Development of a Geometric Model for the Study of Propagating Stall Inception Based on Flow Visualization in a Linear Cascade

by

Donald R. Piatt

Thesis submitted to the Faculty of the
Virginia Polytechnic Institute and State University
in partial fulfillment of the requirements for the degree of

Master of Science
in
Mechanical Engineering

APPROVED

W. F. O'Brien, Chairman

W. F. Ng

J. Moore

July 1986
Blacksburg, Virginia

Development of a Geometric Model for the Study of Propagating Stall Inception Based on Flow Visualization in a Linear Cascade

by

Donald R. Piatt

Mechanical Engineering

(ABSTRACT)

Flow visualization movies of flow through a cascade of compressor blades showed propagating stall at stagger angles of 36.5 and 45 degrees for angles of attack of 20 degrees and higher. At a stagger angle of 25 degrees, the development of a steady, separated boundary layer occurred with no propagation. The observed propagating stall process was the development of a vortex in the boundary layer and its subsequent shedding. The shedding mechanism was observed to be the interference by the reverse flow from the previously stalled passage with the vortex flow in the stalled passage. This dissipated the vortex in the blade passage and the incoming flow then flushed the stagnated vortex out of the passage.

Measurements of propagation speeds showed that the propagation speed is related to the blockage of the passage, that stagger angle has an insignificant effect on propagation speed, and that propagation speed is proportional to the relative velocity.

Based on the observations, a geometric model was developed to predict the onset of propagating stall. This model showed that increased solidity, decreased

stagger angles, and operation at low angles of attack make a cascade more resistant to propagating stall inception. The model shows the relation of the operating point of a compressor to the stall inception point. When expanded to include all significant aspects of blade geometry, the model may provide a basis for controlling propagating, and hence, rotating, stall inception based on the blade row geometry.

Acknowledgements

The author wishes to express his sincere gratitude to the members of his advisory committee: Professors J. Moore, W. F. Ng, and W. F. O'Brien Jr., Chairman. Special thanks go to Professor O'Brien for the degree opportunity and for his insight throughout its completion.

The author also wishes to thank A. Yocum for use of the movies and for his help. The aide of B. Russ is also greatly appreciated.

The author also wishes to gratefully acknowledge Professor G. Scheeler and the Virginia Tech Motion Picture Department for the use of the movie viewing equipment.

Table of Contents

List of Illustrations

List of Symbols

C_x - Absolute velocity, m/sec.

W - Relative velocity, m/sec.

U - Blade velocity, m/sec.

W_x - Axial component of relative velocity, m/sec.

W_y - Tangential component of relative velocity, m/sec.

V_p - Propagation velocity, m/sec.

c - Blade chord, cm.

t - Blade thickness, mm.

h - Blade span, m.

s - Blade spacing, cm.

σ - Solidity, c/s.

γ - Aspect ratio, h/c.

l - Perpendicular distance between blades, cm.

d_f - Flush-out diameter, cm.

d_v - Vortex diameter, cm.

r - Vortex radius, cm.

δ - Boundary layer thickness, cm.

ζ - Stagger angle, degrees.

α - Angle of attack, degrees.

α_m - Mean angle of attack, degrees.

φ - Flow coefficient.

ψ - Pressure rise coefficient, $\Delta P/(\rho U^2/2)$.

x - Axis in the chordwise direction.

x_0 - x coordinate of perpendicular from leading edge of leading blade.

y - Axis perpendicular to the chordwise direction.

m - Length variable.

β - Internal angle variable.

l_c - Characteristic length.

f - Frequency, Hz.

μ - Dynamic viscosity, kg-m/sec.

υ - Kinematic viscosity, μ/ρ.

Str - Strouhal number, fl_c/W.

Str_c - Strouhal number for the cascade, fc/W.

Re - Reynolds number, Wl_c/υ.

Re_c - Reynolds number for the cascade, Wc/υ.

Introduction

When an axial-flow compressor is operating at low mass flow rates, an unstable operating region may be entered where unsteady flow patterns can exist. The flow unsteadiness experienced may be one of two different cases, surge or rotating stall. Surge is characterized by violent fluctuations in total mass flow and pressure rise through the compressor. In surge, the total system operation is unstable. Rotating stall, in contrast, is characterized by stable operation of the compressor at a new operating point which has a lower mass flow rate and reduced pressure rise. The local flow through the blading is, however, unsteady. Local fluctuations in mass flow and pressure rise are experienced, but integration of these values around the compressor annulus is constant. Though much research is needed to fully understand both flow phenomenon, the following work focuses on factors affecting rotating stall.

Rotating stall has been observed and studied in compressor operation and in cascade testing. When a compressor is operating in rotating stall, a portion of the annulus is consumed by a region of greatly reduced mass flow, called a stall 'cell'. The stall cell propagates around the annulus at a velocity related to the blade speed, hence the term 'propagating' or 'rotating' stall. These stall cells may vary in the number present, spanwise extent of the cell, or circumferencial extent of the cell. The cells propagate due to the stalling and unstalling of the blade passages

at the leading and trailing edges of the cell, respectively. Thus, the stall cell seems to move around the annulus.

Propagating stall begins when a compressor, operating at near stall conditions, experiences an inlet flow distortion. The distortion can be caused by discontinuities in the flow, pulsations of flow velocities, an obstruction in the inlet flow, or boundary layer interference from the surrounding environment or blading. This flow distortion causes a sudden increase in incidence angle on one or more of the blades. The sudden increase in incidence causes the affected passage to stall. When the passage stalls, it diverts flow into the passages in front of and behind it. In Fig. 1, passage 2 has stalled and is diverting flow into passage 1, the trailing passage, and passage 3, the leading passage. The flow diverted into passage 1 has a reduced incidence and tends to make the flow through the passage more stable. The flow diverted into passage 3, however, has an increased incidence which causes that passage to stall. As passage 3 stalls, it diverts flow into passages 2 and 4. This causes passage 2 to stabilize and passage 4 to block. Thus, the stall cell seems to propagate along the blade row. This propagation speed has been measured to range from 20 to 70 percent of the blade velocity in the direction opposite to that of the blade rotation. In the stationary reference frame, the stall cell propagates in the same direction as the blade but at a reduced speed.

Among the problems experienced by a compressor operating in rotating stall are reduced performance and structural problems. The reduced performance occurs because the desirable pressure rise cannot be attained in the area of stalled flow. The structural problems arise from the loading and unloading of the blades due to

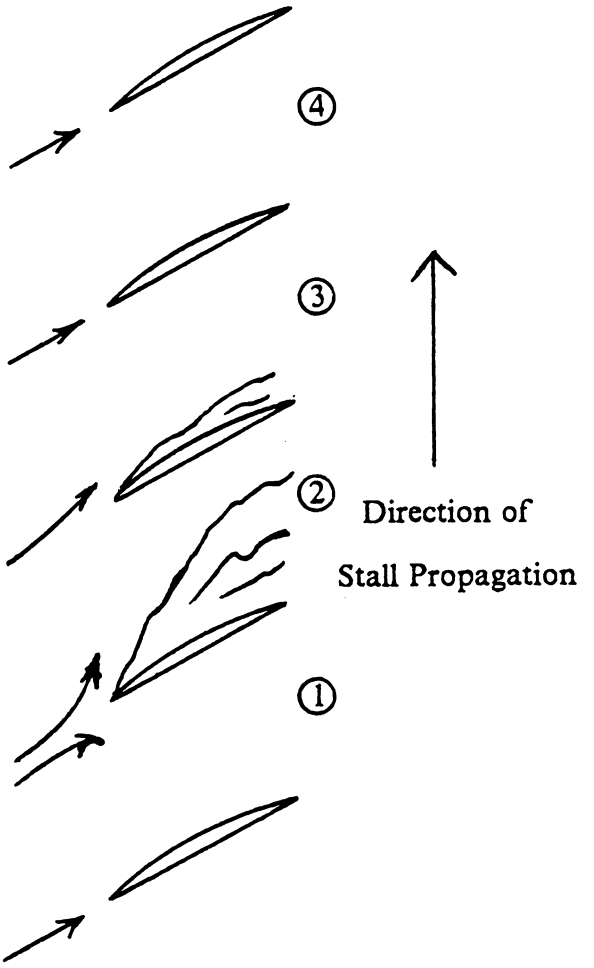

Fig. 1. Diagram of Propagating Stall

the stalling and unstalling of the blade passages. This periodic loading on the blade may cause fatigue stresses in the blade which can cause failure if the compressor is operated under these conditions for an extended period of time.

Recovery from rotating stall is also a major problem. This problem can be observed by examining a typical compressor performance characteristic, as in Fig. 2. A compressor is designed to operate at its operating point, denoted in Fig. 2 as OP. If no large flow transients occur, the compressor will continue to operate on the normal operation curve. If the mass flow is reduced, however, the operating point of the compressor moves along the normal operation curve toward the stall line. When the compressor operates near the stall line, at point A, any small disturbance may cause rotating stall to occur and the compressor will assume stable operation with its new operating point at point B. Recovery from this undesirable condition, if possible, is done by throttling to the stall recovery line. This moves the operating point along the stalled operation line to point C, where the compressor resumes normal operation at operating point D. The stall recovery hysteresis of a compressor is related to the size of the area bounded by the stable operation curves and the stall inception and recovery lines. Compressors with closely-spaced stable operation lines have less hysteresis, i.e. better recovery, than compressors with widely-spaced stable operation lines.

Though much research has been done in the area of rotating stall, the exact physical flow patterns which occur in the blading are still unknown and an accurate universal method for predicting rotating stall behavior is unavailable. What is the nature of the blockage in the stall cells? What characteristics of the stall cell affect

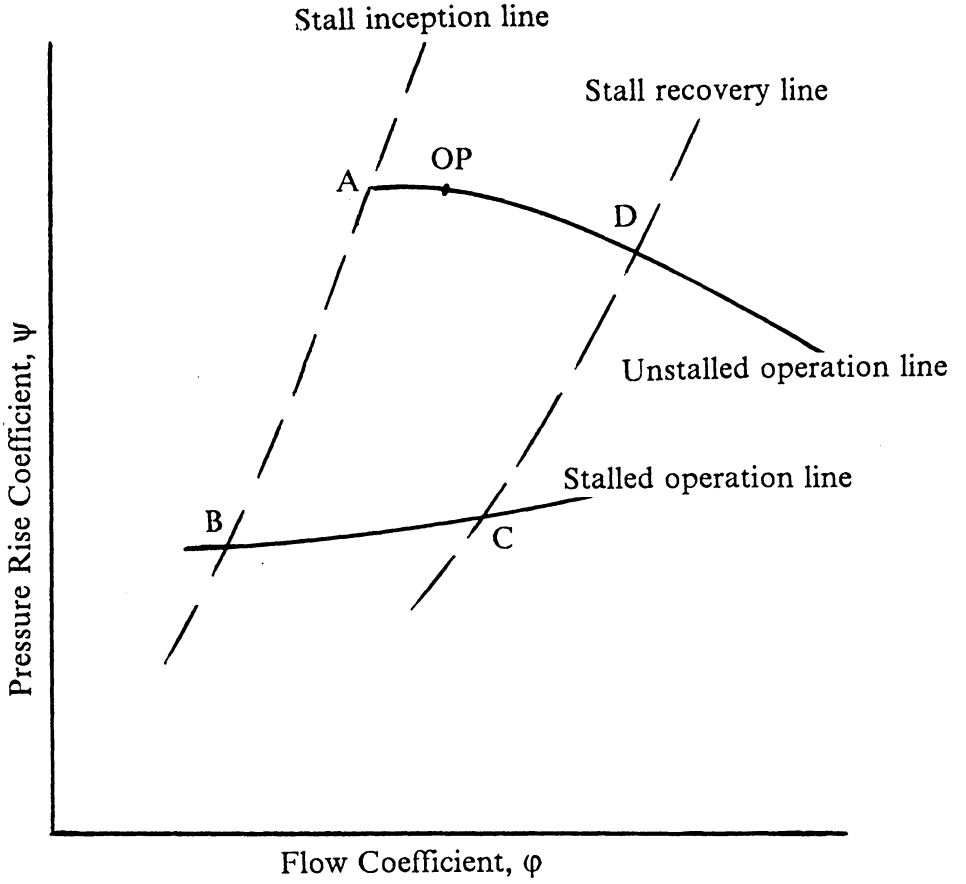

Fig. 2. Compressor Operating Characteristic

the propagation speed? What factors affect the inception of rotating stall? It is the purpose of this paper to gain insight into the phenomenon and formulate some answers based on observations of propagating stall in a cascade in order to provide a sound basis for a fundamentally correct propagating stall model, and, thus, an accurate rotating stall model.

Literature Review

The first observations of rotating stall in axial compressors were made in 1949 by H.P. Grant [1] and, later, in 1951 by W.D. Rannie [2]. Their observations led to a great deal of research into this phenomenon which is of great concern to compressor designers and operators. Even today, the exact flow dynamics which occur in the compressor during rotating stall are unknown. This is the main reason that, although several different theoretical models have been developed to model rotating stall, there has not been one that is universally accurate in prediction of inception of rotating stall or compressor performance during it.

After Grant's and Rannie's observations became public, several people began research and testing of the phenomenon in compressors and blade cascades. Along with Grant and Rannie, among the first were Emmons [1], Iura [2], Stenning and Kriebel [3], et al. Testing was done using hot wire probes to measure velocities and pressure probes to measure the pressures. The results of the experimentation were:

1. Rotating stall is initiated when the compressor is operating near the stall limit.

2. Initially, rotating stall consists of several small cells which cover only a portion of the span of the cell, a condition called 'part span' stall.

3. As the mass flow decreases, more cells appear until they merge to form one large cell.

4. As mass flow is decreased, the cells also grow in spanwise extent until the entire span is covered, a condition called 'full span' stall.

5. The larger stall cells propagate at a faster velocity than the small cells relative to the rotor.

6. The net mass flow through the stalled passages is very small, essentially zero relative to flow through unstalled passages.

7. Reverse flow is present in the stall cells.

8. Greatly reduced pressure rise occurs across the stall cell.

9. The major stalling process occurs with leading edge stall.

10. Stall cell propagation speeds range from 20 to 70 percent of the blade velocity and are in the direction opposite to the direction of the blade velocity.

11. Overall pressure losses increase drastically with the onset of rotating stall.

The testing provided valuable information which laid the basis for the theoretical models of propagating stall which followed.

In the years following Grant's and Rannie's observations, several theoretical models were developed to predict the onset of stall, propagation velocity, and stall cell size. Sears [4], Marble [5], and Emmons, et al. [6], were the first to develop models. The first models solved the linearized flow equations to predict, most often, propagation speed and inception of rotating stall. The blades were modeled using actuator disk theory, where the blade row is replaced by a plane which imparts the blade effects to the flow. Each was unique, but still accurate in certain cases. The Sears model utilized a time lag parameter to predict propagation speed. Marble's analysis was done in a reference frame fixed to the stall cell, but it required a stall cell propagation velocity as an input. The model of Emmons, et al., and those that followed, relied on pressure fluctuations or lift coefficients to predict propagation speed. The amount of flow blockage was often calculated to predict the size of the stall cell. These linear models used a small perturbation analysis to predict the onset of rotating stall. In this type of analysis, a small flow perturbation is imbedded in the upstream flow. The downstream flow is then analyzed to see if the perturbation grew or shrank. If the perturbation grew, rotating stall inception would be predicted.

Stenning and Kriebel took a different approach to modeling rotating stall. Their research indicated the presence of a vortex in a stalled passage. They therefore looked at stall propagation as a vortex shedding problem. They based their model on the flow velocities and angles of the shed vortices to predict propagation

speed. Recently, Spalart [7] has extended vortex methods over isolated bodies to vortex shedding in a cascade of blades. The flow patterns he developed using this method correlated well with the observed flow patterns of Stenning and Kriebel.

These early researchers gave valuable insight into the modeling of rotating stall. Each model contained different parameters which made it a good model for its particular case. The models were limited, however, in their range of valid use. There has not been a model developed which accurately predicts rotating stall phenomenon for all cases, which is the desired result.

Models which naturally followed the linear models were non-linear models. Takata and Nagano [8] and Adamczyk and Carta [9] were among the first to develop non-linear models. These models solved the non-linear flow equations using numerical techniques. Further improvement came from modeling the blades using semi-actuator disk theory. Again, these models used pressure loss and a small perturbation analysis to predict rotating stall inception and propagation speed.

One aspect of these non-linear models which remained unchanged from the linear models is the response of the blade effects to changes in flow. Throughout the models, the response is assumed to be first order. Sexton [10] improved on these non-linear models by developing a dynamic response curve, based on on-rotor pressure measurements, to model the dynamic blade row characteristics.

The non-linear models were improvements over the linear models, but they still concentrated the analysis on global fluctuations. The local flow dynamics were basically ignored. It is felt that only through knowledge of the flow over the individual blades can a general rotating stall model be developed.

A different approach to the understanding of rotating stall was taken by Greitzer [11,12,13]. He pointed out that a compressor operates, not just as a set of blade rows, but as a compressor system. The compressor system stability should therefore be analyzed. His compressor system model was based on the compressor operating characteristic, a compressor length, a discharge plenum volume, etc.... Using this model he was able to calculate a critical value of a parameter for a compressor which would predict the type of stall experienced by the compressor, surge or rotating stall. Moore [14,15,16] also approached the problem this way. His theory showed that rotating stall is an eigenvalue problem of the total system stability.

These approaches led to certain conclusions concerning the recovery ability of a compressor. Greitzer showed that compressors which had large hysteresis loops, the loop formed by points A,B,C,D in Fig. 3, had poor recovery ability. Similarly, those with small hysteresis loops had better recovery ability. Figure 3 shows these two cases and their hysteresis loops. Day, Greitzer, and Cumpsty [17] determined that a critical blockage value of thirty percent occured at the stall limit and that this critical blockage was related to the amount of hysteresis in the system. Conclusions reached were that compressors with low values of design C_x/U (< 0.55) had closely-spaced stable operation lines and, thus, little or no hysteresis. Those with higher values had widely-spaced lines and more hysteresis.

While the previous models gave predictions for inception, cell size, and propagation speed, the actual process of rotating stall is not clear. Some researchers have investigated the effects of different aspects of blade geometry on rotating stall

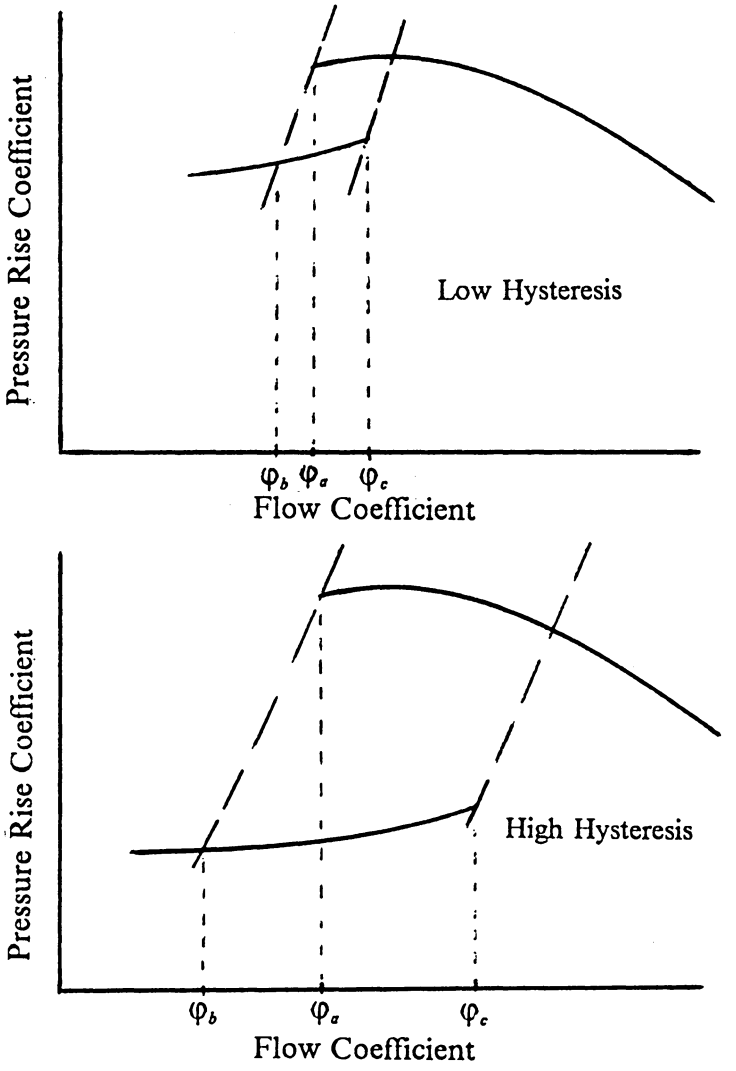

Fig. 3. Hysteresis Loops on Compressor Characteristics

and others have developed models which incorporate these effects. Because an understanding of the local flow dynamics are essential to understanding rotating stall, blade geometry is definitely important.

Lieblein [18] was among the first to study blade geometry effects. He developed a diffusion factor, D, based on blading, which was indicative of the losses in a compressor. At a value of D of 0.6, it was noticed that the losses rapidly increased. This, along with the knowledge that losses drastically increased when stall occured, has been used to predict stall inception.

Cheers and Funnell [19] studied the effect of the shape of the nose of the blade on rotating stall. They based their work on studies done on the stalling behavior of isolated airfoils. These studies showed that airfoils with well-rounded noses experienced trailing edge separation which moved closer to the leading edge as the incidence angle was increased until the entire blade was stalled. Airfoils with more pointed noses experienced this same stalling behavior at low incidence angles, but as the incidence was increased, a critical value of incidence would be reached where the stalling behavior would abruptly change to leading edge separation. Very sharp noses on airfoils led to leading edge separation immediately with reattachment at some point downstream. As the incidence is increased, this reattachment point moves toward the trailing edge of the blade until it is gone. Cheers and Funnell calculated a G_m parameter which described the nose shape with respect to the inlet flow angle. They then compared the observed propagation speeds of the stall cells in compressors with blades with similar blade nose shape. Their investigations showed definite correlations between the two parameters. Because the main stall-

ing behavior in the present experiment occurs with leading edge stall, it is felt the shape of the leading edge is significant in predicting stall inception.

Other factors of blade geometry have been investigated by Koch and Smith [20,21], and Russ [22]. Koch and Smith investigated the effect of endwall boundary layer growth on rotating stall. Endwall boundary layer growth is related to blade shape and rotor tip clearance. The boundary layer growth is important because it contributes to flow blockage and contributes to three-dimensional flow patterns. They also studied the effect of aspect ratio. Results showed that low aspect ratio machines stalled at lower flow coefficients than high aspect ratio machines and, thus, were more resistant to rotating stall inception. Russ has studied the effect of endwall boundary layer separation and found it to make a significant contribution to transition of a blade from trailing edge to leading edge separation.

Recently, Mathioudakis and Breugelmans [23,24] have conducted extensive research on local flow patterns in stalled flows. Their research showed definite reverse flow and radial flow on the blades and gave insight into three-dimensional flow patterns in stall.

Models have been developed which employ local flow data and some blade geometry effects. Cumpsty and Greitzer [25] have developed a model for predicting stall propagation speed which is based on the local pressure variations around the annulus during rotating stall. Zika [26] and Cousins [27] have developed models for rotating stall which incorporate blade geometry. These models do not, however, focus on the actual flow in the stalled passages.

The Cumpsty and Greitzer model for calculating the stall propagation speed is based on the pressure spikes which occur at the leading and trailing edges of the stall cell. The magnitudes of these pressure variations and an experimentally-determined constant are the keys to the model. Their predictions of propagation speed for a wide variety of compressors showed relatively good correlation.

Zika's model was based on a finite discontinuity analysis of rotating stall. He concluded that solidity, stagger, and the amount of prewhirl all had a significant effect on the inception of rotating stall. These factors, however, did not affect the propagation speed of the cell. It was only dependent on the turning angle of the blading.

Cousins' model was a non-linear model along the lines of Sexton's work. He incorporated into his model the chord length, stagger angle, turning angle, and blade tangential velocity. His model yielded some conclusions on the recovery of a compressor from rotating stall. The model showed that compressors which had stable stalled and unstalled operating lines which were closely-spaced had better recovery characteristics than those with widely-spaced operating lines. This agreed with the conclusions reached by Greitzer and Moore concerning the relation of recovery and the compressor operating characteristics. Cousins proposed a parameter, R, to quantify the amount of stall hysteresis of a compressor. R, the recovery factor, was defined as the ratio of the difference of the stall inception and cessation flow coefficients on the stalled operating line over the flow coefficient of the stall inception point on the unstalled line. Using the notation of Fig. 3, R is defined as

$$R = \frac{(\varphi_c - \varphi_b)}{\varphi_a}$$

Low R values indicate low hysteresis while high values indicate a large amount of hysteresis.

While many of the theoretical models have sought to predict rotating stall inception, cell size, and propagation speeds, few are based on the local flow dynamics over the blade during stall. Most of the models were based on global parameters such as loss, flow coefficients, or pressure distribution. To date, Cousins' non-linear model, which incorporates some blade geometry effects, is the most complete. Accurate prediction of stall inception and recovery, thought to be the primary concern, can only be done through a thorough understanding of the mechanism by which it occurs. Inception is directly related to blade geometry and more research is needed to determine how it is affected. Recovery from stall has been shown to be related to the compressor characteristic, which is determined by the blade geometry. Thus, a better understanding of the effects of solidity, stagger, turning angle, prewhirl, and blade nose shape on rotating stall is essential for the development of an accurate theoretical model.

Discussion of Literature

Since the first observations of rotating stall, much research has been done in an attempt to fully understand this phenomenon. Along with testing, linear and non-linear models were developed to predict the onset of and recovery from rotating stall, stall cell size, and cell propagation speeds. These developments all certainly enhanced the knowledge of rotating stall, but each model had its limitations. It is felt that these limitations can only be overcome through a complete understanding of the mechanism by which rotating stall occurs. Further research based on local flow analysis must be done to achieve this.

One factor which plays a vital role in local flow behavior is the geometric configuration of the blades. This affects stall inception and the shape of the compressor characteristic, and thus recovery. The relationship between solidity, stagger, aspect ratio, turning angle, prewhirl, blade nose shape, and tip spacing and rotating stall must be evaluated.

Cheers and Funnel [19] showed that the shape of the nose of the blade has an effect on propagation velocity. Since the primary stalling behavior is associated with leading edge stall [22], their research would indicate that a critical value of incidence angle, dependent on the nose shape, is a key element in the prediction of rotating stall. From a recovery standpoint, rounder noses should have better recovery characteristics, since the separation point can be moved along the blade by varying the incidence angle. When leading edge separation occurs, the passage

is more resistant to recovery. Thus, a very high critical incidence value (those associated with rounder noses) means the blade is more resistant to inception of leading edge stall and has better recovery ability to unstalled operation.

Koch and Smith [20,21] studied effects of aspect ratio and, indirectly, tip clearance and blade shape. Their findings showed that low aspect ratios corresponded with low values of flow coefficients for stall inception. Therefore, low aspect ratio compressors should be more resistant to rotating stall inception. Their research on the effect of endwall boundary layer growth, which is dependent on blade shape and tip clearance, showed it to be important in multistage machines. Russ' study [22] of endwall boundary layer separation in a cascade showed it to be important in determining the transition point from trailing edge separation to leading edge separation. The endwall boundary layer therefore plays an important role in determining the inception point of rotating stall.

Blade geometry is related to stall recovery because it determines the compressor operating characteristic. Good recovery ability, associated with low hysteresis, was shown by Greitzer [11,12,13], Moore [14,15,16], and Cousins [27] to correspond to compressors which had closely spaced stalled and unstalled stable operation curves. This may be explained by the fact that the reduction in pressure rise experienced by compressors operating in stall is greater in compressors with widely-spaced characteristics than in compressors with closely-spaced characteristics. There is a greater amount of pressure rise that must be recovered to resume normal operation so recovery is more difficult. Greitzer correlated recovery be-

havior with design values of C_x/U. Compressors with low values of design C_x/U had characteristics with low hysteresis and better recovery.

The work that follows investigates what happens locally to the flow during stalled behavior. From these observations, a theory is developed to relate the effect of blade geometry on rotating stall. This research gives further knowledge of the local flow dynamics and, when combined with previous and future research, will lay a sound basis for the development of a universally acceptable model.

Experimental Procedure

As part of a project to investigate loss sources in an axial-flow compressor, a linear cascade was designed, constructed, and is currently in use in the Mechanical Engineering Turbomachinery Lab at Virginia Polytechnic Institute and State University. The cascade was originally built by Tkacik [28] in 1980-81. Currently, it is being used in the research of Yocum [29] and Russ [22]. The project objective is to examine the flow losses produced by the cascade blading and to use the results to predict losses experienced by a compressor. To aid in this research, Yocum took flow visualization movies of flow through the cascade. These movies showed the existence of a propagating stall phenomenon and are the basis for the following work.

The cascade contains flat-bottomed blades with a circular arc suction surface. The geometry of the cascade is shown in Fig. 4. The chord length of the blades, c, is 6.55 centimeters and the blade thickness, t, is 6.53 millimeters. The blade span, h, is 0.308 meters in length, giving an aspect ratio, γ , of 4.70. The cascade has a solidity, σ , of 1.00. The blades are made of aluminum and are mounted on movable, circular walls. These walls are constructed of plexiglas and are designed to rotate inside a plywood frame. The stagger angle, ζ , can be varied by changing the blade position in the cascade. By rotating the walls, the desired angle of attack, α , can be set. Thus, any combination of stagger angle and angle of attack is

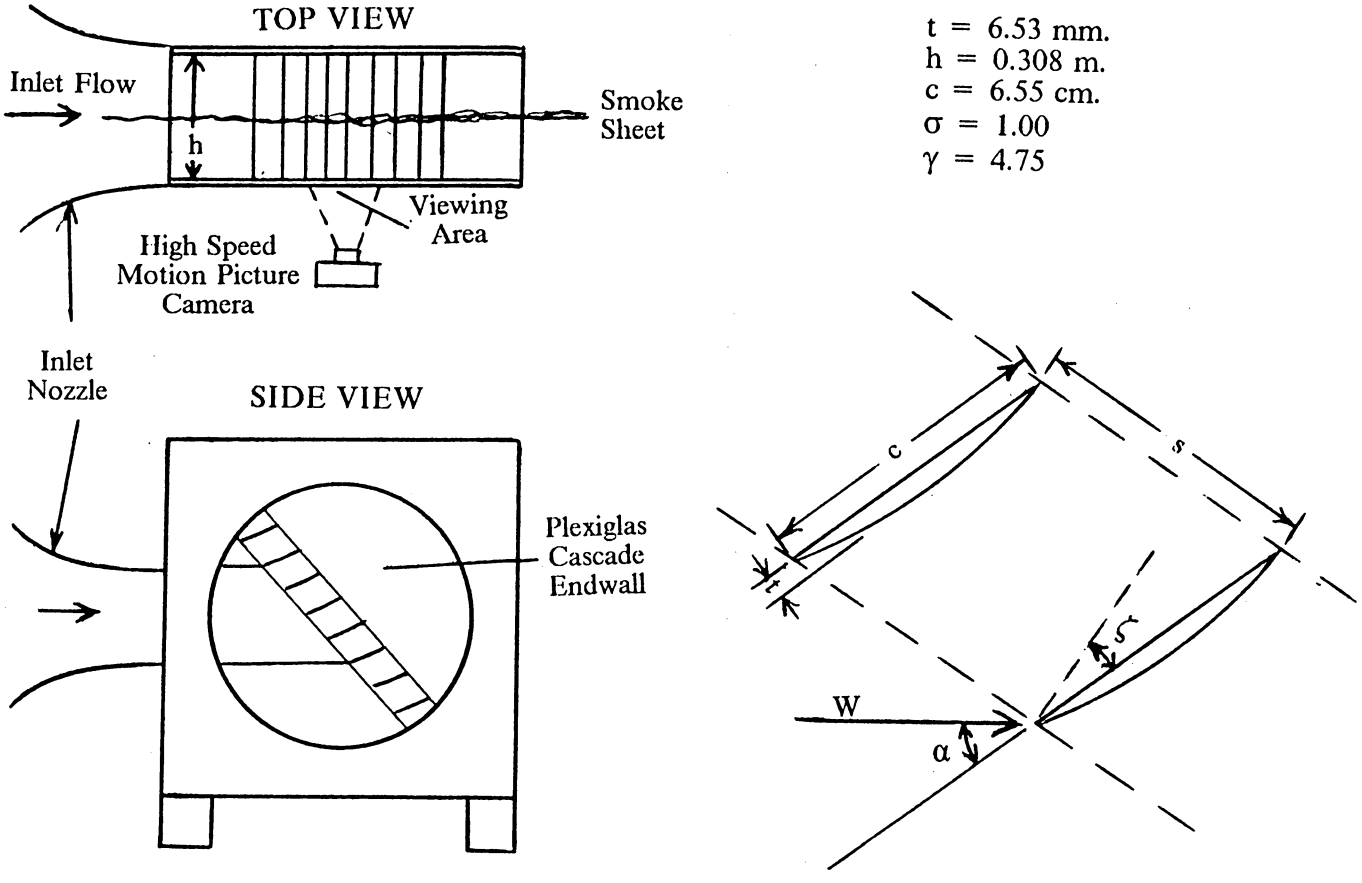

Fig. 4. Cascade Geometry

available for research purposes. A 0.305 meter by 0.308 meter inlet duct directs the inlet flow to the blading.

The flow visualization recorded in the movies was performed by injecting a vertical smoke sheet into the upstream flow at the midspan of the blades. This smoke sheet had a thickness of 4.8 millimeters the injection point and diffused to a thickness of approximately 13 millimeters at the blading. The movies provided a two-dimensional view of the flow patterns which existed in this high aspect ratio cascade. Russ' work [22] showed that the primary stalling behavior at high angles of attack is due to two-dimensional leading edge separation on the stalled blades. This can be seen by examining a diagram of a sample of Russ' results, as shown in Fig. 5. Russ painted the cascade blades with titanium dioxide paint and then recorded the flow for a wide range of angles of attack in small degree increments. In Fig. 5, blade 1 shows very little separated flow on the blade face. This is at a low angle of attack. Blade 2 is at a slightly higher angle of attack and shows the development of a trailing edge separated boundary layer and the growth of an endwall boundary layer. As the angle of attack increases further, as on blade 3, the extent of the trailing edge separation and endwall boundary layer influence increases. Blade 3 is at an angle of attack which is in the developing stall region. In this region, the stalling behavior is three-dimensional, as evidenced by the location of the separation points on the blades. Further increasing the angle of attack causes flow separation similar to that diagrammed on blade 4. The flow over this blade is experiencing leading edge two-dimensional separation. This is the fully-developed stall region. The transition of a blade from the stalling behavior of blade 3 to the

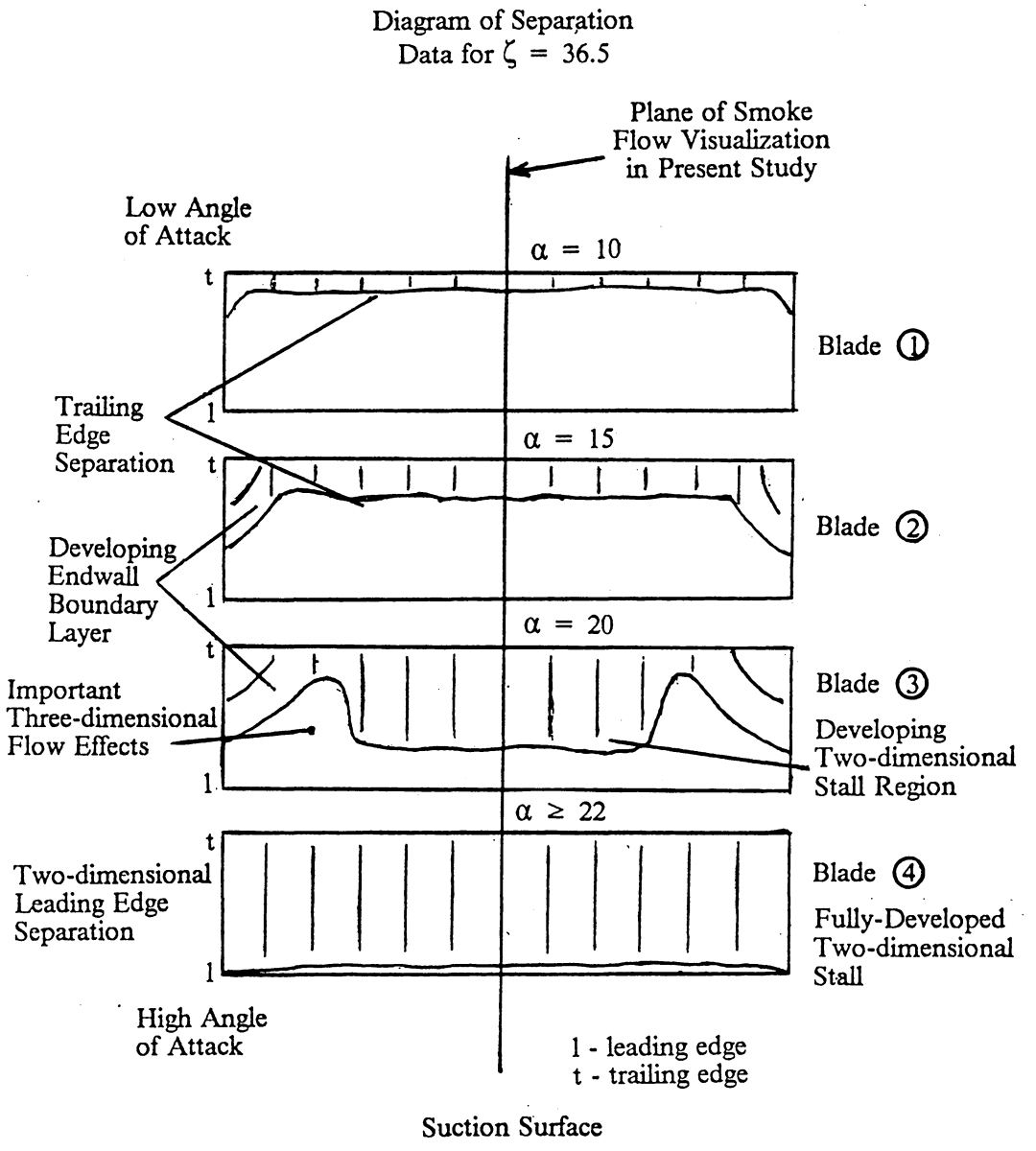

Fig. 5. Diagram of Surface Flow Visualization Showing Developing Flow Separation on a Blade [22]

stalling behavior of blade 4 occurs with a change of only 2 or 3 degrees in angle of attack. The observed fully-developed propagating stall behavior discussed in this thesis occurred at angles of attack which gave flow separation corresponding to that of blade 4.

A Hycam II High Speed Rotating Prism Camera (model no. 41-0014), a product of the Redlake Corporation, was used to film the movies. The movies were filmed on 16 mm color film at a film speed of 4000 frames per second. One 100 foot film was made for each test case. Since there are 40 frames per foot on the movies, the movie frames are spaced at 0.25 millisecond intervals. Movies were taken at stagger angles of 25, 36.5 and 45 degrees for angles of attack ranging from 10 to 45 degrees. A low speed test, with an inlet velocity of approximately 17 meters per second, and a high speed test, with an inlet velocity of approximately 47 meters per second, were photographed. Thus, a study of the effects of stagger angle, angle of attack, and relative velocity could be made with the movies.

The movies showed the development of a vortex in the blade passages and its subsequent shedding. This flow behavior was fairly periodic and showed a definite propagation along the blade row. After further scrutinization, the observed behavior was determined to be a propagating stall phenomenon. Figures 9 through 80 will show the observed flow behavior for the different test conditions.

A quantitative expression of the observed vortex growth and shedding process was desired. It was decided that viewing the movies and counting the propagating stall occurrences was the best available method. This could not be done using a conventional movie projector because the occurrences happen too quickly and ref-

erencing the observations to any sort of time frame would be extremely difficult. To overcome this problem, manual movie viewing equipment was obtained from the Virginia Tech Motion Picture Department. This equipment consisted of a portable viewing screen, a frame counter, and a set of manual rewinds, as shown in Fig. 6. The movies were viewed by running the film from one rewind, through the viewing screen and the frame counter, and onto the other rewind. A movie, once readied for viewing, was then viewed by manually winding the rewinds, thus pulling the movie through the screen. With one rewind on either side of the viewer and frame counter, the movies could be shown at any desired speed, forward or backward, or viewed one frame at a time, as a series of still photos taken in 0.25 millisecond intervals. The frame counter was used to count the number of frames between observations of similar flow patterns. The recorded data could then be used to reference the observations with an associated time period since the frame speed was known.

Two observations were recorded by viewing the movies, frequency of occurrences in one passage and a rate of vortex propagation. For this study, it was necessary to develop a criteria for defining an occurrence. This reference criteria was defined to be the point at which a vortex flow was well defined and maximum blockage of the passage was attained. Determination of this point was done by observation of the vortex flow and was very dependent on the judgement of the viewer. When viewing the movies, each time flow behavior similar to the behavior described above was observed, an occurrence was counted. The judgement of the viewer in determining the exact point at which this occurred was vital to the

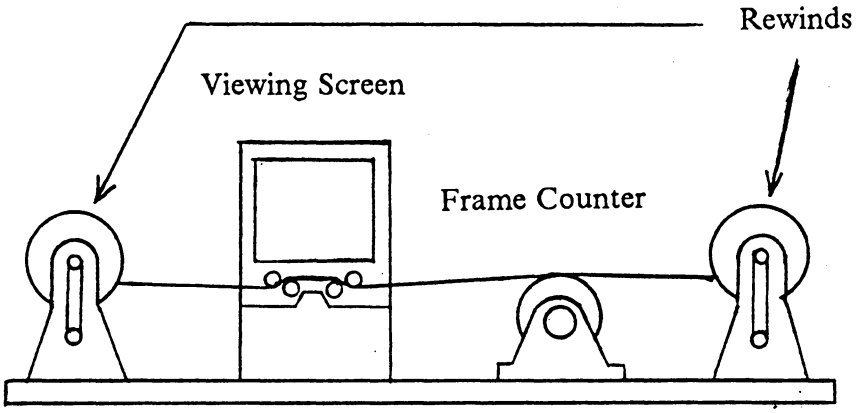

Fig. 6. Sketch of Movie Viewing Equipment

measurement procedure. Even though great care was taken to determine an occurrence at equivalent points in the vortex development, definition of this point could easily fall within a 10 or 15 frame span, or more. To reduce the error involved in the measurements, as many occurrences as were discernable were counted and then averaged. The averages were then assumed to be the actual values for the measurements.

The measurement of frequency of occurrence in a passage was measured in the center passage, that is, the passage in the center of the frame. An example of the data taken for this measurement is shown in Fig. 7. The foot and frame number at which each occurrence took place on the film was recorded. These data were then used to calculate the number of frames between occurrences, DFRAME in Fig. 7. Since the film speed is known, an associated time period and frequency were then calculated.

The second value, the rate of propagation, VPROP in Fig. 7, was measured in much the same way. The movies generally showed three or four passages in which the flow patterns could be distinguished. To measure the propagation velocity, the foot and frame number of an occurrence in the uppermost passage was noted to define the initiation of a stall cell propagation measurement. The associated boundary layer growth and vortex development and shedding in the adjacent passage due to the stalling of the initial passage was followed along the blade row. When the occurrence reached the last discernable passage, that foot and frame number were also recorded. The data thus consisted of the beginning and concluding foot and frame numbers and the number of blade passages through which

Stagger angle= 36.5 , Angle of attack= 25 , Inlet velocity= 54.1 ft/sec.

OCCURRENCES IN CENTER PASSAGE

THERE ARE 10 OCCURRENCES

NO.	FT FRAME		DFRAME	PERIOD <SEC>	FREQUENCY <HZ>
0	1.0	21.0			
1	2.0	10.0	29.0	0.007250	137.93
2	3.0	0.0	30.0	0.007500	133.33
3	4.0	10.0	50.0	0.012500	80.00
4	10.0	18.0	248.0	0.062000	16.13
5	11.0	25.0	47.0	0.011750	85.11
6	16.0	22.0	197.0	0.049250	20.30
7	21.0	31.0	209.0	0.052250	19.14
8	27.0	32.0	241.0	0.060250	16.60
9	46.0	18.0	746.0	0.186500	5.36
10	56.0	16.0	398.0	0.099500	10.05

THE 9 ENTRY IS NOT INCLUDED IN THE STATS
MEAN= 161.0000 STD.DEV.= 129.2478 PER.= 0.040250 FREQ.= 24.8447

CALCULATION OF PROPAGATION SPEED FROM PROPAGATING DATA

THERE ARE 6 PROPAGATING STALL CELLS NOTED

NO.	FRAMES	PASS.	PERIOD SEC.	FREQ. HZ.	VPROP FT/SEC	VPROP/W
1	94.000	2.000	0.01175000	85.106	18.1560	0.33560
2	167.000	3.000	0.01391666	71.856	15.3293	0.28335
3	118.000	2.000	0.01475000	67.797	14.4633	0.26734
4	114.000	2.000	0.01425000	70.175	14.9708	0.27672
5	131.000	1.000	0.03275000	30.534	6.5140	0.12041
6	97.000	2.000	0.01212500	82.474	17.5945	0.32522

MEAN= 66.3611 STD.DEV.= 0.320257E+02

AVERAGE VALUES
PER.= 0.016590 FREQ= 60.276 VPROP= 12.8589 VPROP/W= 0.23769

Fig. 7. Data Example

propagation occurred. The frame numbers were converted to a time period as in the first measurement. Then, since the blade spacing was known, the number of passages was converted into a distance. The propagation speed was then the ratio of the distance to the time period. The results were then non-dimensionalized using the relative inlet velocity.

Results and Discussion

Two important conclusions were reached as a result of the evaluations of the observations. First, the measurements gave quantitative values which could be used to determine the effects of geometry on propagation speed. Secondly, the movies provided information about the mechanism which causes the vortex in the passage to shed, or 'flush-out'. The latter observations led to the development of a geometric model for predicting propagating stall inception.

Flow Observations

The movies showed the existence of propagating stall at stagger angles of 36.5 and 45 degrees for angles of attack of 20 degrees or greater. At a stagger angle of 25 degrees, no such behavior was observed. This can be seen by examining the flow behavior in Figs. 9 through 80. For each stagger angle and angle of attack there are 6 sequential photos which show the flow development in the blade passages. In each figure, a photo appears with a diagram of the significant flow behavior which occurs in it. A key for examining the propagating stall photos is given below.

At an angle of attack of 15 degrees and for all three staggers, Figs. 9 through 14, 33 through 38, and 57 through 62, the movies showed little or no separated boundary layer development and relatively smooth flow between all blade passages.

At a stagger angle of 25 degrees, the higher angles of attack cause the development of a steady separated boundary layer from the leading edge on the suction side of the blade. This boundary layer is steady with time and the same behavior occurs in each passage, as seen in Figs. 15 through 32. This indicates that no propagation occurred at a 25 degree stagger angle. Thus, stagger angle must affect the propagating stall inception point.

The figures showing the flow patterns at stagger angles of 36.5 and 45 degrees and higher angles of attack, Figs. 39 through 56 and 63 through 80, show the development of a separated boundary layer and then a vortex in the blade passages. This behavior varies from passage to passage and in time. Furthermore, the development of a vortex in one blade passage caused the next passage to also develop a vortex. This is the propagation of the stall cell.

A schematic, or 'key', of the typical propagating stall flow behavior appears in Fig. 8. Each photo shows several blade passages but the significant flow behavior in the photos occurs in passages 1 and 2 where passage 1 is denoted as the passage to the upper left of the passage in the center of each picture and the center passage is denoted as passage 2. For stagger angles of 36.5 and 45 degrees and angles of attack greater than 20 degrees, each sequence of photos show, in order:

picture.	description
1.	Vortex development in passage 1 and smooth flow in passage 2.
2.	Vortex occurrence in passage 1.

3. Flush-out of vortex in passage 1 and corresponding vortex development in passage 2.

4. Vortex occurrence in passage 2.

5. Flush-out of vortex in passage 2.

6. Resumption of smooth flow through passage 2.

This flow development can be followed in Fig. 8 and by following the diagram of the flow corresponding to each photo.

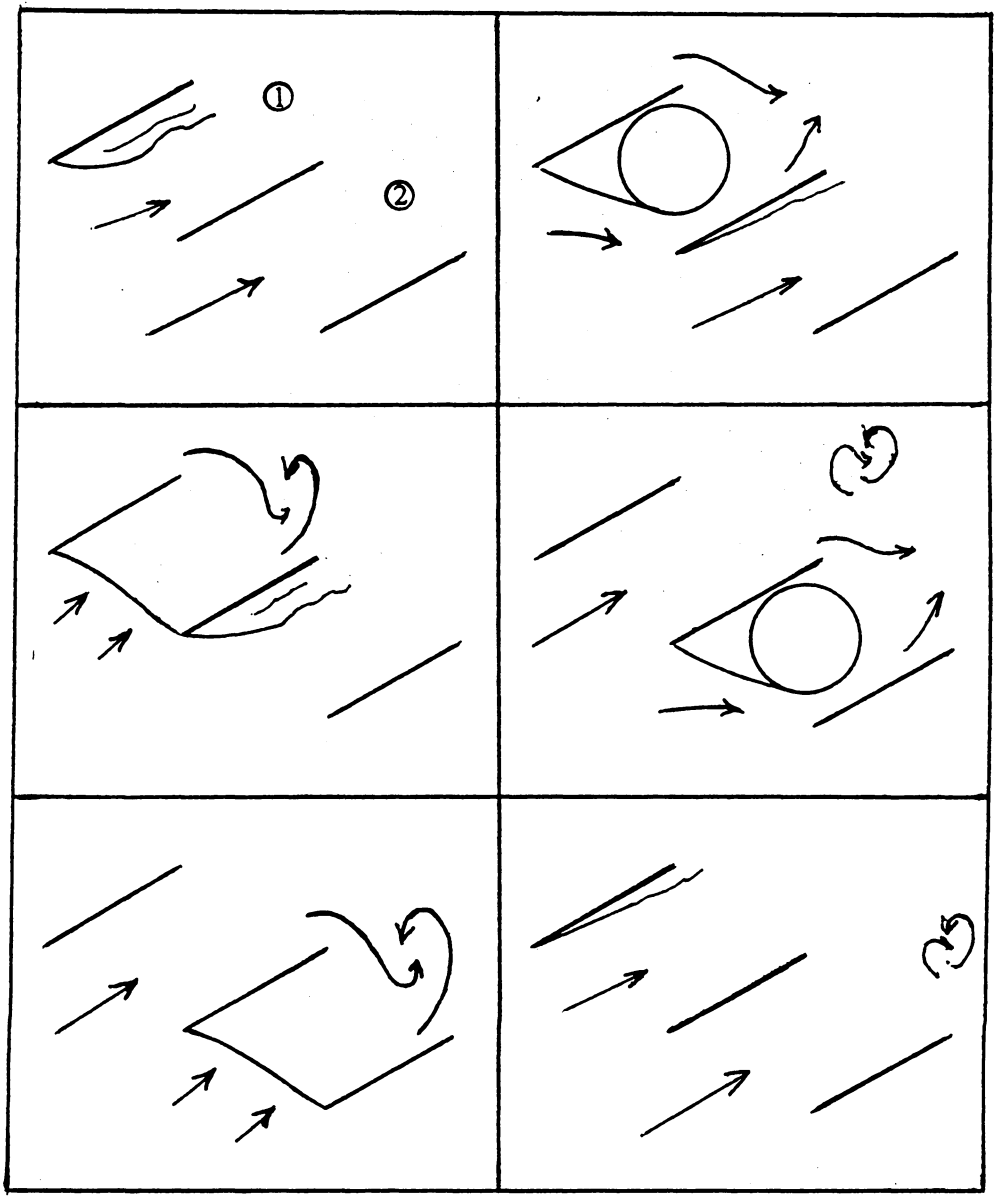

Picture 1
Picture 3
Picture 5

Picture 2
Picture 4
Picture 6

Fig. 8. Schematic of Observed Flow

(a)

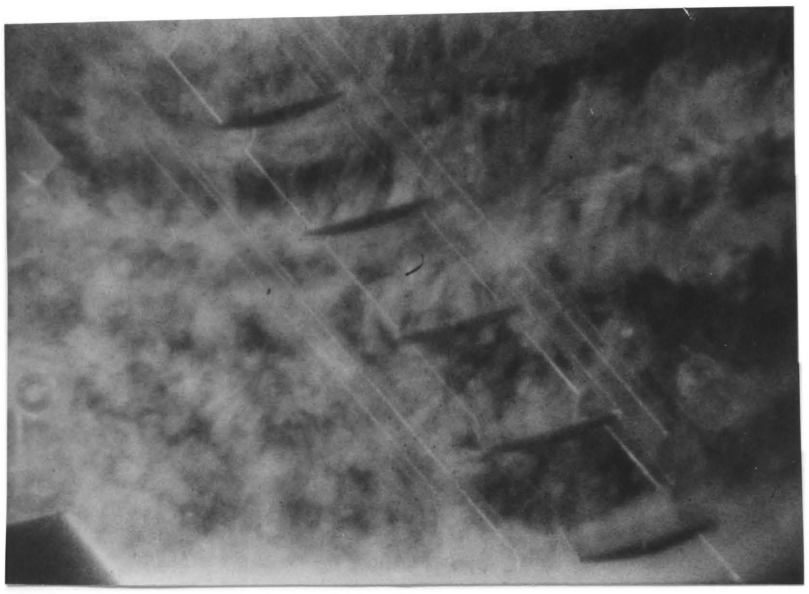

(b)

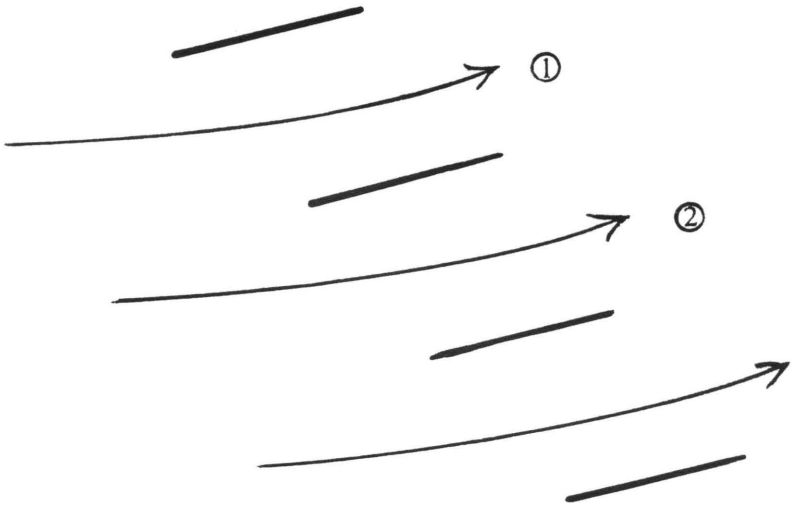

Fig. 9. Observed Flow; Stagger = 25, Angle of Attack = 15
(a) Picture 1, time = 0.00 ms., ref.
(b) Diagram of Picture 1

(a)

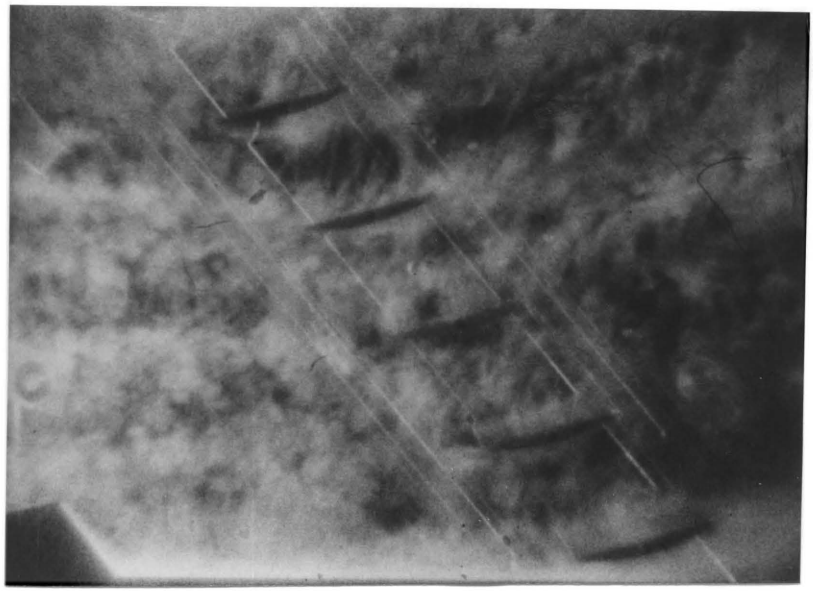

(b)

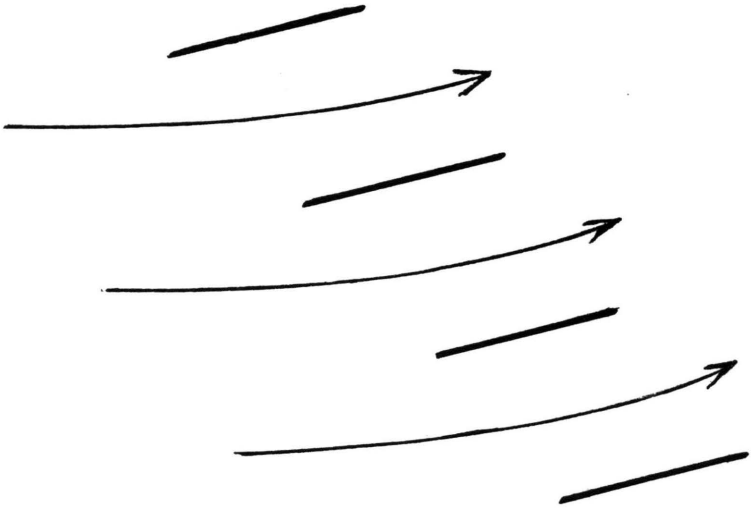

Fig. 10. Observed Flow; Stagger = 25, Angle of Attack = 15
(a) Picture 2, time = 5.00 ms.
(b) Diagram of Picture 2

(a)

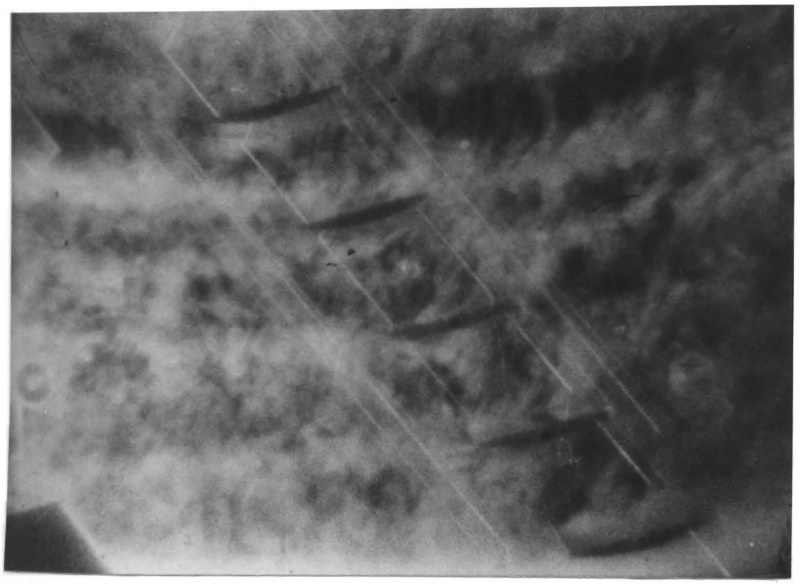

(b)

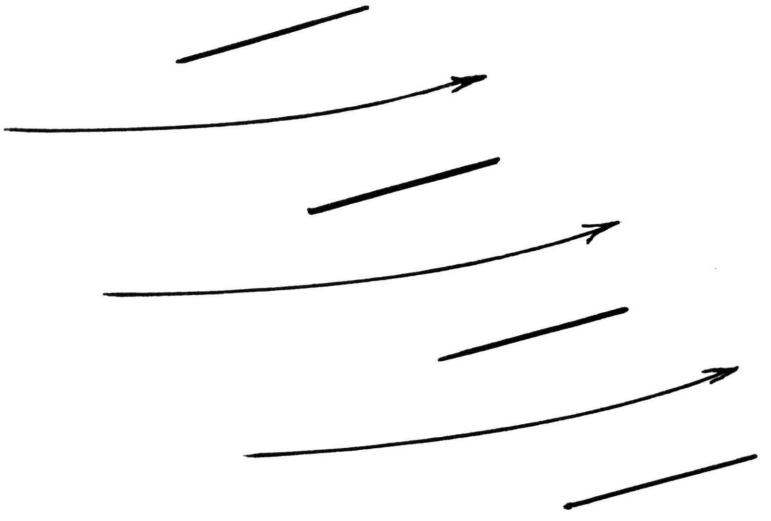

Fig. 11. Observed Flow; Stagger = 25, Angle of Attack = 15
(a) Picture 3, time = 10.00 ms.
(b) Diagram of Picture 3

(a)

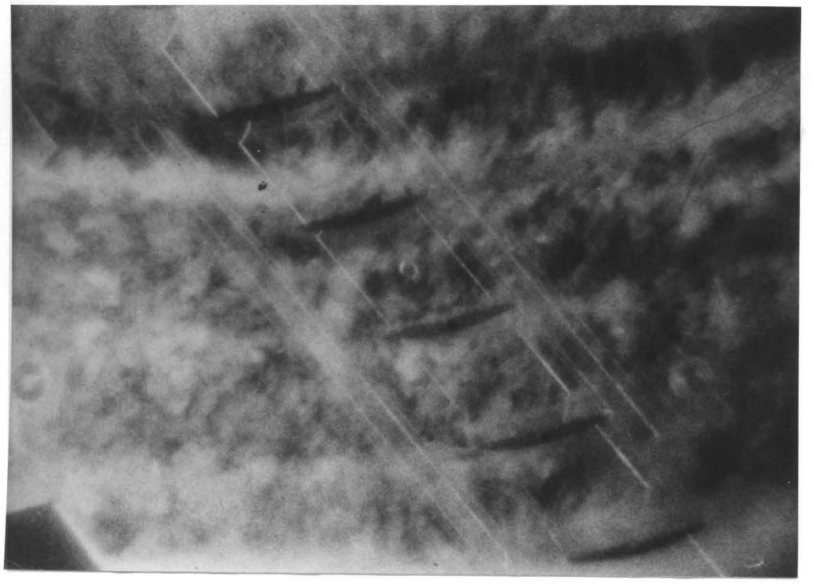

(b)

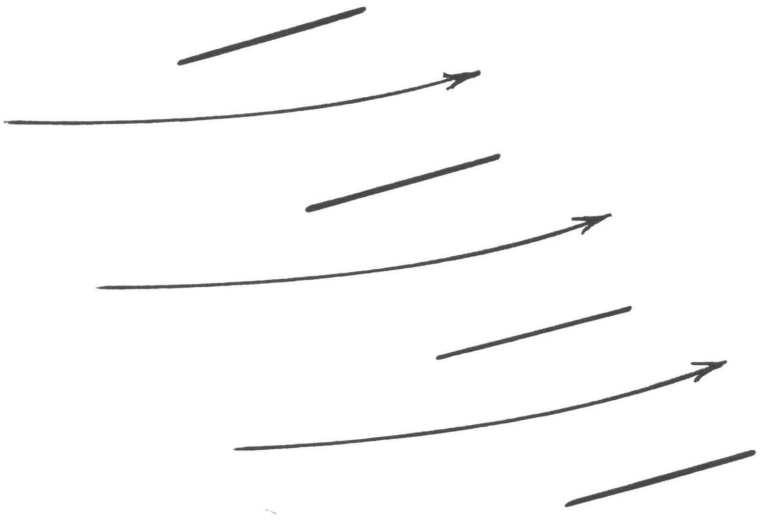

Fig. 12. Observed Flow; Stagger = 25, Angle of Attack = 15
(a) Picture 4, time = 15.00 ms.
(b) Diagram of Picture 4

(a)

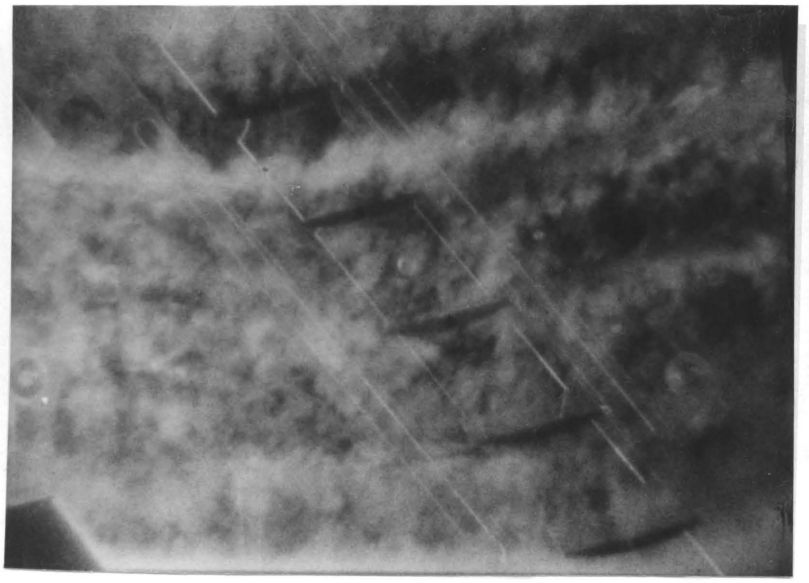

(b)

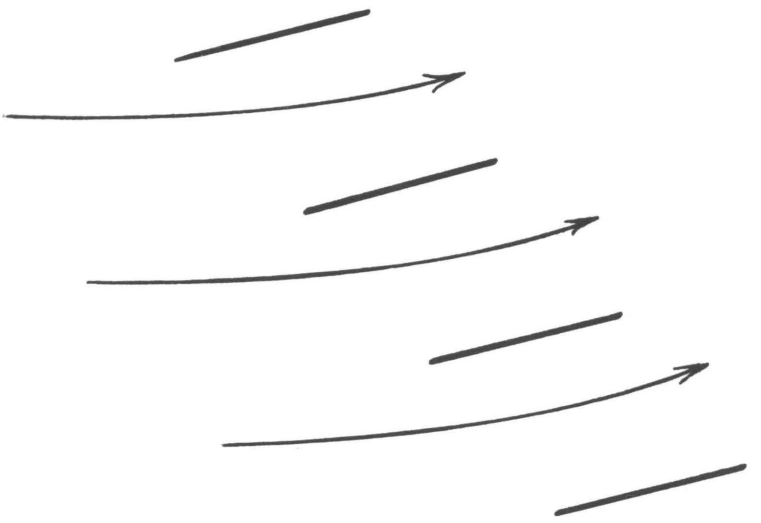

Fig. 13. Observed Flow; Stagger = 25, Angle of Attack = 15
(a) Picture 5, time = 20.00 ms.
(b) Diagram of Picture 5

(a)

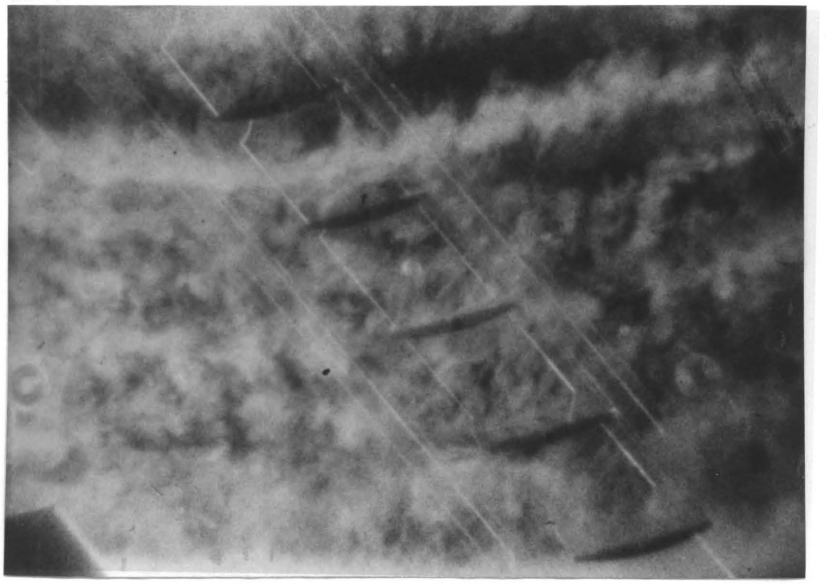

(b)

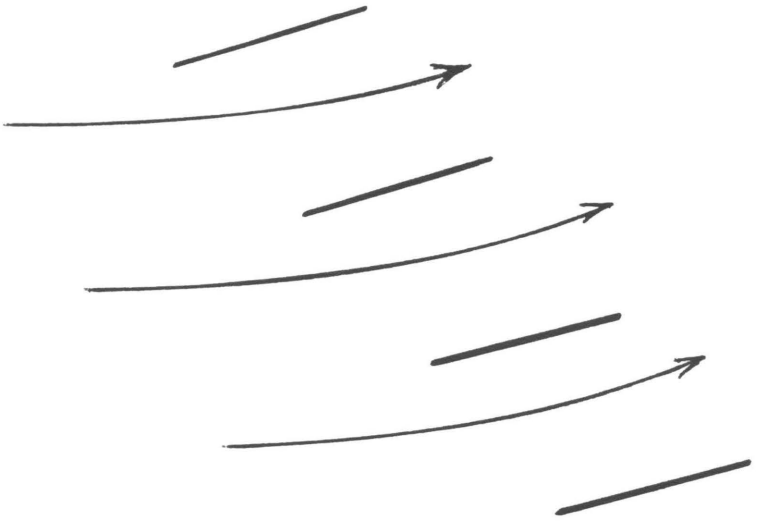

Fig. 14. Observed Flow; Stagger = 25, Angle of Attack = 15
(a) Picture 6, time = 25.00 ms.
(b) Diagram of Picture 6

(a)

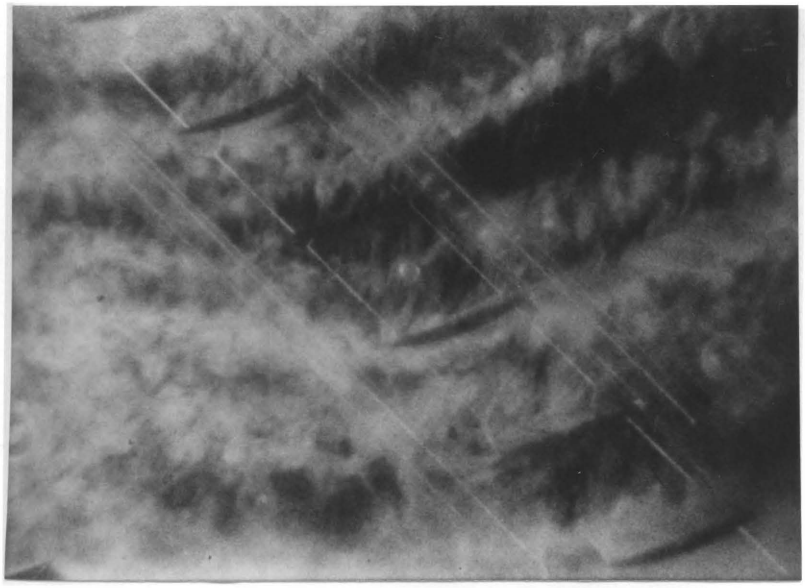

(b)

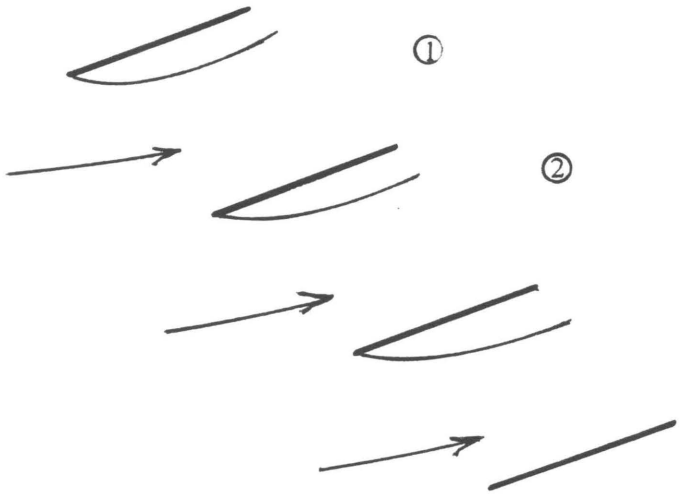

Fig. 15. Observed Flow; Stagger = 25, Angle of Attack = 20
(a) Picture 1, time = 0.00 ms., ref.
(b) Diagram of Picture 1

(a)

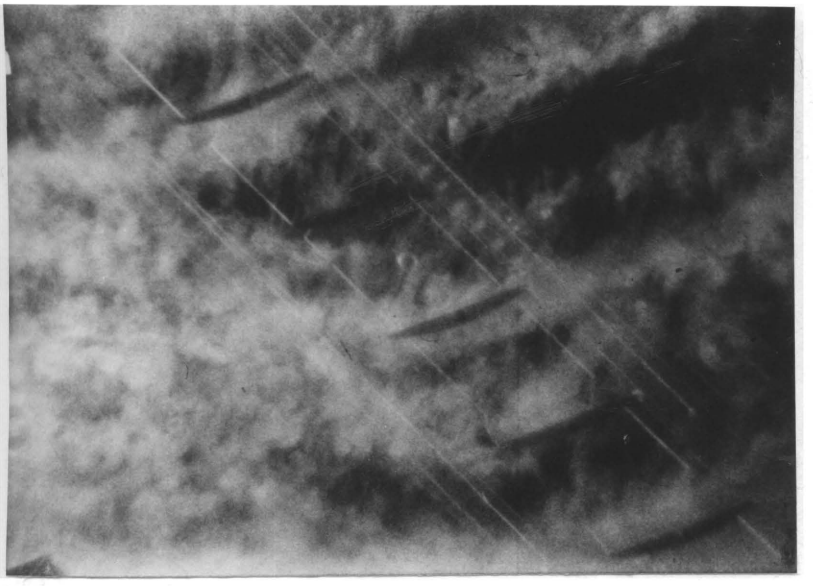

(b)

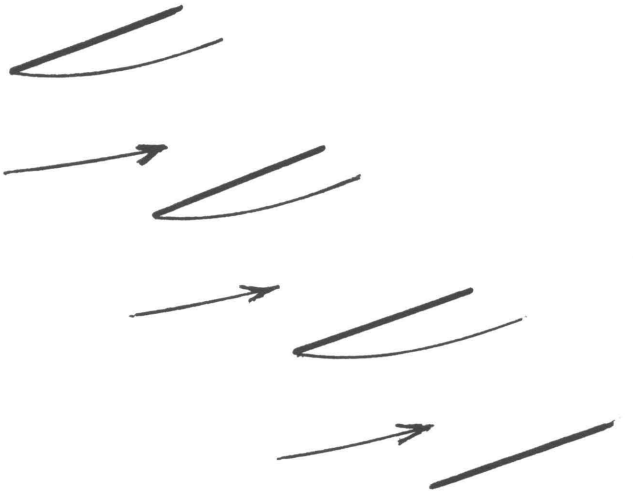

Fig. 16. Observed Flow; Stagger = 25, Angle of Attack = 20
(a) Picture 2, time = 5.00 ms.
(b) Diagram of Picture 2

(a)

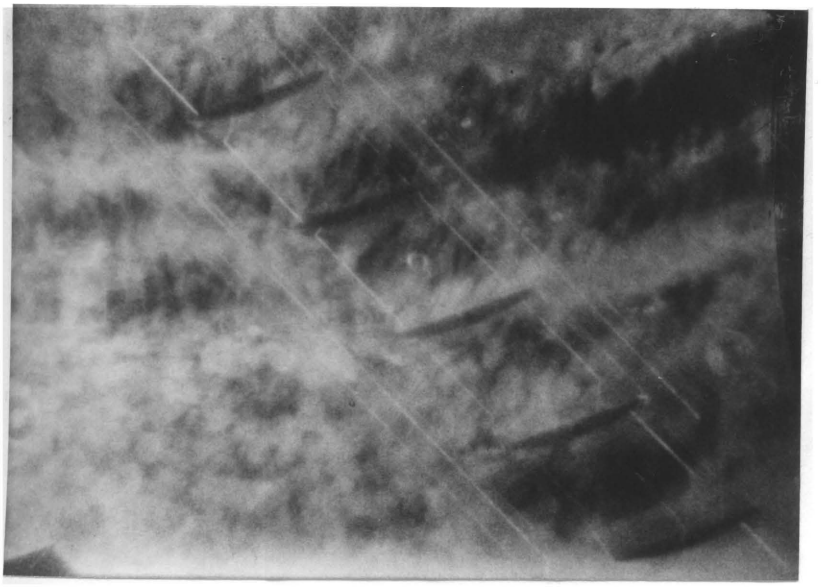

(b)

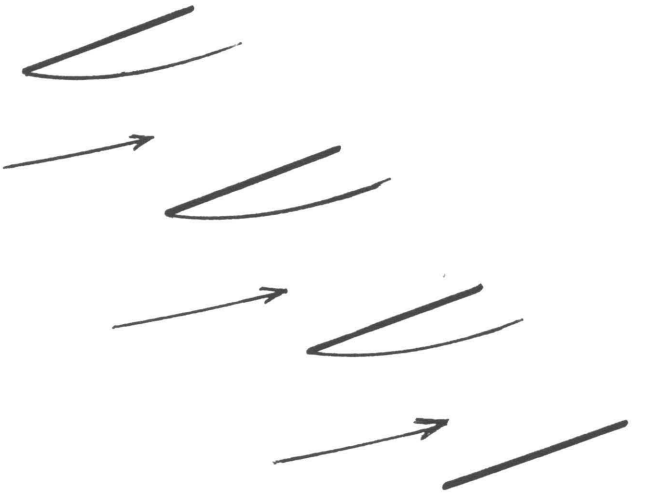

Fig. 17. Observed Flow; Stagger = 25, Angle of Attack = 20
(a) Picture 3, time = 10.00 ms.
(b) Diagram of Picture 3

(a)

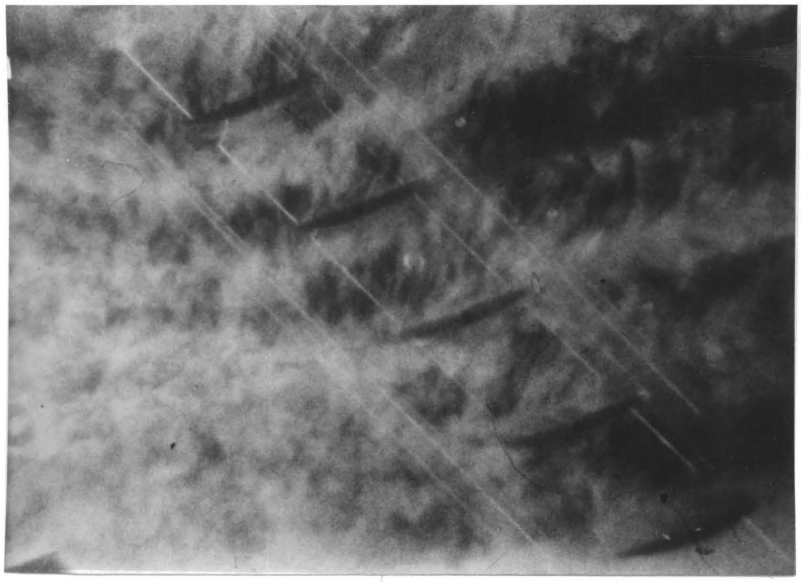

(b)

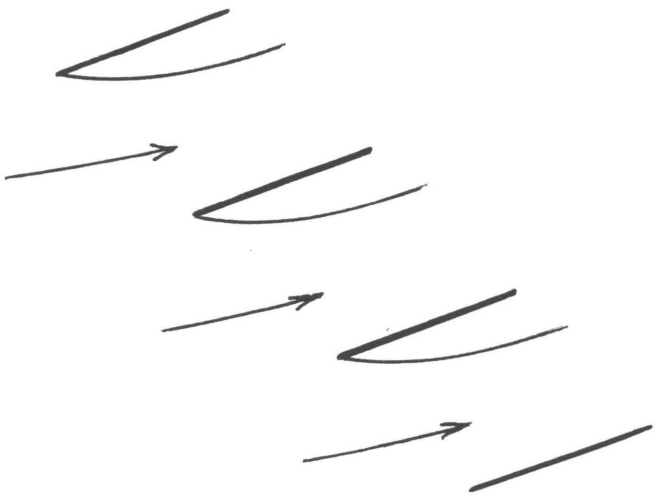

Fig. 18. Observed Flow; Stagger = 25, Angle of Attack = 20
(a) Picture 4, time = 15.00 ms.
(b) Diagram of Picture 4

(a)

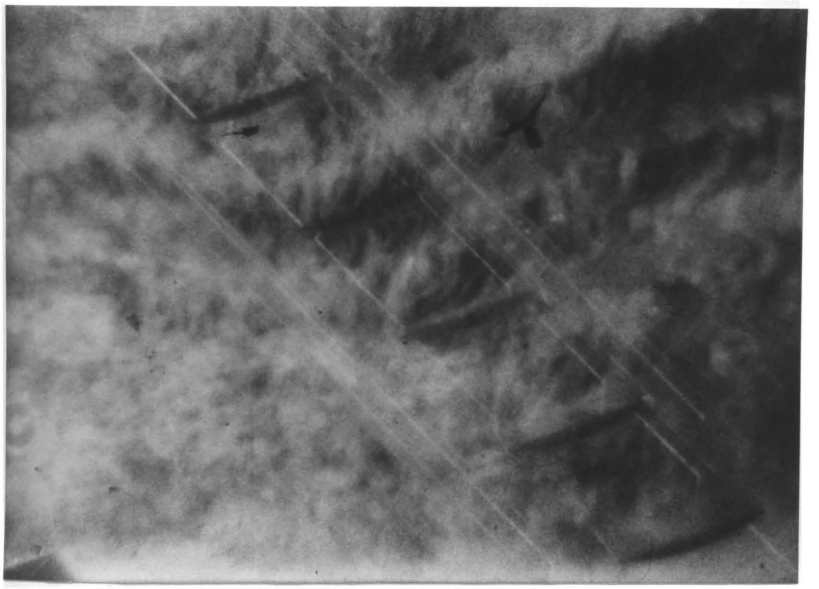

(b)

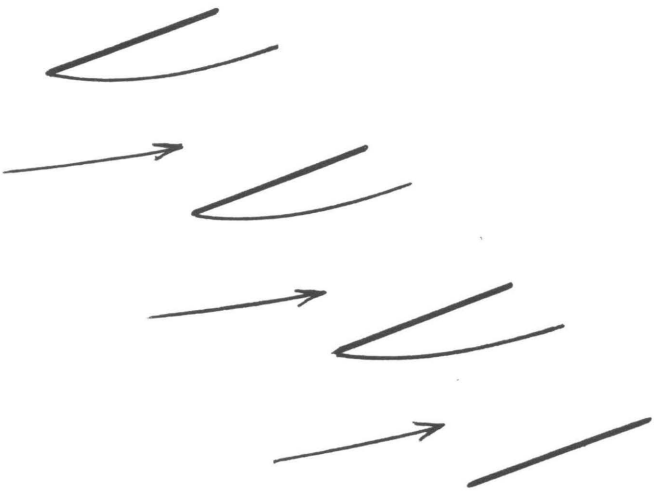

Fig. 19. Observed Flow; Stagger = 25, Angle of Attack = 20
(a) Picture 5, time = 20.00 ms.
(b) Diagram of Picture 5

(a)

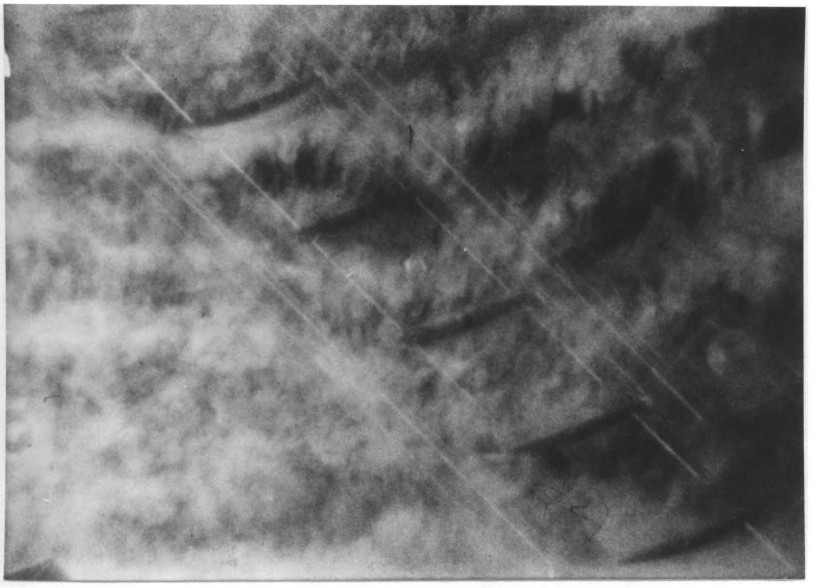

(b)

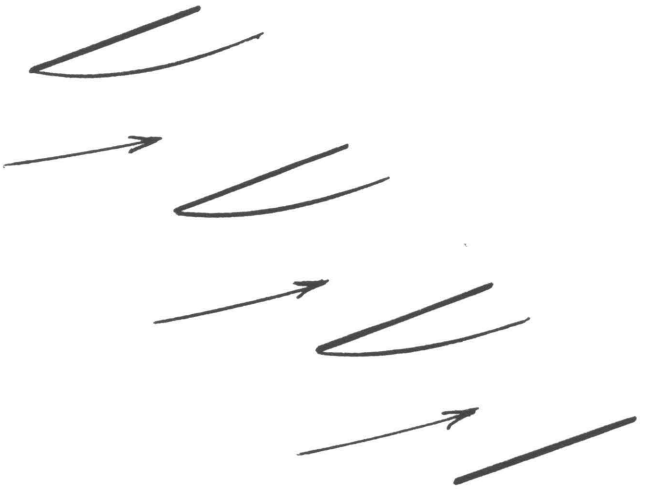

Fig. 20. Observed Flow; Stagger = 25, Angle of Attack = 20
(a) Picture 6, time = 25.00 ms.
(b) Diagram of Picture 6

(a)

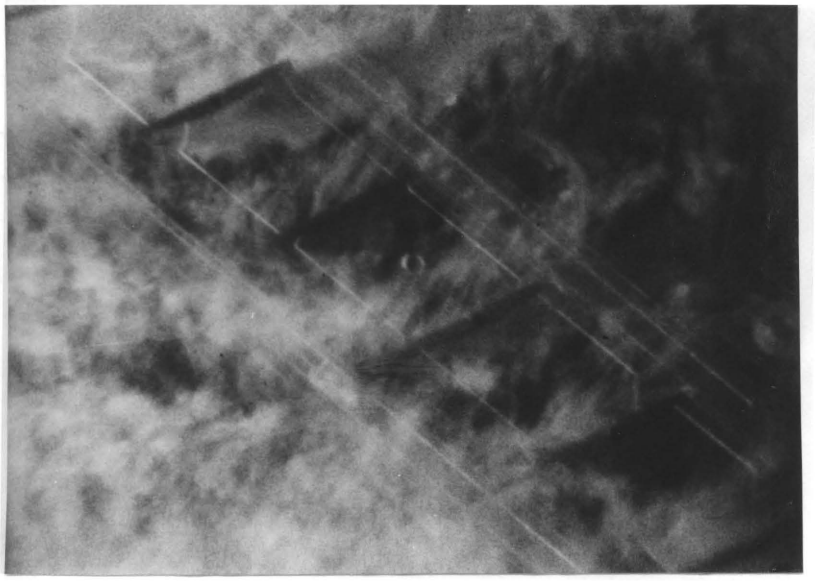

(b)

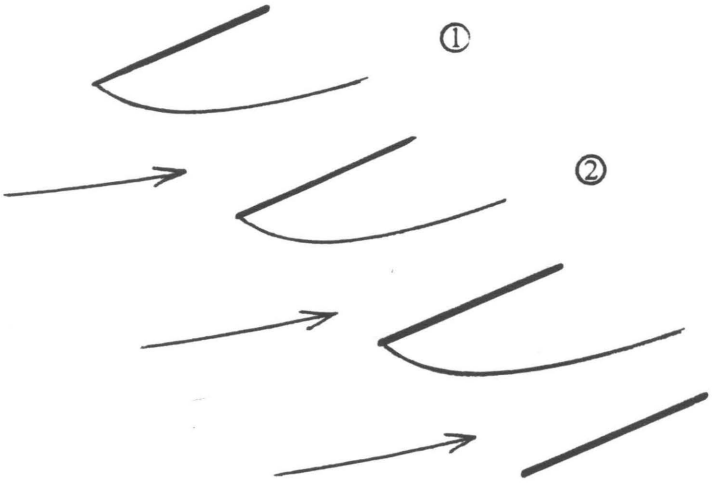

Fig. 21. Observed Flow; Stagger = 25, Angle of Attack = 25
(a) Picture 1, time = 0.00 ms., ref.
(b) Diagram of Picture 1

(a)

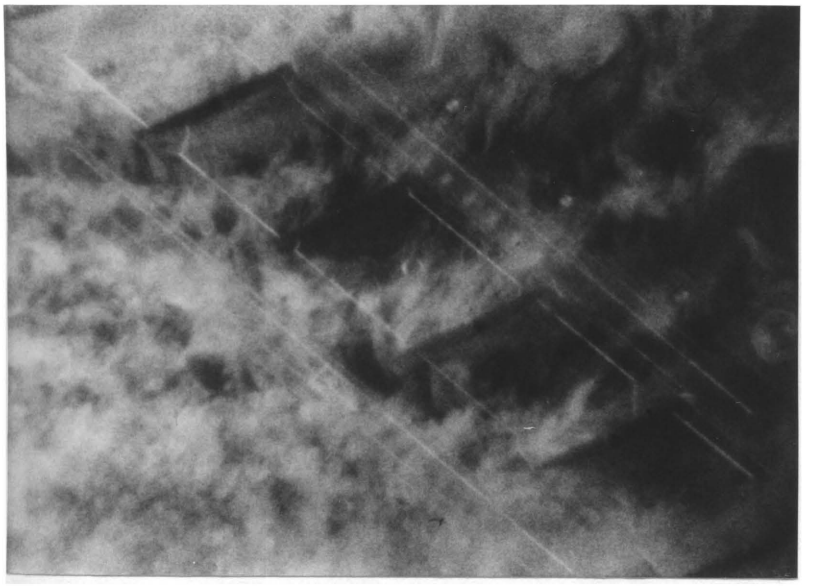

(b)

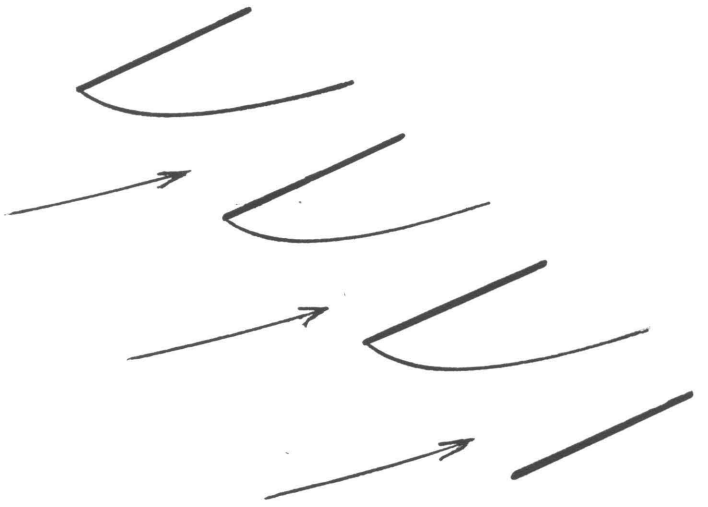

Fig. 22. Observed Flow; Stagger = 25, Angle of Attack = 25
(a) Picture 2, time = 5.00 ms.
(b) Diagram of Picture 2

(a)

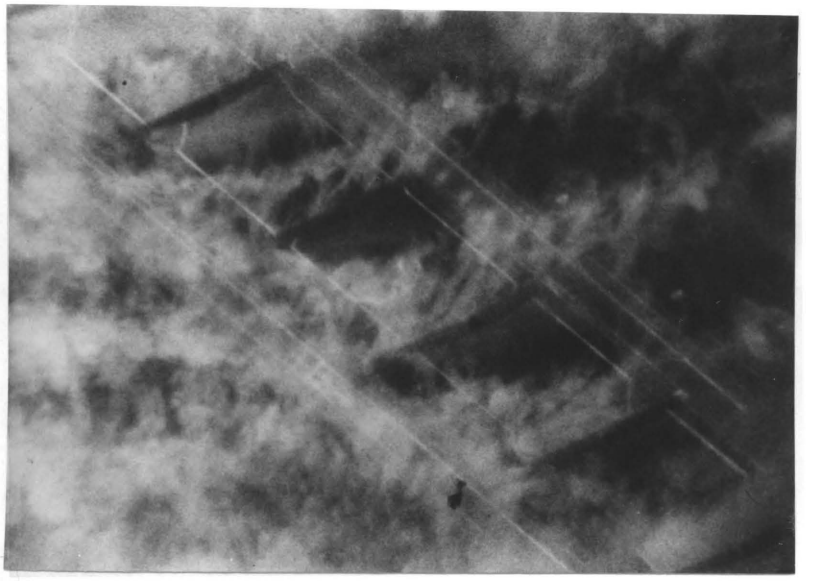

(b)

Fig. 23. Observed Flow; Stagger = 25, Angle of Attack = 25
(a) Picture 3, time = 10.00 ms.
(b) Diagram of Picture 3

(a)

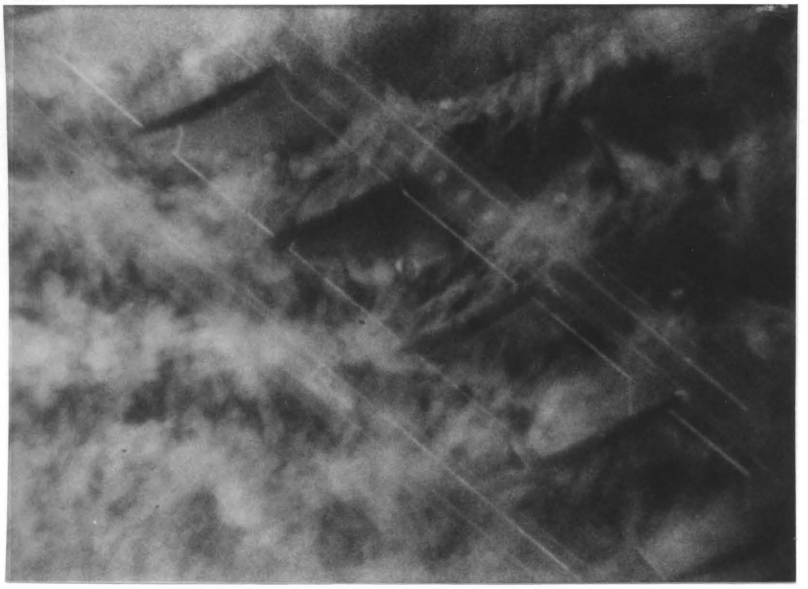

(b)

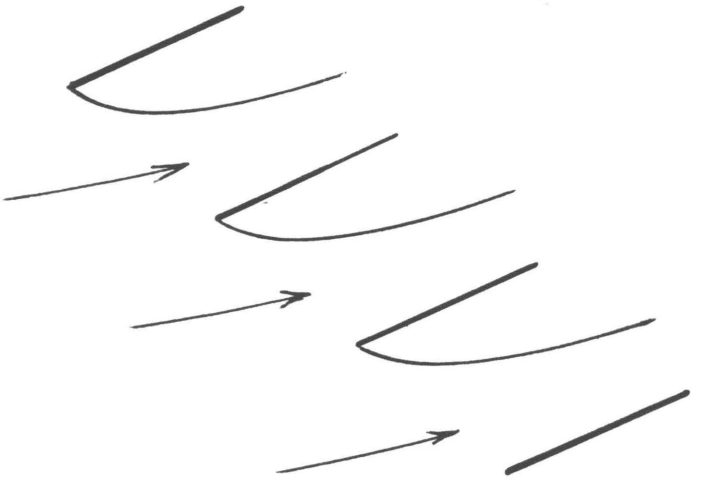

Fig. 24. Observed Flow; Stagger = 25, Angle of Attack = 25
(a) Picture 4, time = 15.00 ms.
(b) Diagram of Picture 4

(a)

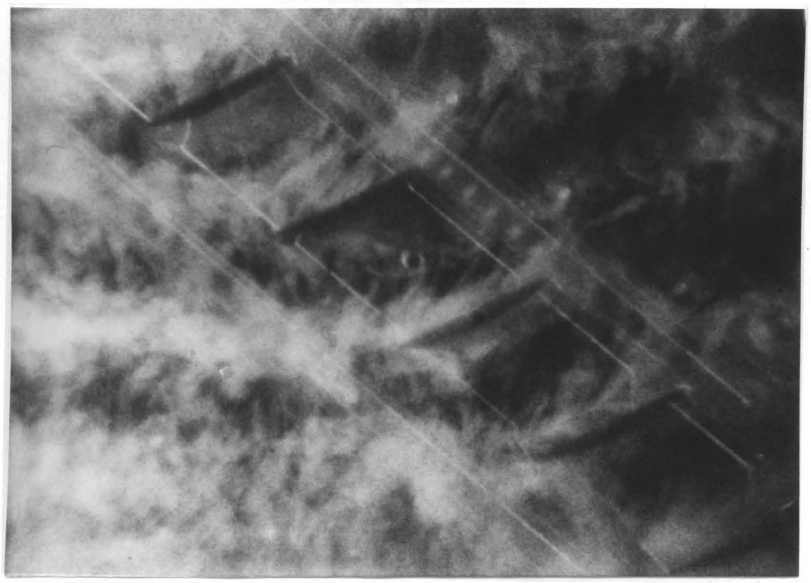

(b)

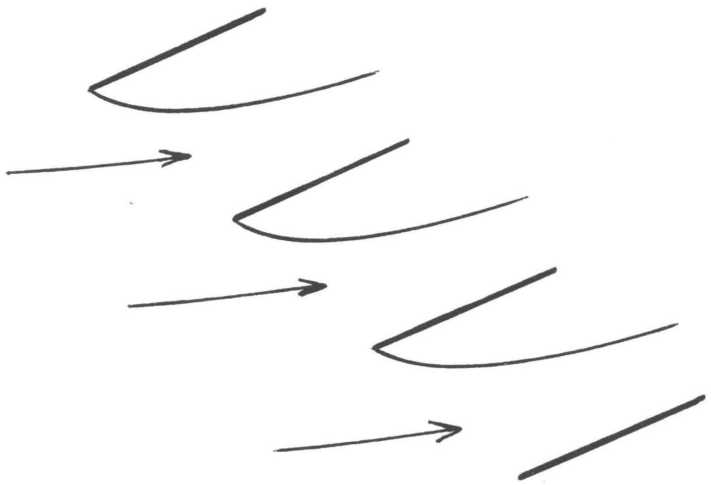

Fig. 25. Observed Flow; Stagger = 25, Angle of Attack = 25
(a) Picture 5, time = 20.00 ms.
(b) Diagram of Picture 5

(a)

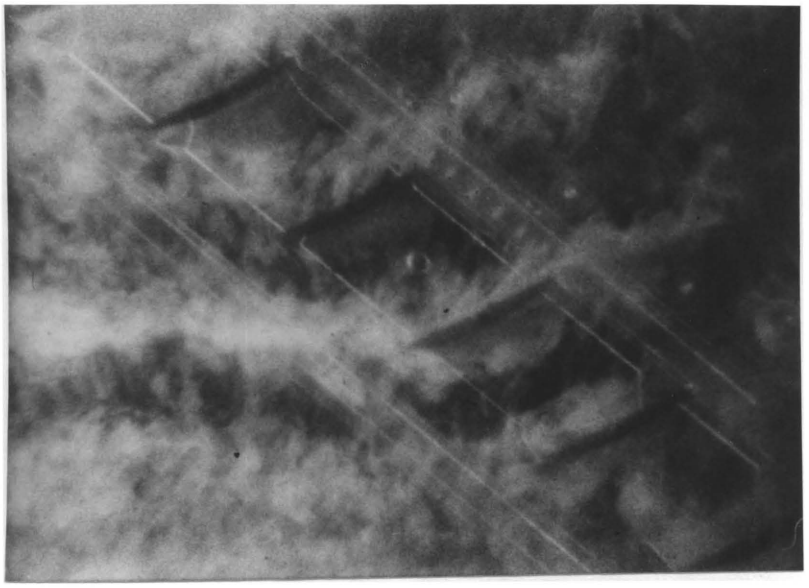

(b)

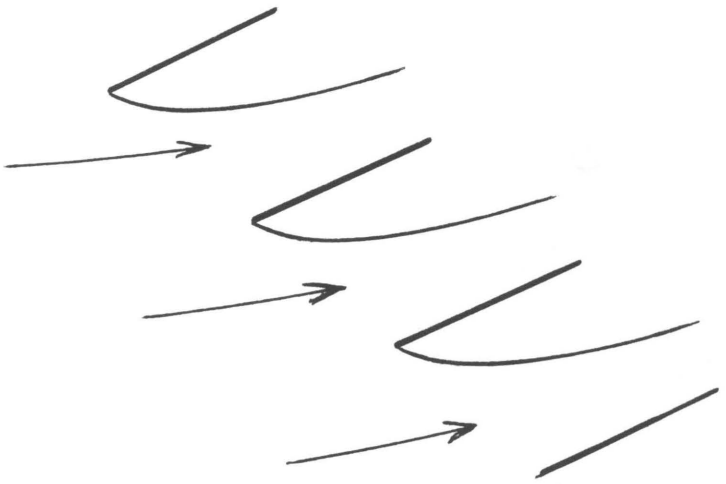

Fig. 26. Observed Flow; Stagger = 25, Angle of Attack = 25
(a) Picture 6, time = 25.00 ms.
(b) Diagram of Picture 6

(a)

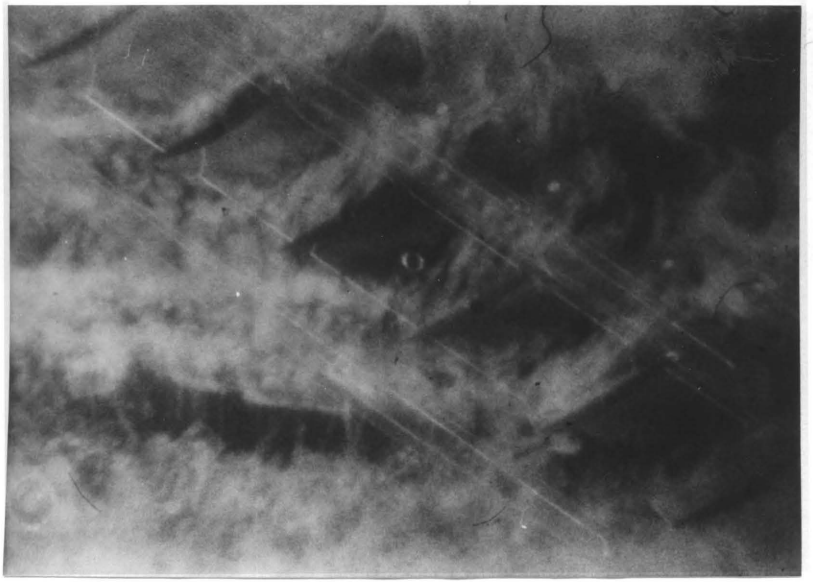

(b)

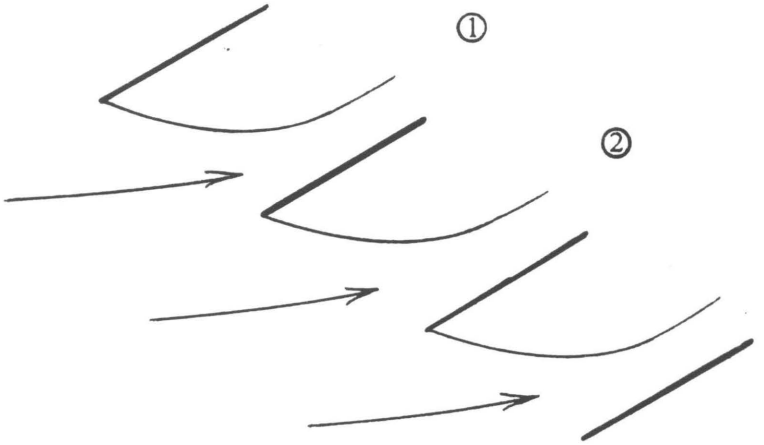

Fig. 27. Observed Flow; Stagger = 25, Angle of Attack = 30
(a) Picture 1, time = 0.00 ms., ref.
(b) Diagram of Picture 1

(a)

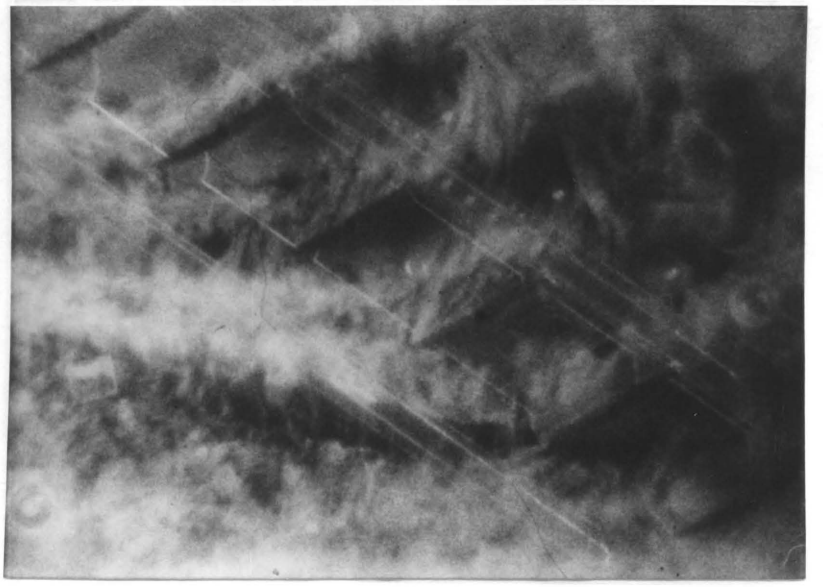

(b)

Fig. 28. Observed Flow; Stagger = 25, Angle of Attack = 30
(a) Picture 2, time = 5.00 ms.
(b) Diagram of Picture 2

(a)

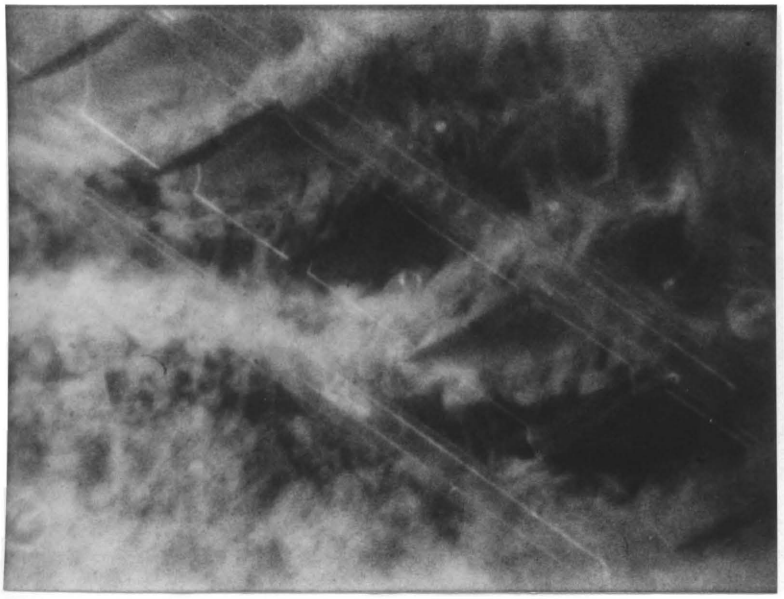

(b)

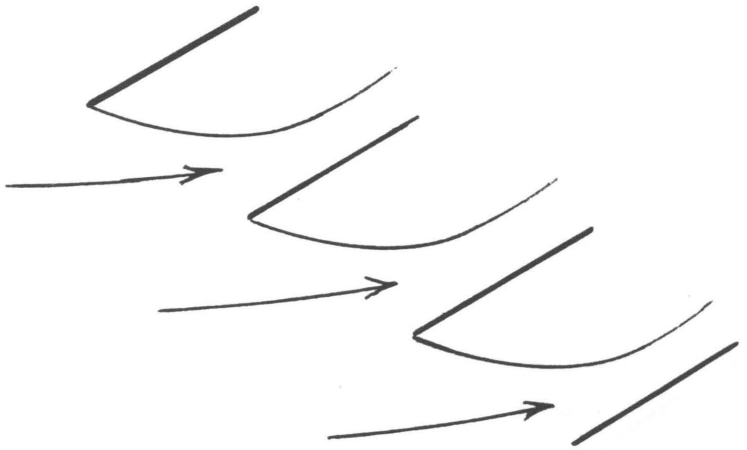

Fig. 29. Observed Flow; Stagger = 25, Angle of Attack = 30
(a) Picture 3, time = 10.00 ms.
(b) Diagram of Picture 3

(a)

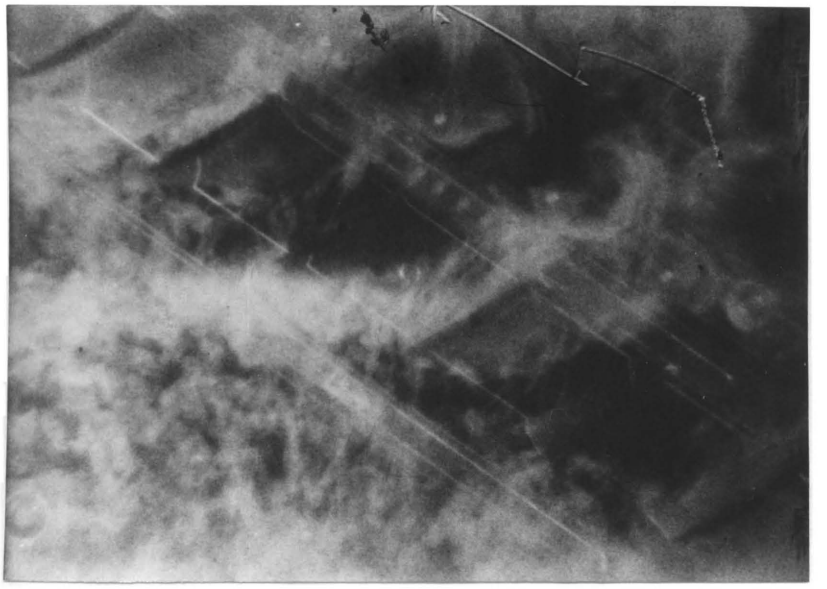

(b)

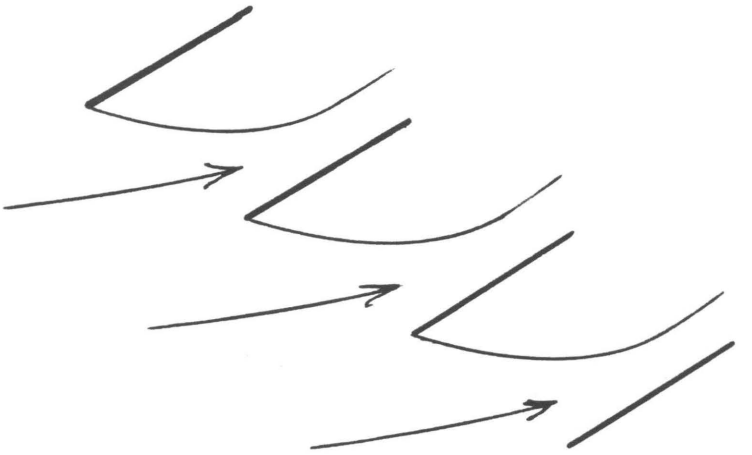

Fig. 30. Observed Flow; Stagger = 25, Angle of Attack = 30
(a) Picture 4, time = 15.00 ms.
(b) Diagram of Picture 4

(a)

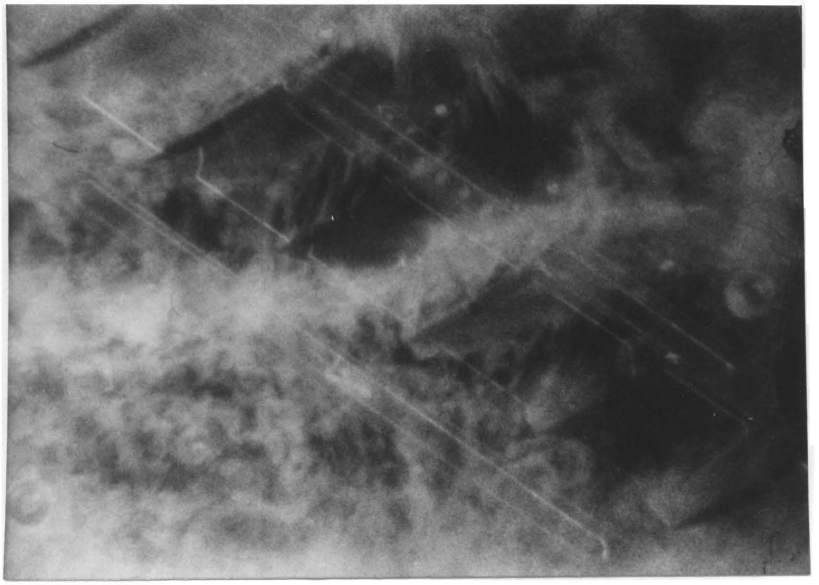

(b)

Fig. 31. Observed Flow; Stagger = 25, Angle of Attack = 30
(a) Picture 5, time = 20.00 ms.
(b) Diagram of Picture 5

(a)

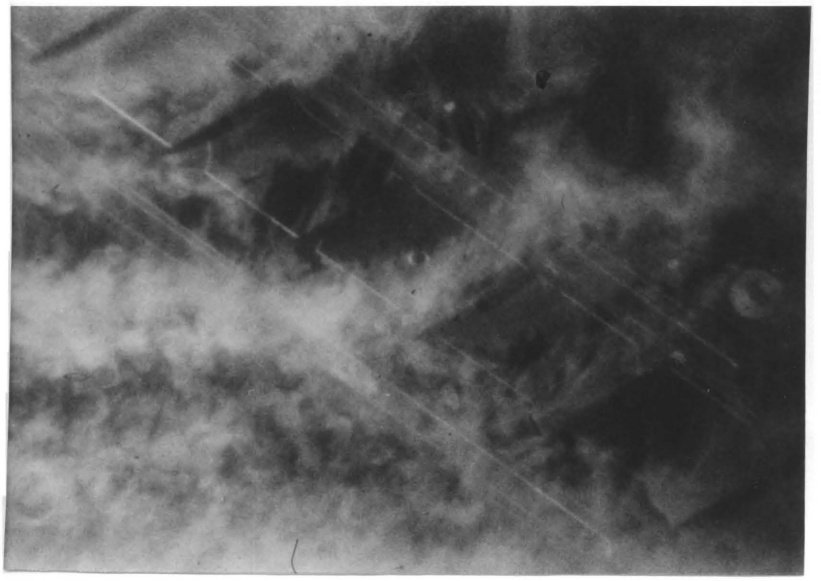

(b)

Fig. 32. Observed Flow; Stagger = 25, Angle of Attack = 30
(a) Picture 6, time = 25.00 ms.
(b) Diagram of Picture 6

(a)

(b)

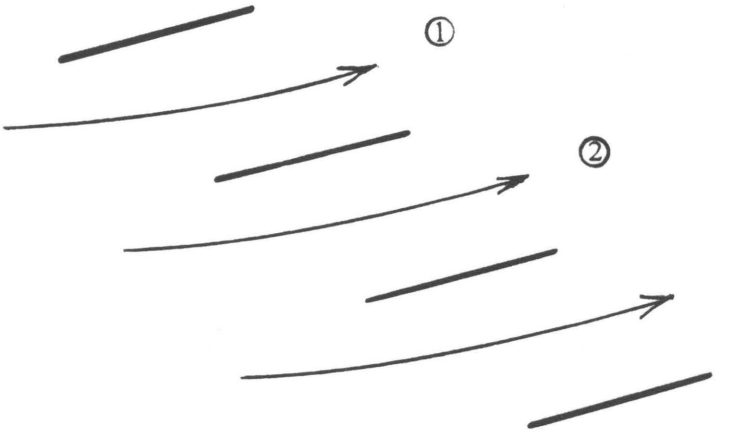

Fig. 33. Observed Flow; Stagger = 36.5, Angle of Attack = 15
(a) Picture 1, time = 0.00 ms., ref.
(b) Diagram of Picture 1

(a)

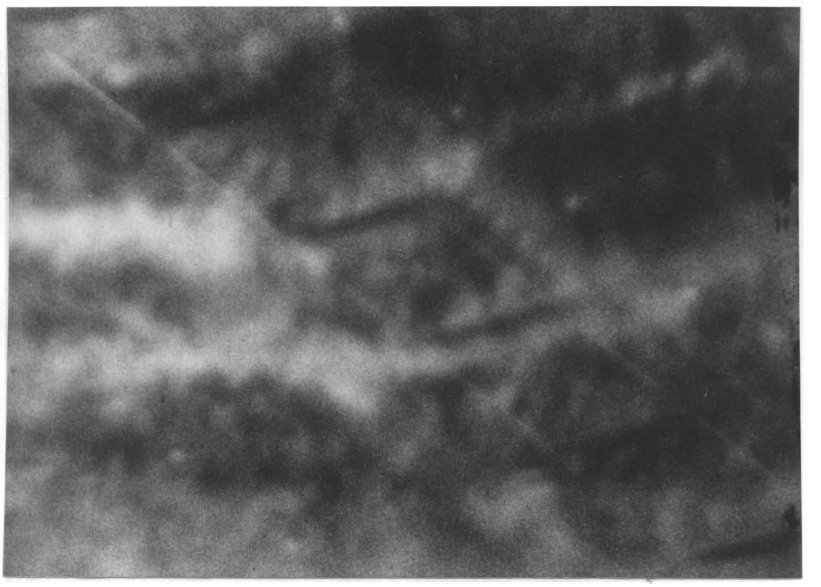

(b)

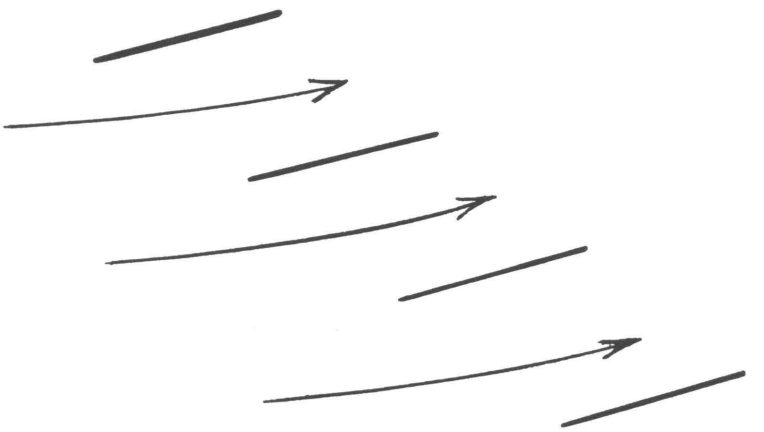

Fig. 34. Observed Flow; Stagger = 36.5, Angle of Attack = 15
(a) Picture 2, time = 5.00 ms.
(b) Diagram of Picture 2

(a)

(b)

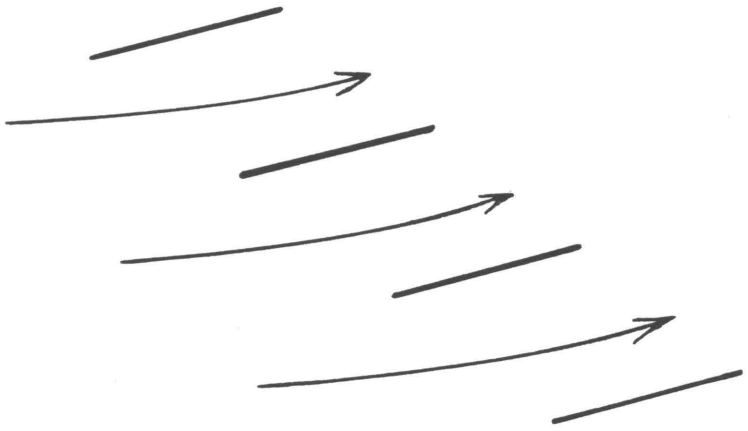

Fig. 35. Observed Flow; Stagger = 36.5, Angle of Attack = 15
(a) Picture 3, time = 10.00 ms.
(b) Diagram of Picture 3

(a)

(b)

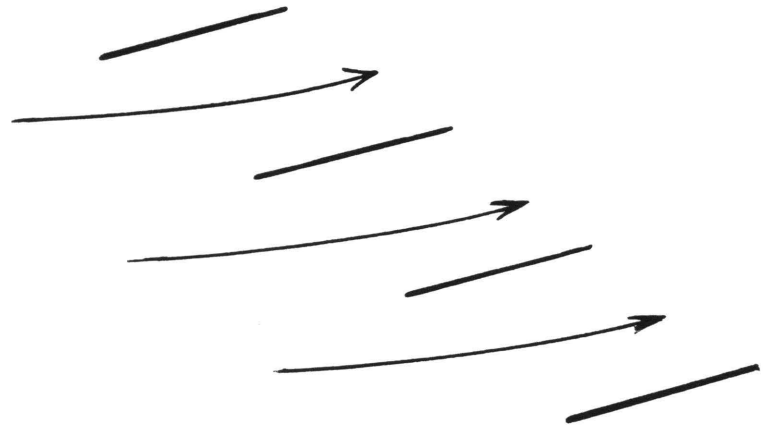

Fig. 36. Observed Flow; Stagger = 36.5, Angle of Attack = 15
(a) Picture 4, time = 15.00 ms.
(b) Diagram of Picture 4

(a)

(b)

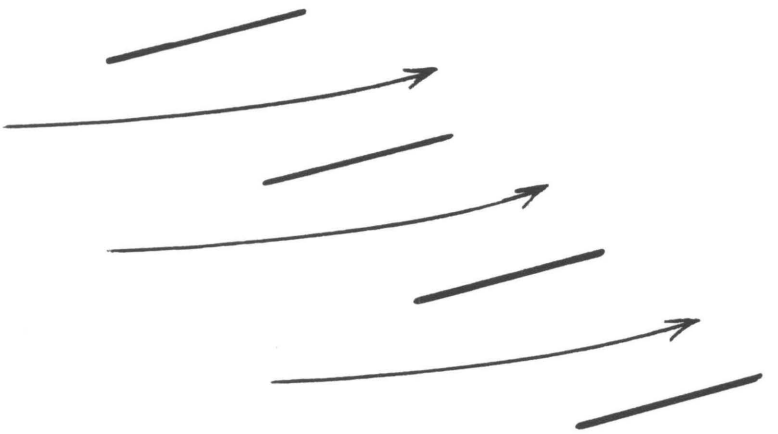

Fig. 37. Observed Flow; Stagger = 36.5, Angle of Attack = 15
(a) Picture 5, time = 20.00 ms.
(b) Diagram of Picture 5

(a)

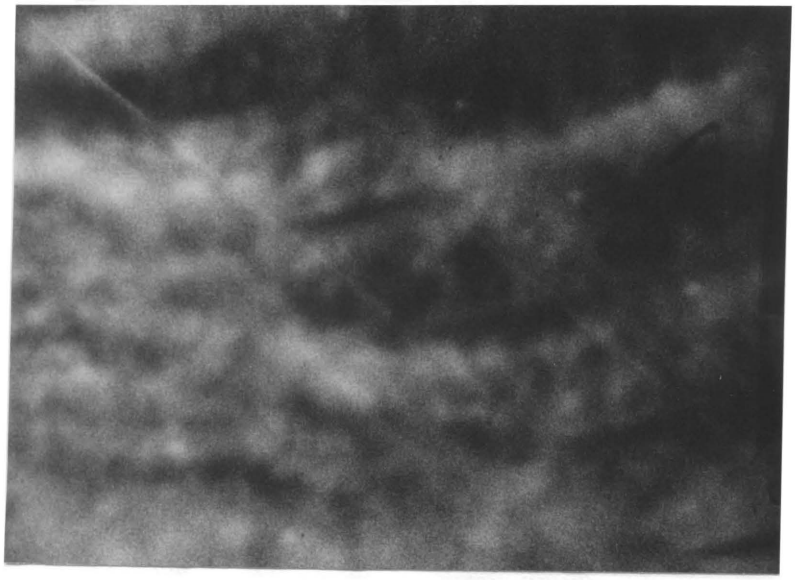

(b)

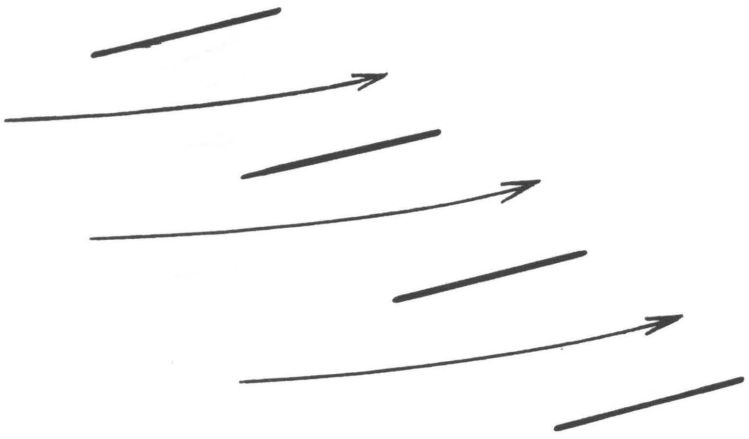

Fig. 38. Observed Flow; Stagger = 36.5, Angle of Attack = 15
(a) Picture 6, time = 25.00 ms.
(b) Diagram of Picture 6

(a)

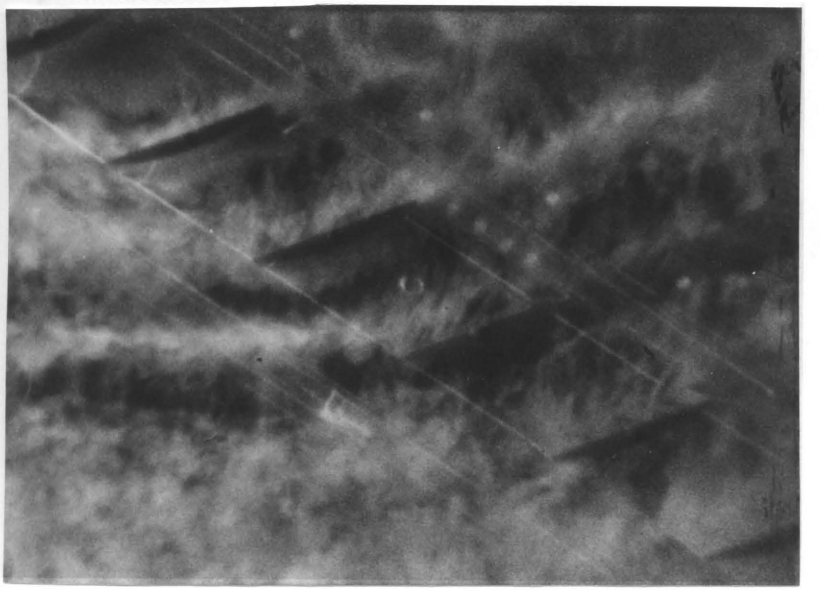

(b)

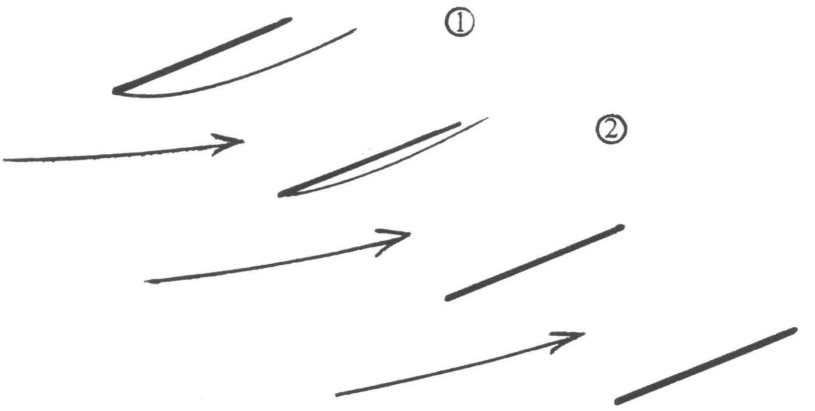

Fig. 39. Observed Flow; Stagger = 36.5, Angle of Attack = 20
(a) Picture 1, time = 0.00 ms., ref.
(b) Diagram of Picture 1

(a)

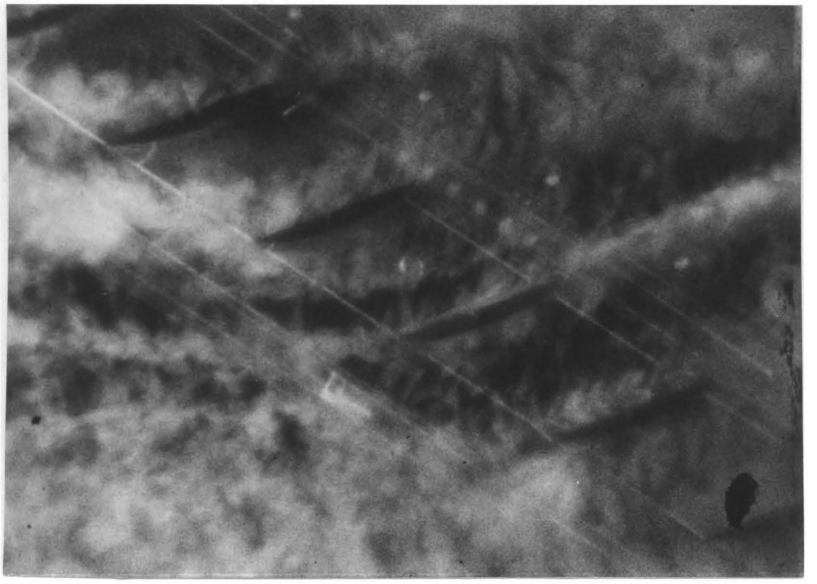

(b)

Fig. 40. Observed Flow; Stagger = 36.5, Angle of Attack = 20
(a) Picture 2, time = 14.25 ms.
(b) Diagram of Picture 2

(a)

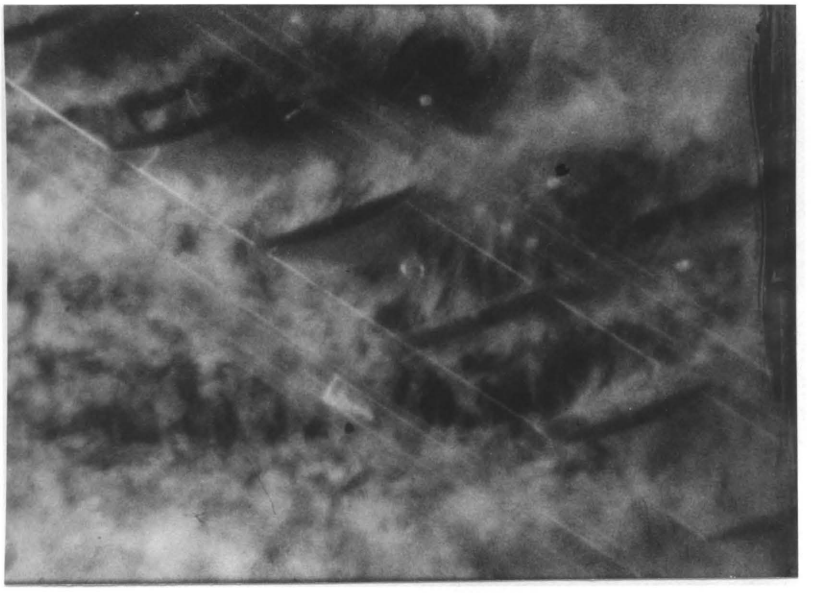

(b)

Fig. 41. Observed Flow; Stagger = 36.5, Angle of Attack = 20
(a) Picture 3, time = 26.75 ms.
(b) Diagram of Picture 3

(a)

(b)

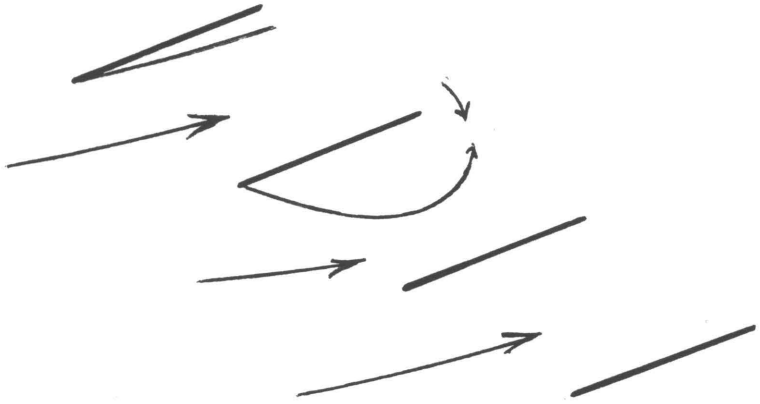

Fig. 42. Observed Flow; Stagger = 36.5, Angle of Attack = 20
(a) Picture 4, time = 36.50 ms.
(b) Diagram of Picture 4

(a)

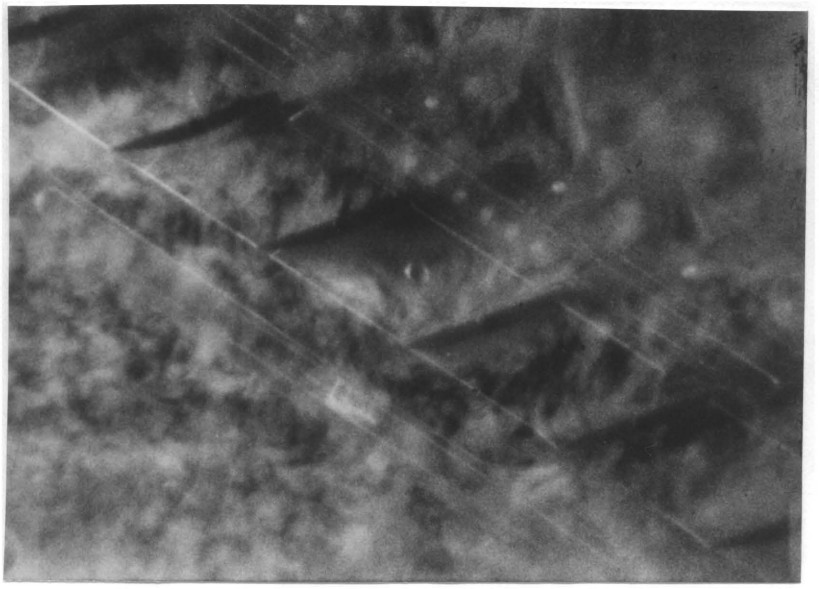

(b)

Fig. 43. Observed Flow; Stagger = 36.5, Angle of Attack = 20
(a) Picture 5, time = 45.50 ms.
(b) Diagram of Picture 5

(a)

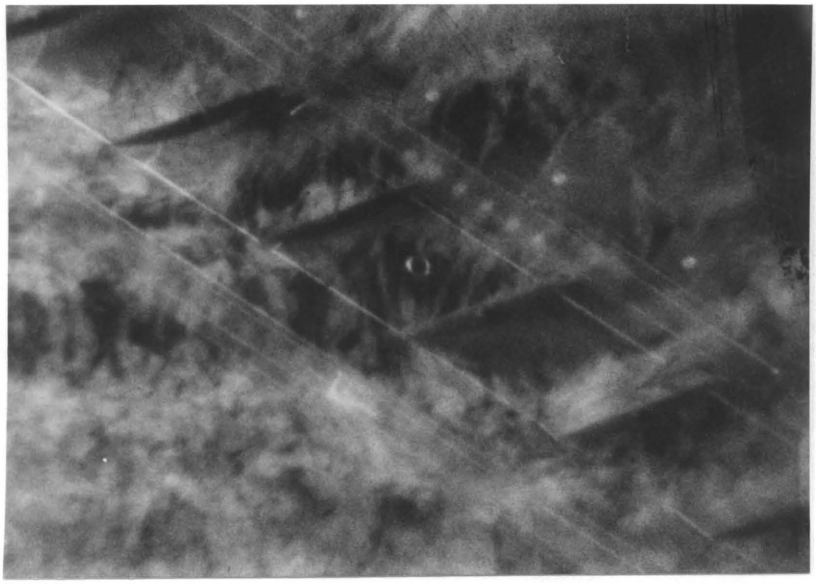

(b)

Fig. 44. Observed Flow; Stagger = 36.5, Angle of Attack = 20
(a) Picture 6, time = 65.75 ms.
(b) Diagram of Picture 6

(a)

(b)

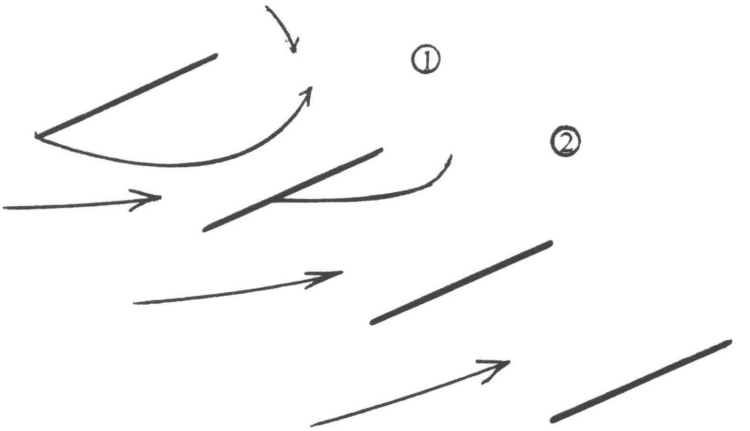

Fig. 45. Observed Flow; Stagger = 36.5, Angle of Attack = 25
(a) Picture 1, time = 0.00 ms., ref.
(b) Diagram of Picture 1

(a)

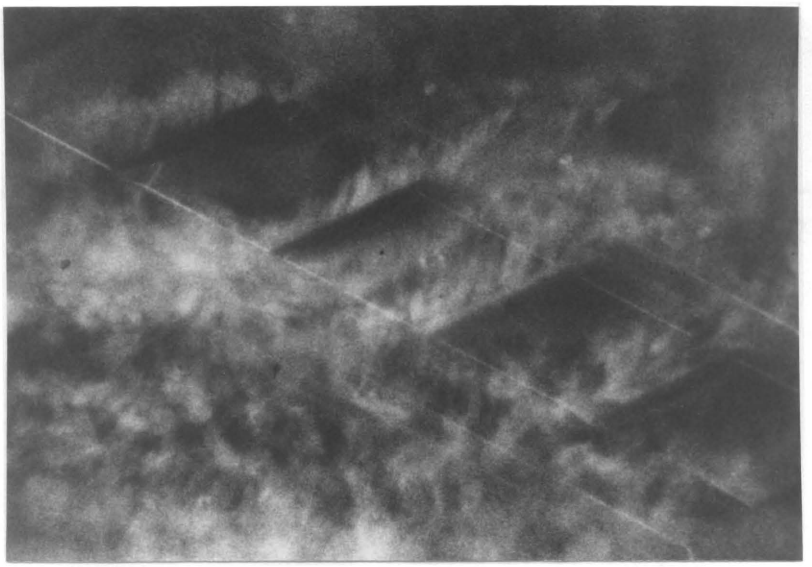

(b)

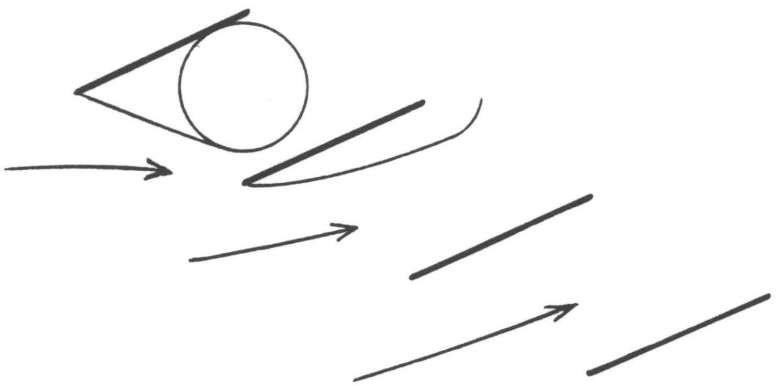

Fig. 46. Observed Flow; Stagger = 36.5, Angle of Attack = 25
(a) Picture 2, time = 10.75 ms.
(b) Diagram of Picture 2

(a)

(b)

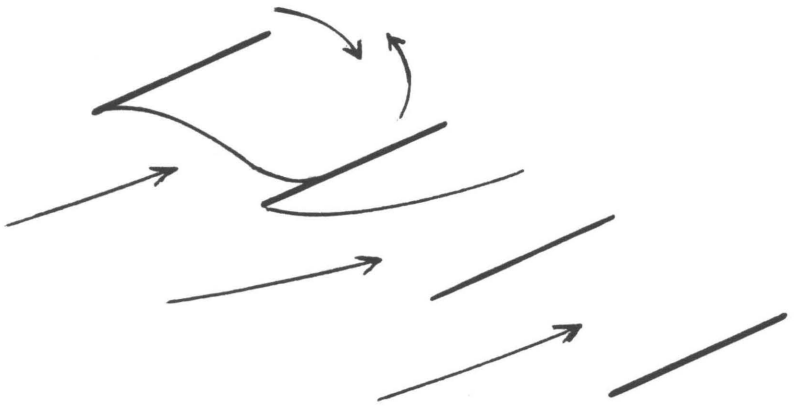

Fig. 47. Observed Flow; Stagger = 36.5, Angle of Attack = 25
(a) Picture 3, time = 14.75 ms.
(b) Diagram of Picture 3

(a)

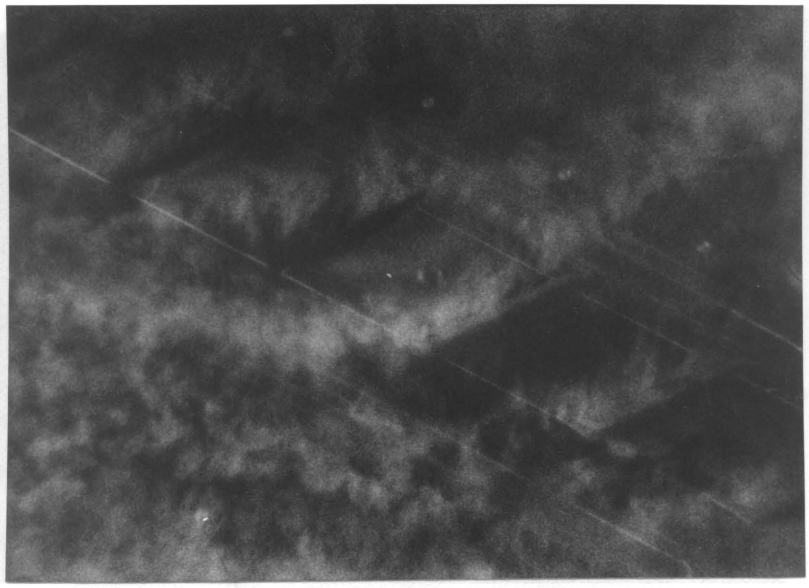

(b)

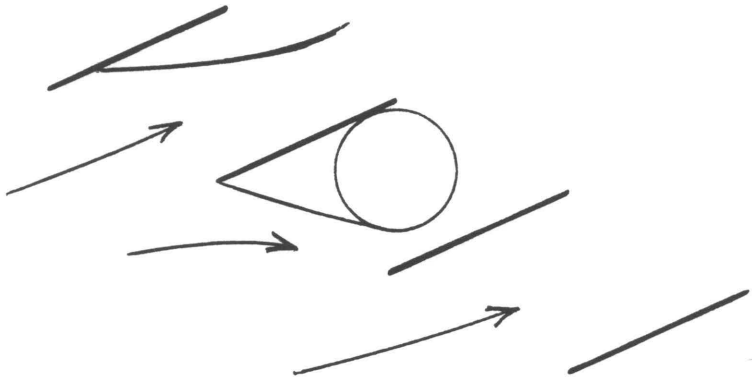

Fig. 48. Observed Flow; Stagger = 36.5, Angle of Attack = 25
(a) Picture 4, time = 23.50 ms.
(b) Diagram of Picture 4

(a)

(b)

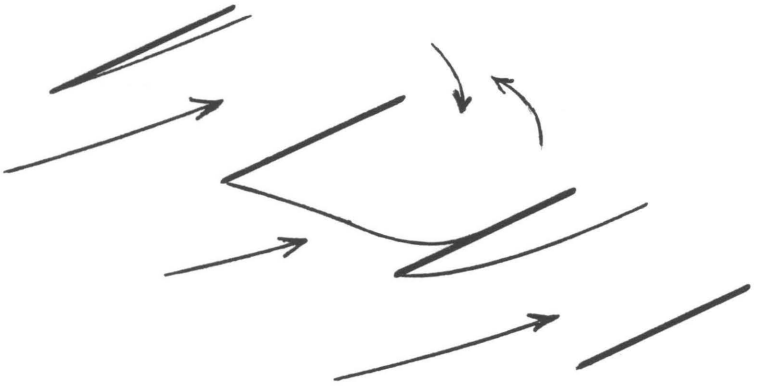

Fig. 49. Observed Flow; Stagger = 36.5, Angle of Attack = 25
(a) Picture 5, time = 28.25 ms.
(b) Diagram of Picture 5

(a)

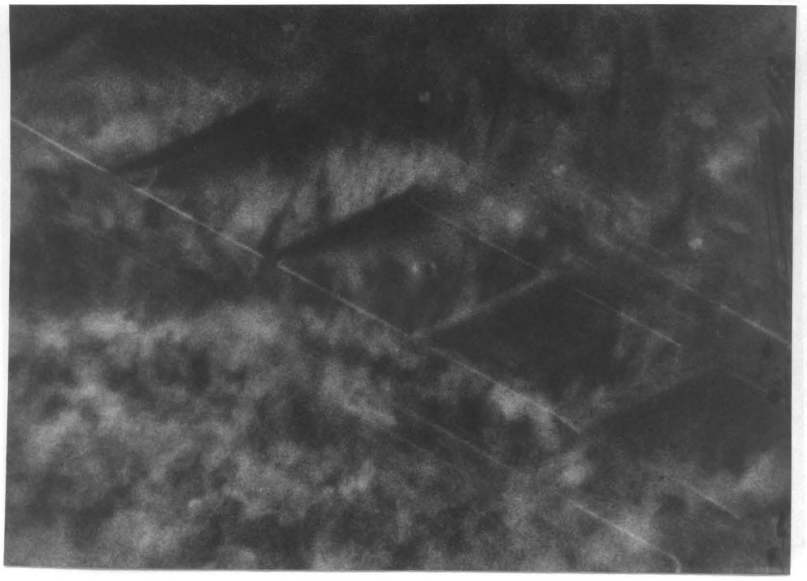

(b)

Fig. 50. Observed Flow; Stagger = 36.5, Angle of Attack = 25
(a) Picture 6, time = 43.25 ms.
(b) Diagram of Picture 6

(a)

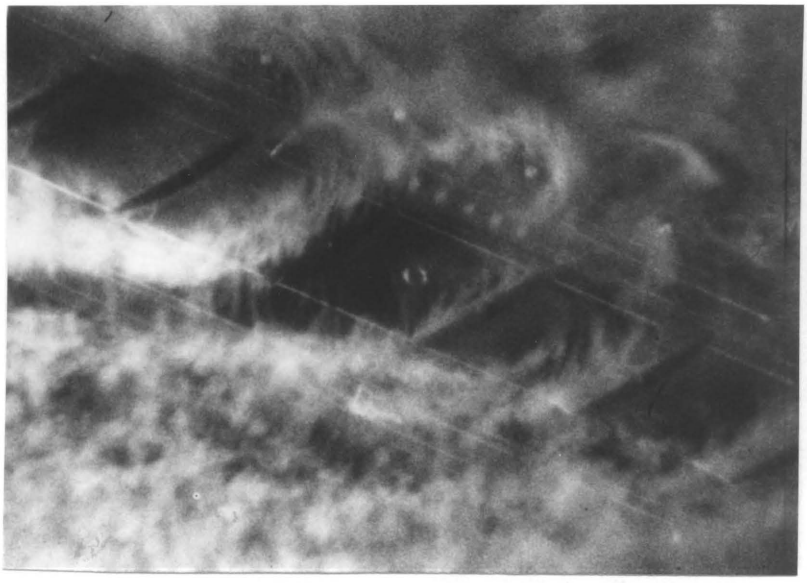

(b)

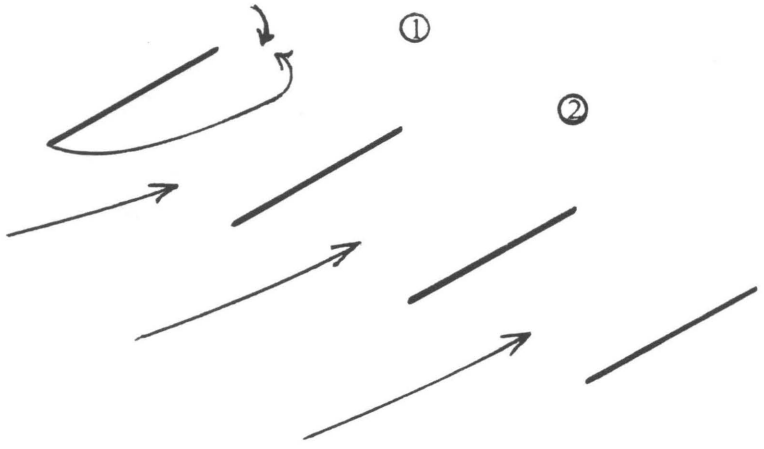

Fig. 51. Observed Flow; Stagger = 36.5, Angle of Attack = 30
(a) Picture 1, time = 0.00 ms., ref.
(b) Diagram of Picture 1

(a)

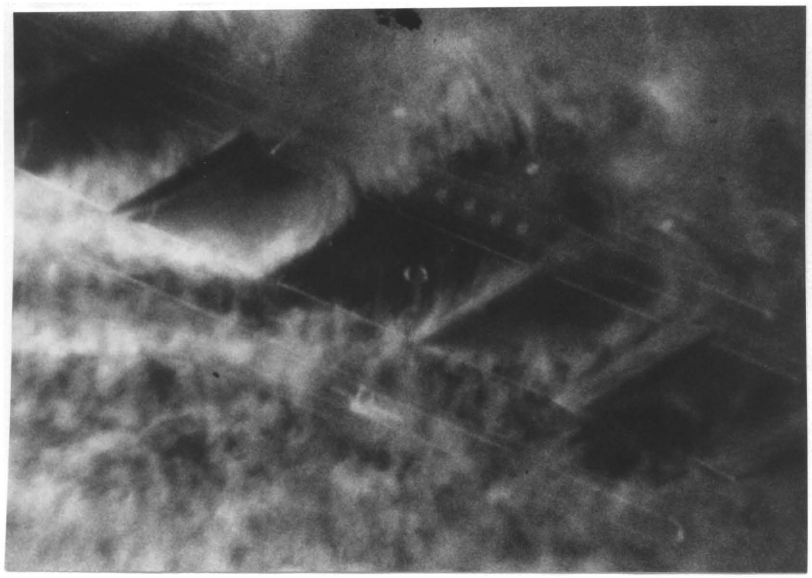

(b)

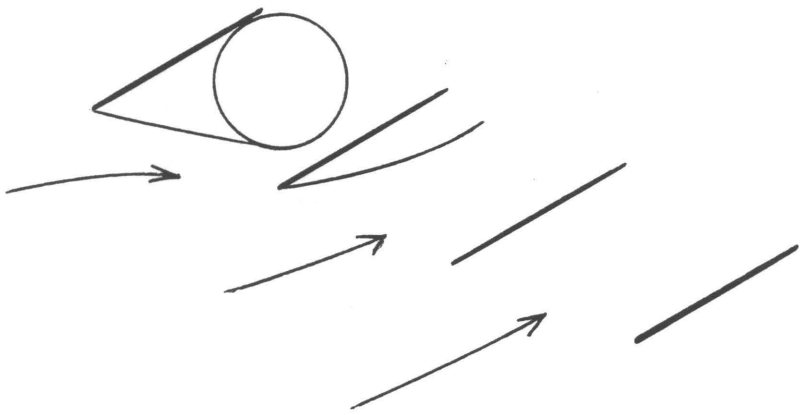

Fig. 52. Observed Flow; Stagger = 36.5, Angle of Attack = 30
(a) Picture 2, time = 6.75 ms.
(b) Diagram of Picture 2

(a)

(b)

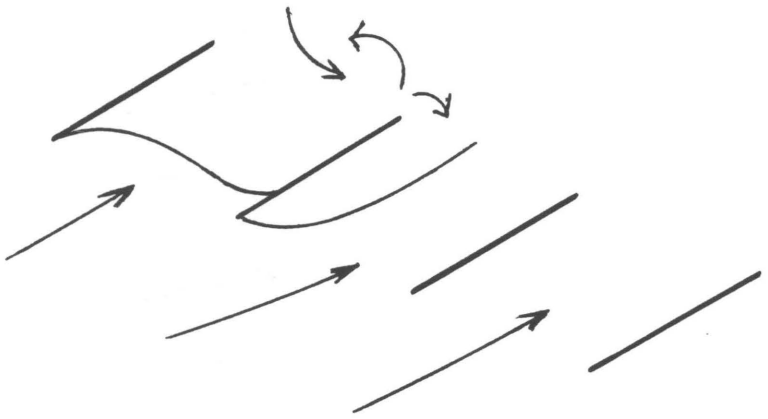

Fig. 53. Observed Flow; Stagger = 36.5, Angle of Attack = 30
(a) Picture 3, time = 13.00 ms.
(b) Diagram of Picture 3

(a)

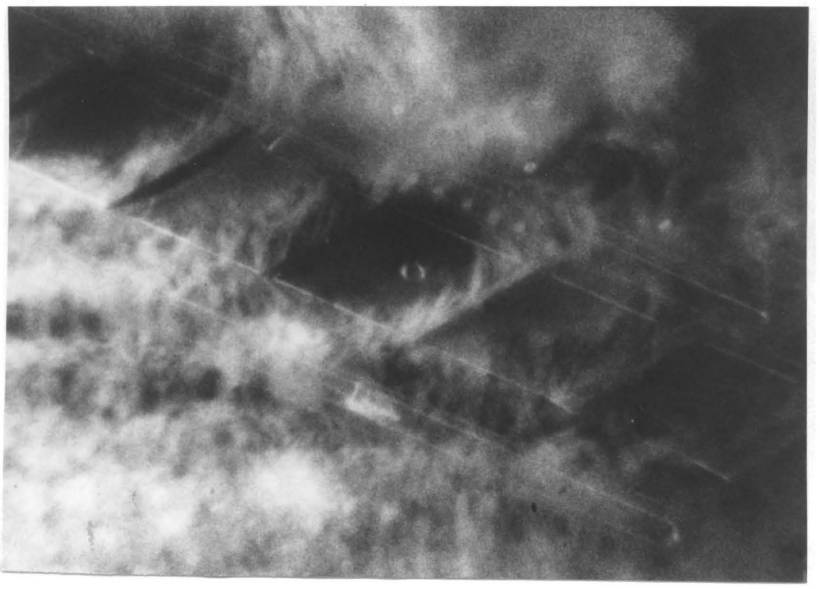

(b)

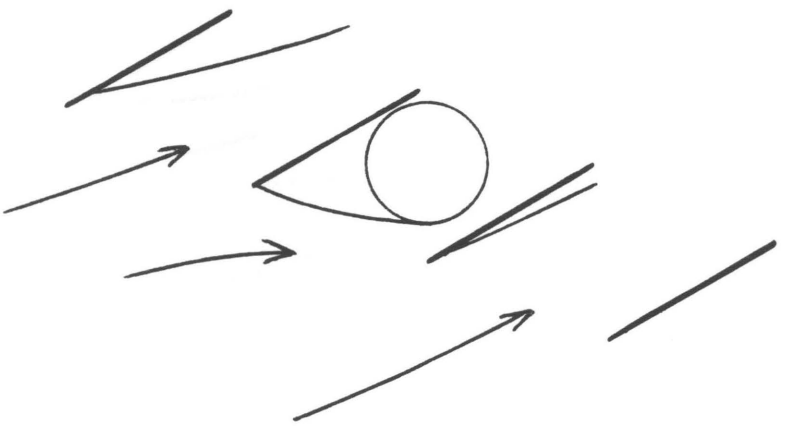

Fig. 54. Observed Flow; Stagger = 36.5, Angle of Attack = 30
(a) Picture 4, time = 21.50 ms.
(b) Diagram of Picture 4

(a)

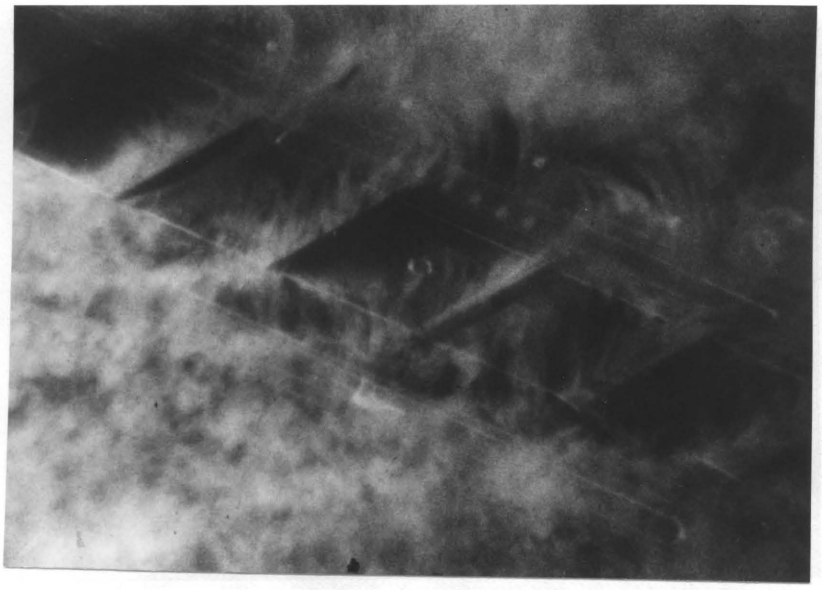

(b)

Fig. 55. Observed Flow; Stagger = 36.5, Angle of Attack = 30
(a) Picture 5, time = 27.50 ms.
(b) Diagram of Picture 5

(a)

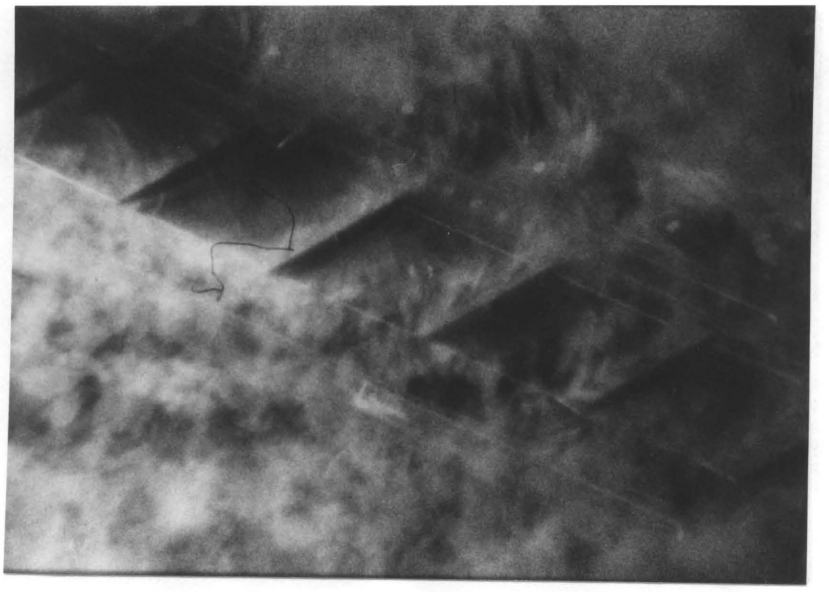

(b)

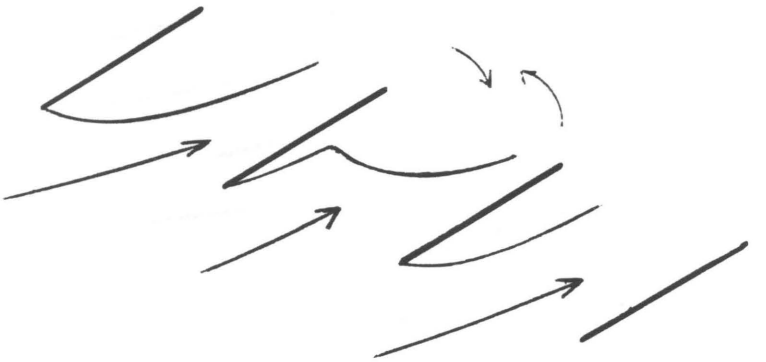

Fig. 56. Observed Flow; Stagger = 36.5, Angle of Attack = 30
(a) Picture 6, time = 42.75 ms.
(b) Diagram of Picture 6

(a)

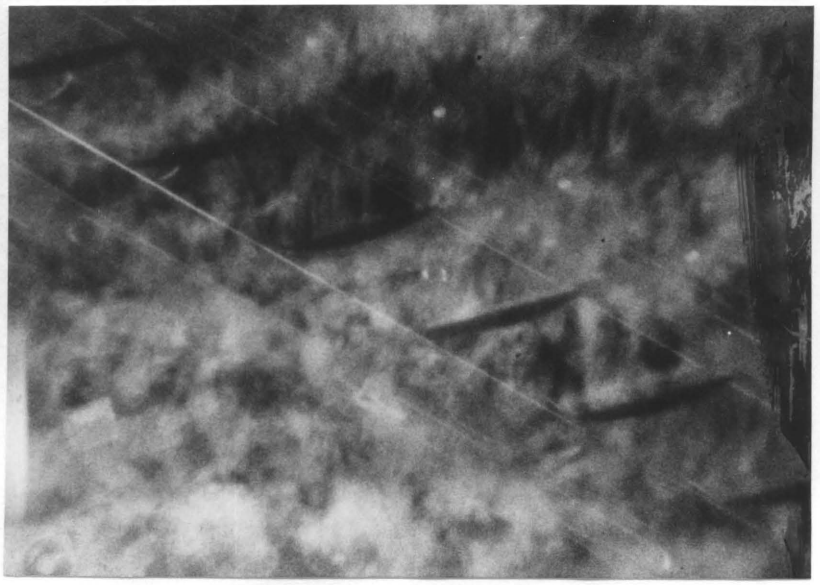

(b)

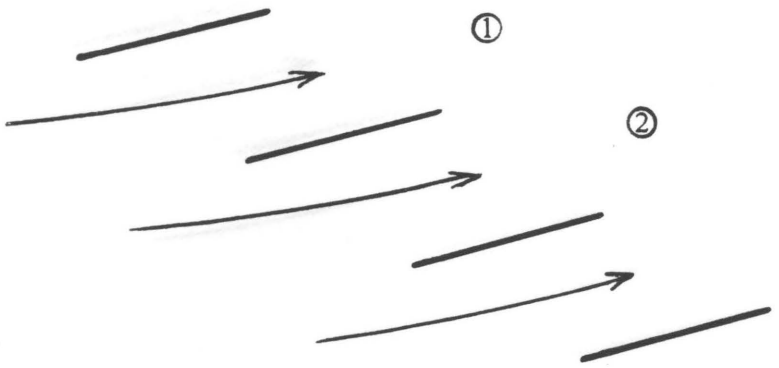

Fig. 57. Observed Flow; Stagger = 45, Angle of Attack = 15
(a) Picture 1, time = 0.00 ms., ref.
(b) Diagram of Picture 1

(a)

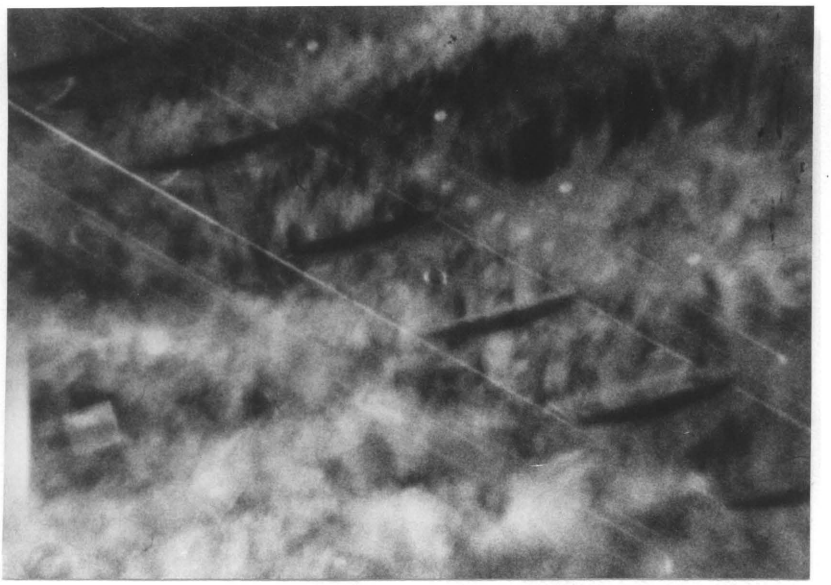

(b)

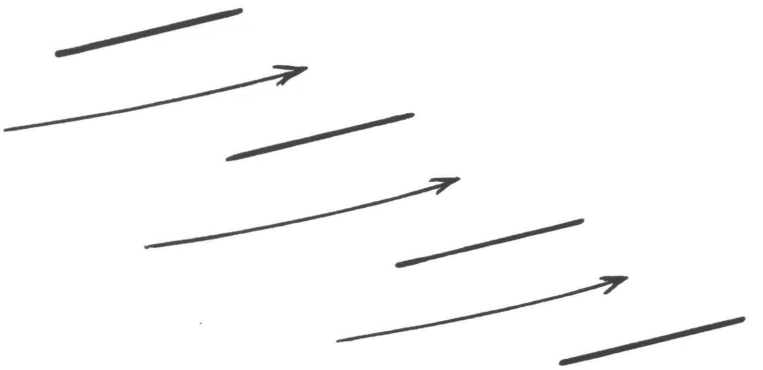

Fig. 58. Observed Flow; Stagger = 45, Angle of Attack = 15
(a) Picture 2, time = 5.00 ms.
(b) Diagram of Picture 2

(a)

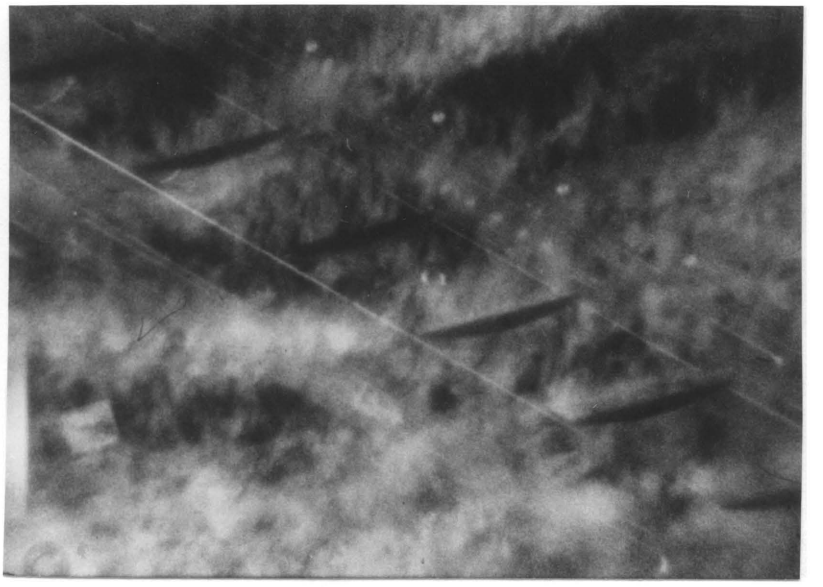

(b)

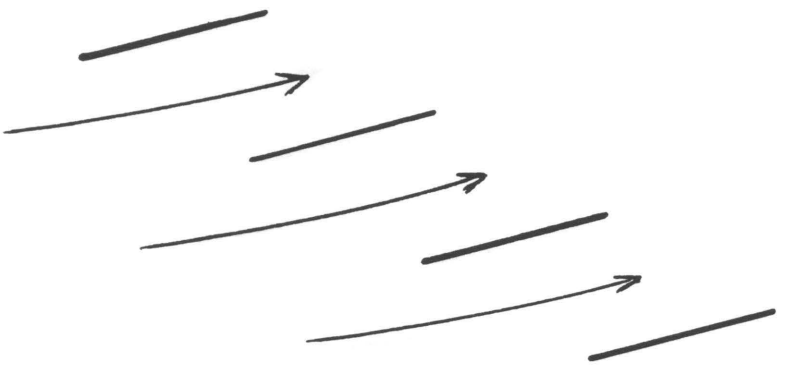

Fig. 59. Observed Flow; Stagger = 45, Angle of Attack = 15
(a) Picture 3, time = 10.00 ms.
(b) Diagram of Picture 3

(a)

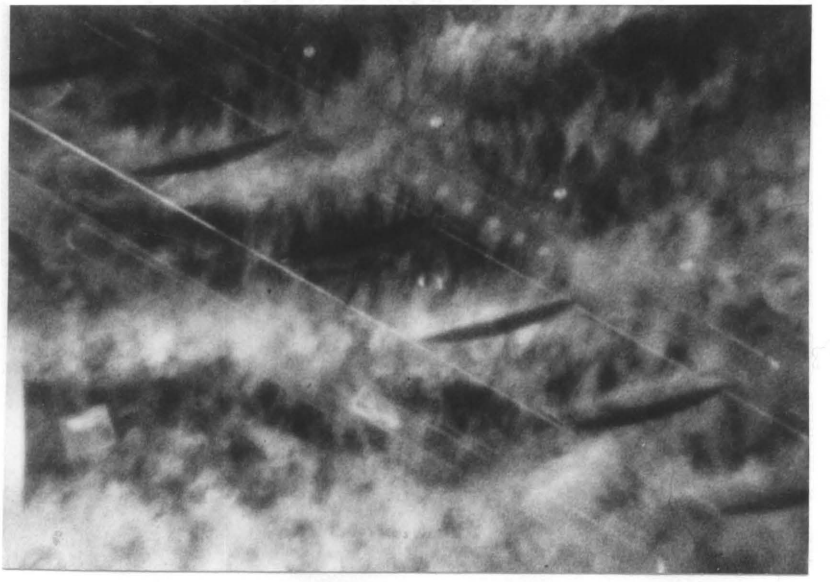

(b)

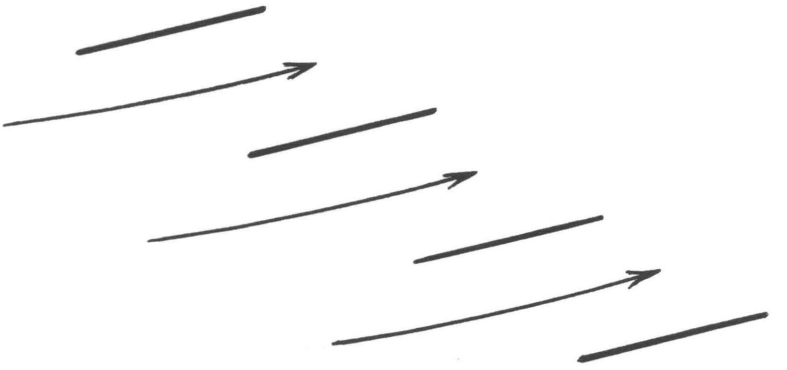

Fig. 60. Observed Flow; Stagger = 45, Angle of Attack = 15
(a) Picture 4, time = 15.00 ms.
(b) Diagram of Picture 4

(a)

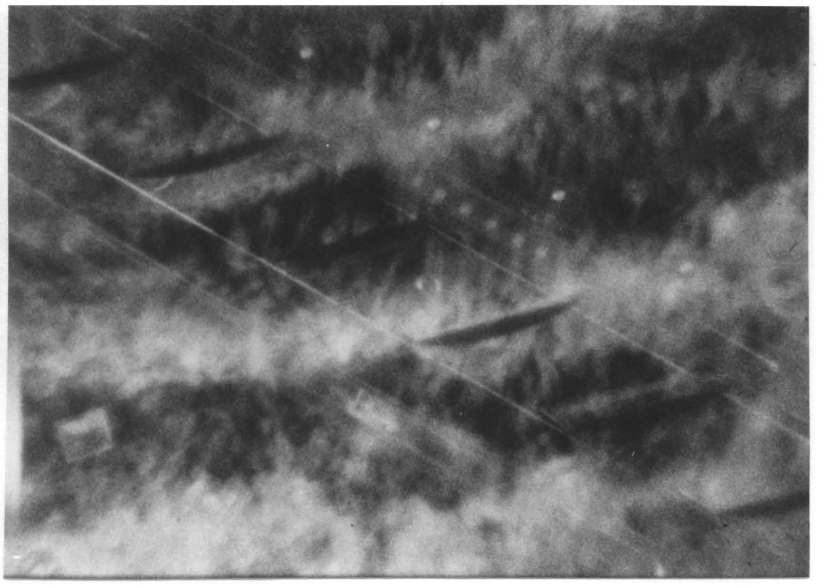

(b)

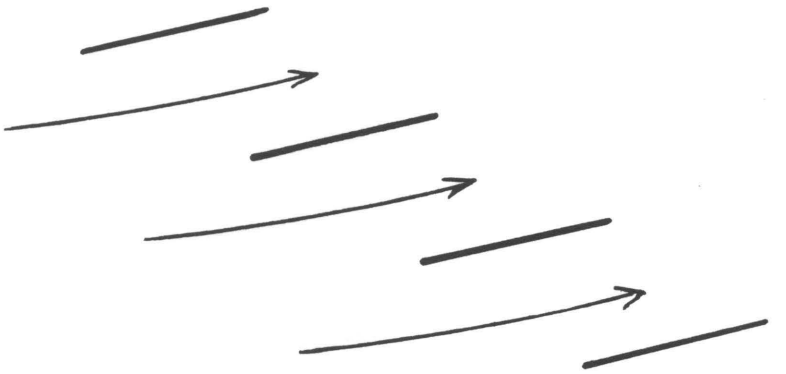

Fig. 61. Observed Flow; Stagger = 45, Angle of Attack = 15
(a) Picture 5, time = 20.00 ms.
(b) Diagram of Picture 5

(a)

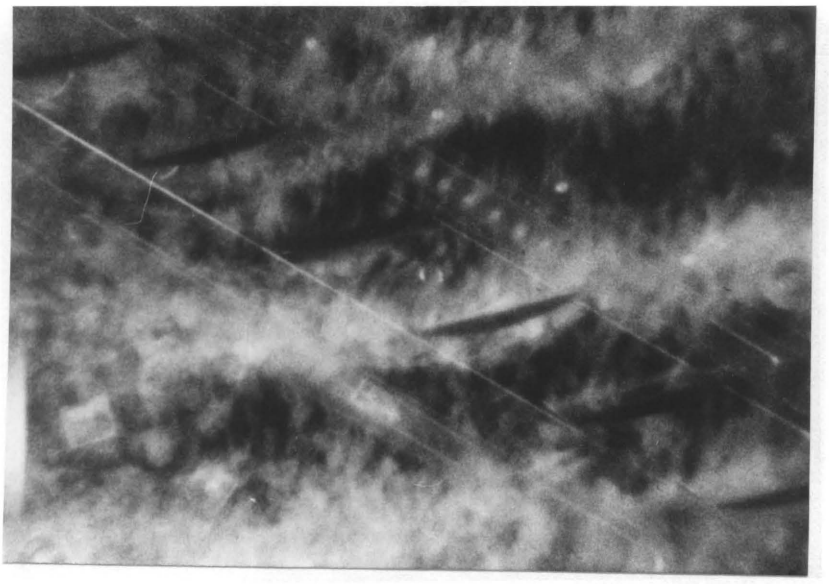

(b)

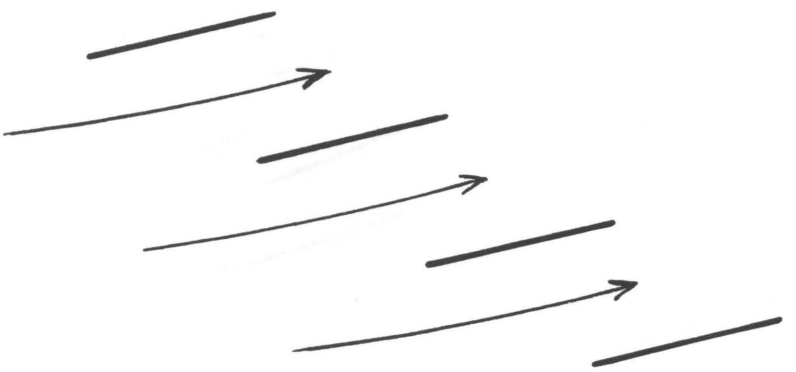

Fig. 62. Observed Flow; Stagger = 45, Angle of Attack = 15
(a) Picture 6, time = 25.00 ms.
(b) Diagram of Picture 6

(a)

(b)

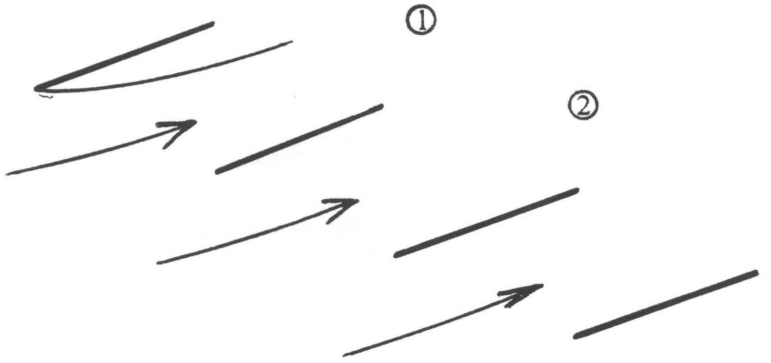

Fig. 63. Observed Flow; Stagger = 45, Angle of Attack = 20
(a) Picture 1, time = 0.00 ms., ref.
(b) Diagram of Picture 1

(a)

(b)

Fig. 64. Observed Flow; Stagger = 45, Angle of Attack = 20
(a) Picture 2, time = 9.75 ms.
(b) Diagram of Picture 2

(a)

(b)

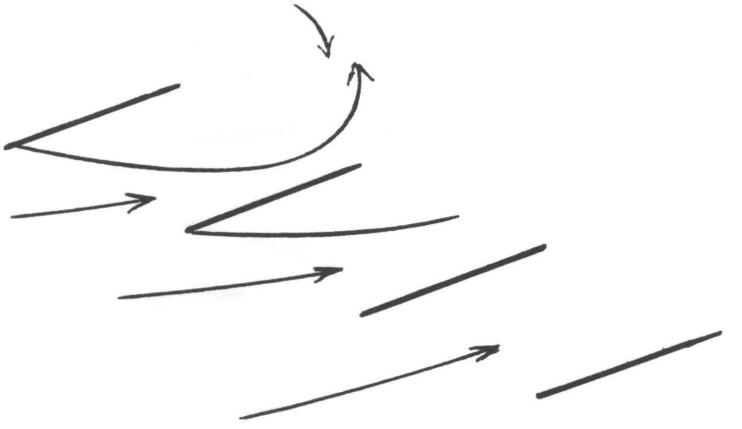

Fig. 65. Observed Flow; Stagger = 45, Angle of Attack = 20
(a) Picture 3, time = 28.00 ms.
(b) Diagram of Picture 3

(a)

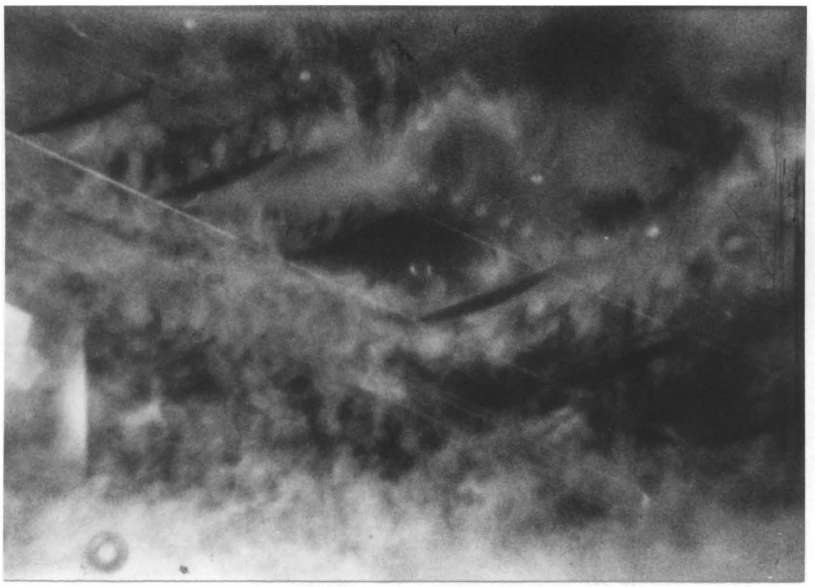

(b)

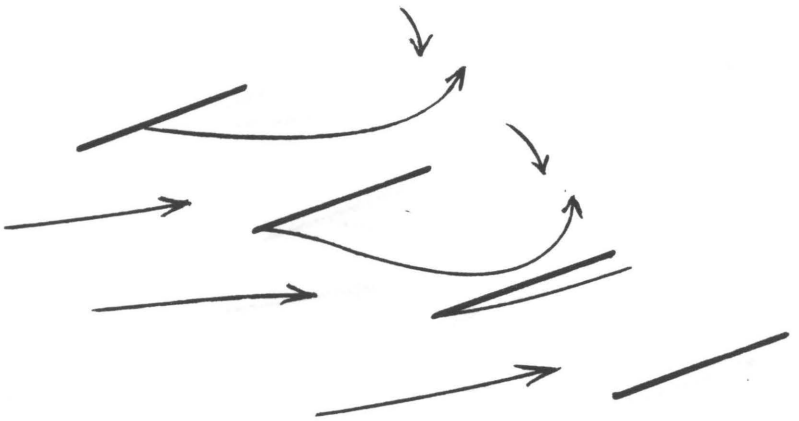

Fig. 66. Observed Flow; Stagger = 45, Angle of Attack = 20
(a) Picture 4, time = 30.00 ms.
(b) Diagram of Picture 4

(a)

(b)

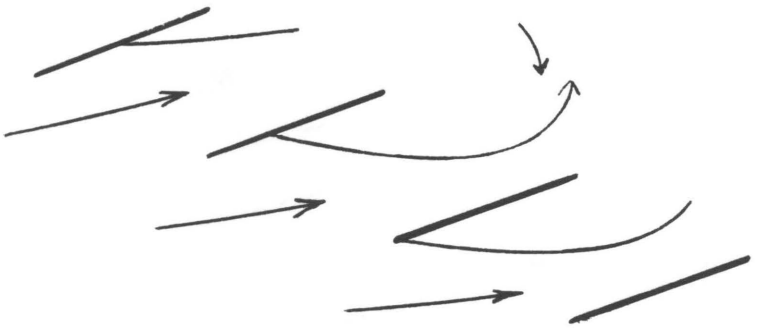

Fig. 67. Observed Flow; Stagger = 45, Angle of Attack = 20
(a) Picture 5, time = 33.00 ms.
(b) Diagram of Picture 5

(a)

(b)

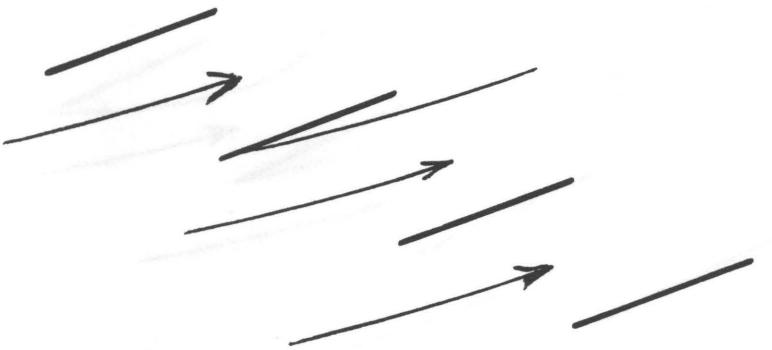

Fig. 68. Observed Flow; Stagger = 45, Angle of Attack = 20
(a) Picture 6, time = 52.50 ms.
(b) Diagram of Picture 6

(a)

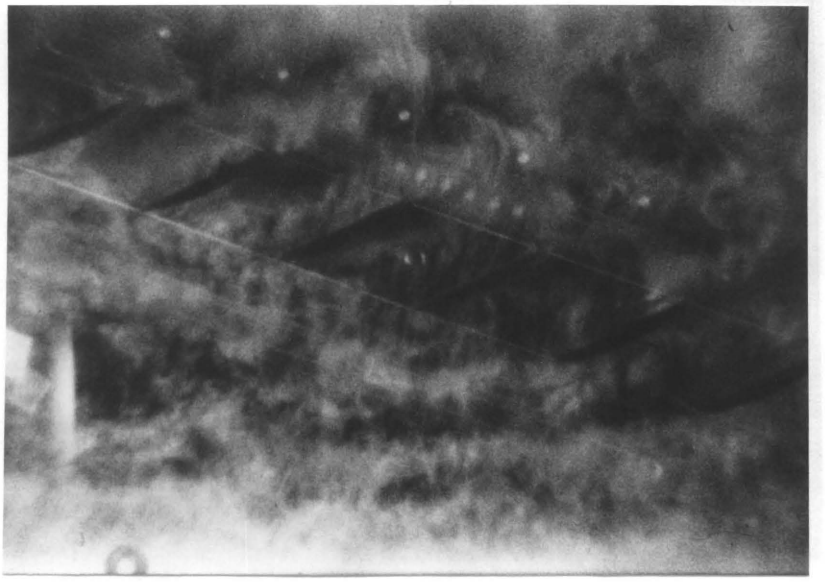

(b)

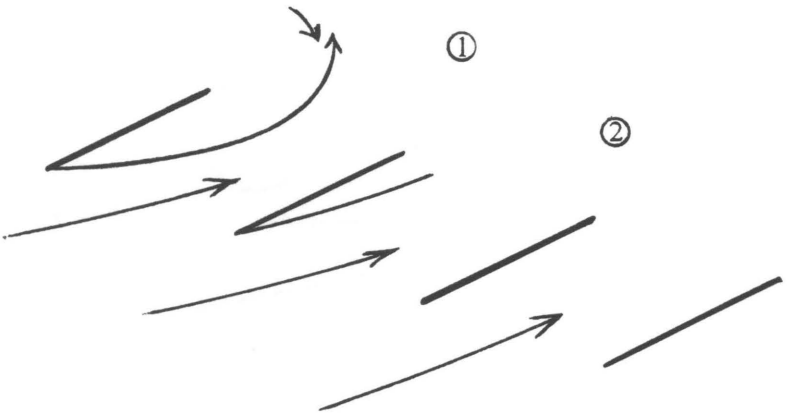

Fig. 69. Observed Flow; Stagger = 45, Angle of Attack = 25
(a) Picture 1, time = 0.00 ms., ref.
(b) Diagram of Picture 1

(a)

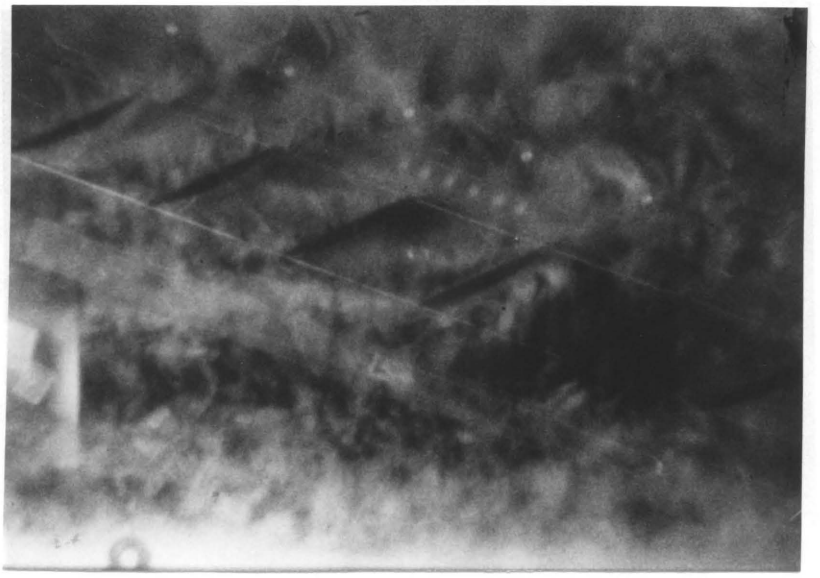

(b)

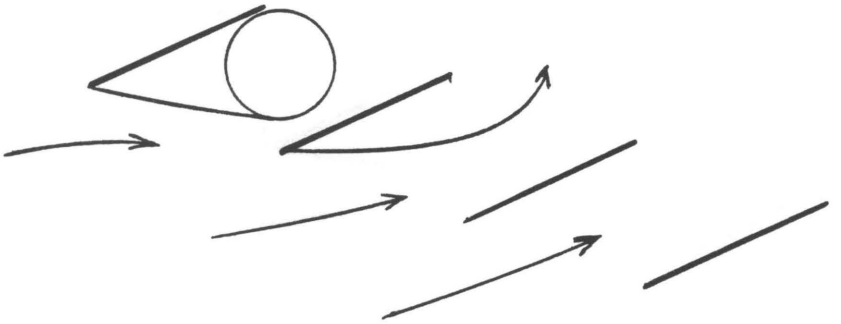

Fig. 70. Observed Flow; Stagger = 45, Angle of Attack = 25
(a) Picture 2, time = 15.75 ms.
(b) Diagram of Picture 2

(a)

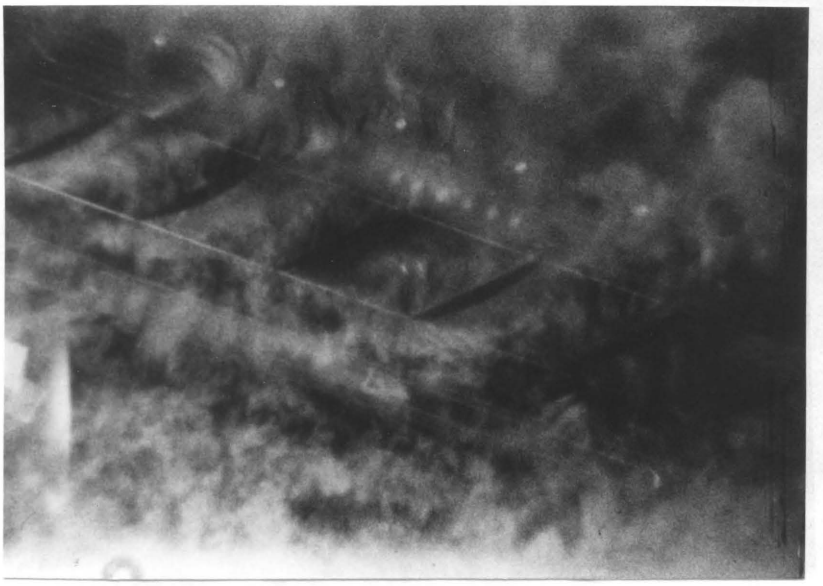

(b)

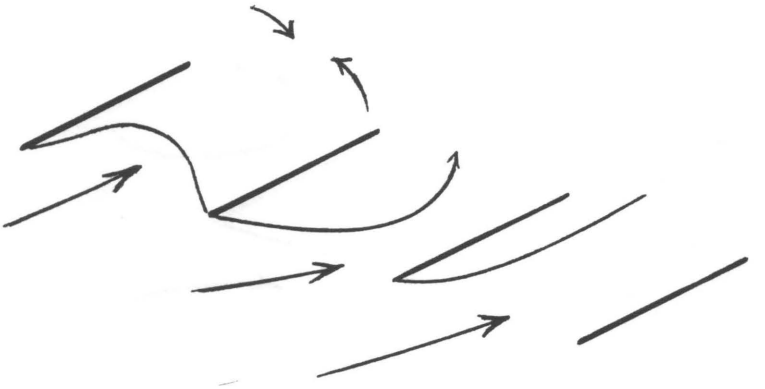

Fig. 71. Observed Flow; Stagger = 45, Angle of Attack = 25
(a) Picture 3, time = 24.00 ms.
(b) Diagram of Picture 3

(a)

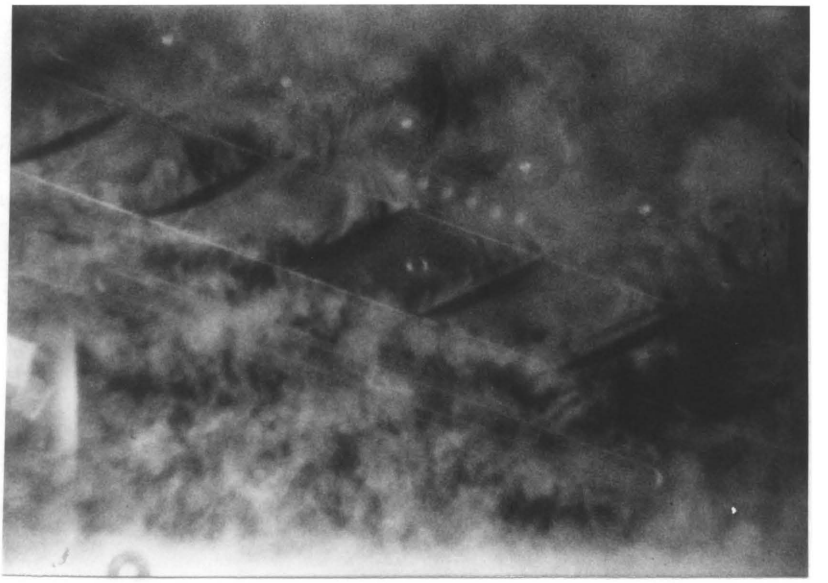

(b)

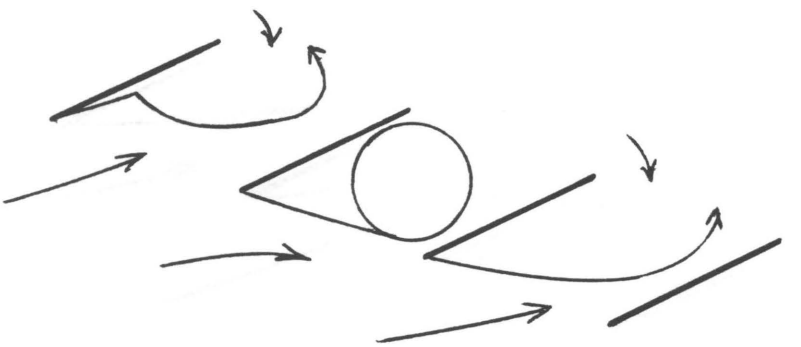

Fig. 72. Observed Flow; Stagger = 45, Angle of Attack = 25
(a) Picture 4, time = 30.00 ms.
(b) Diagram of Picture 4

(a)

(b)

Fig. 73. Observed Flow; Stagger = 45, Angle of Attack = 25
(a) Picture 5, time = 40.75 ms.
(b) Diagram of Picture 5

(a)

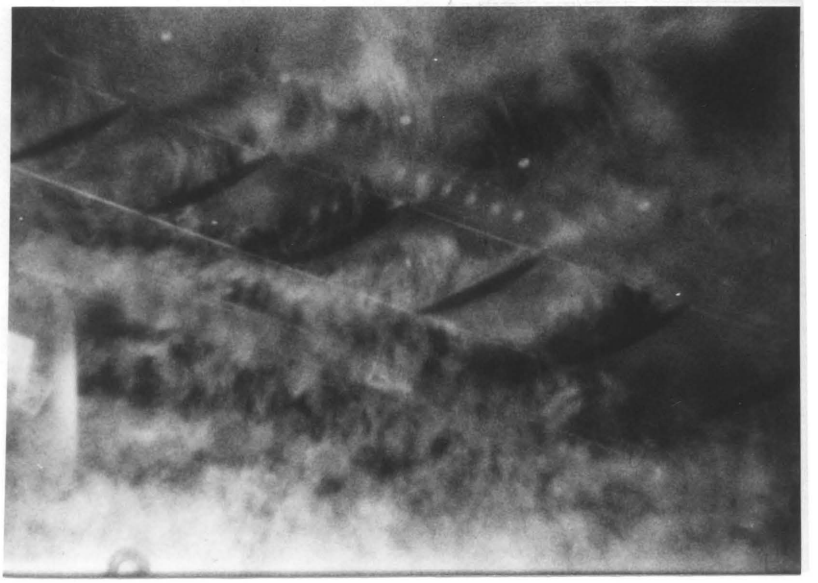

(b)

Fig. 74. Observed Flow; Stagger = 45, Angle of Attack = 25
(a) Picture 6, time = 61.75 ms.
(b) Diagram of Picture 6

(a)

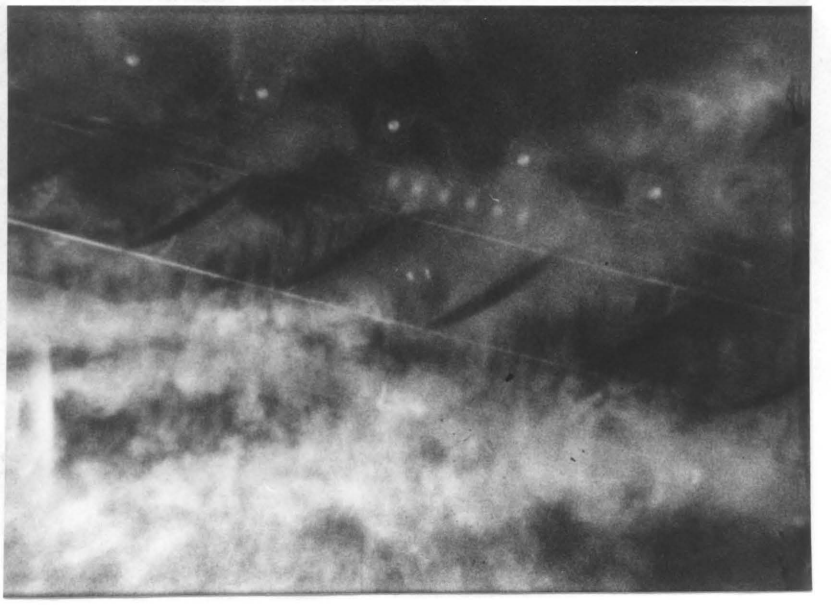

(b)

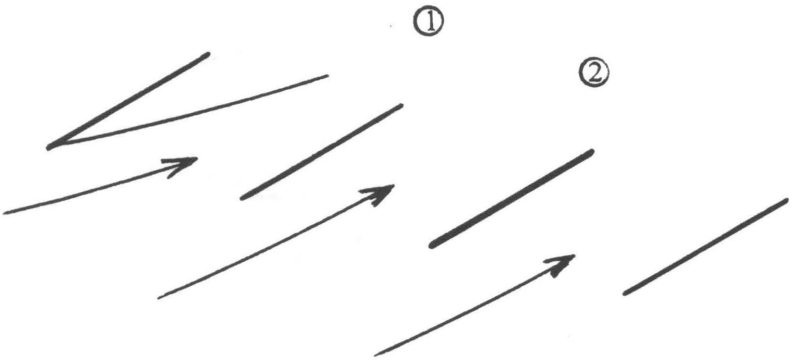

Fig. 75. Observed Flow; Stagger = 45, Angle of Attack = 30
(a) Picture 1, time = 0.00 ms., ref.
(b) Diagram of Picture 1

(a)

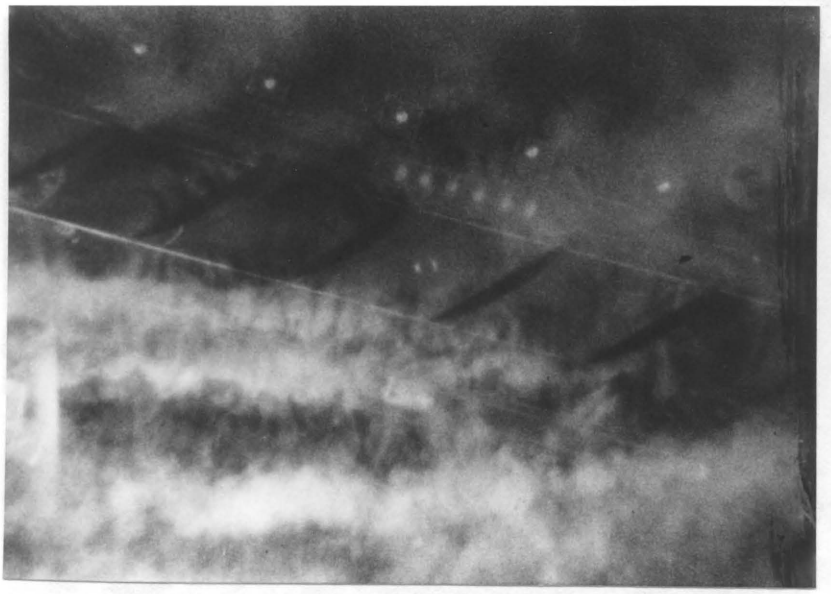

(b)

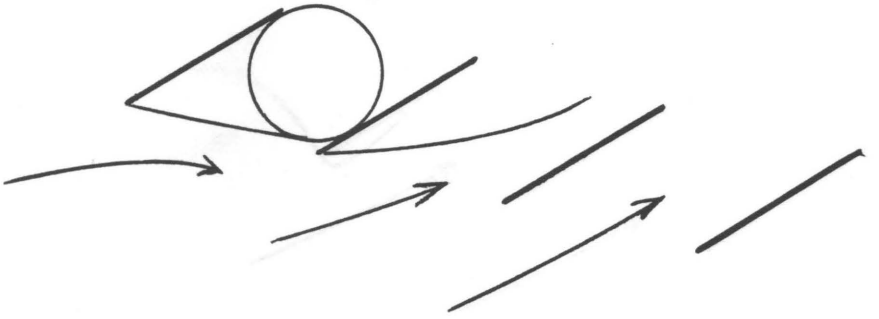

Fig. 76. Observed Flow; Stagger = 45, Angle of Attack = 30
(a) Picture 2, time = 12.00 ms.
(b) Diagram of Picture 2

(a)

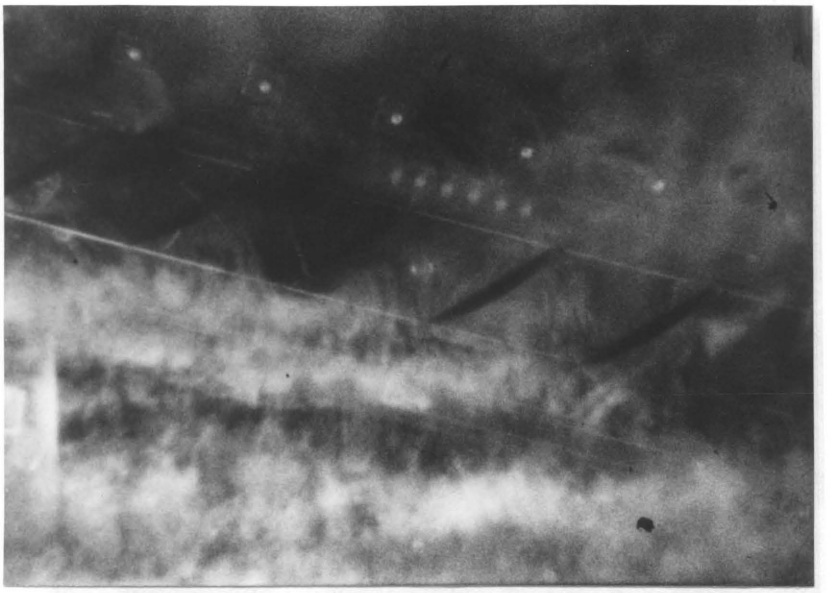

(b)

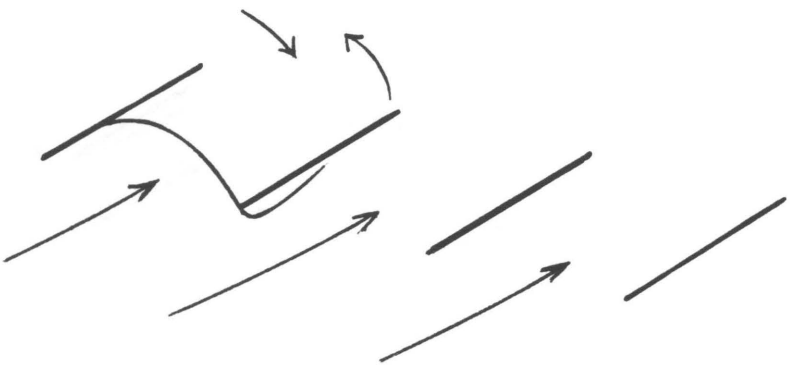

Fig. 77. Observed Flow; Stagger = 45, Angle of Attack = 30
(a) Picture 3, time = 18.00 ms.
(b) Diagram of Picture 3

(a)

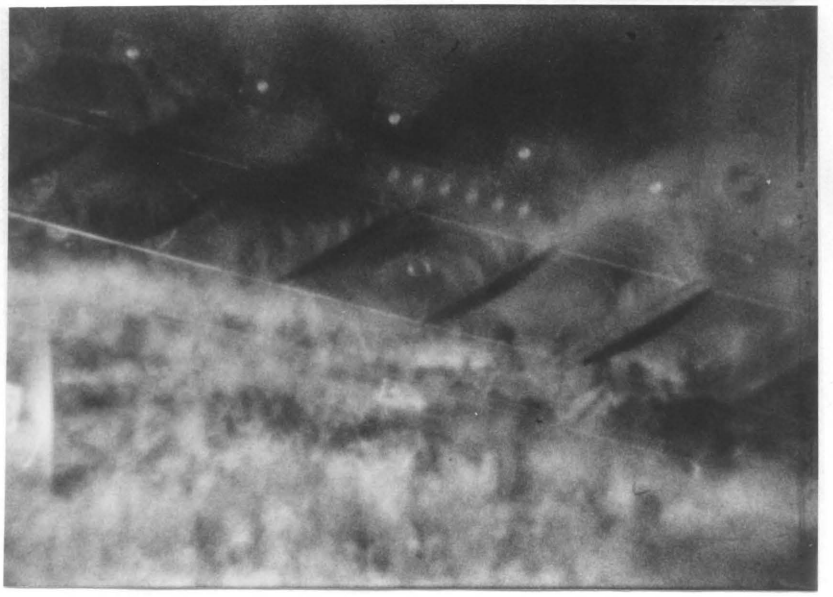

(b)

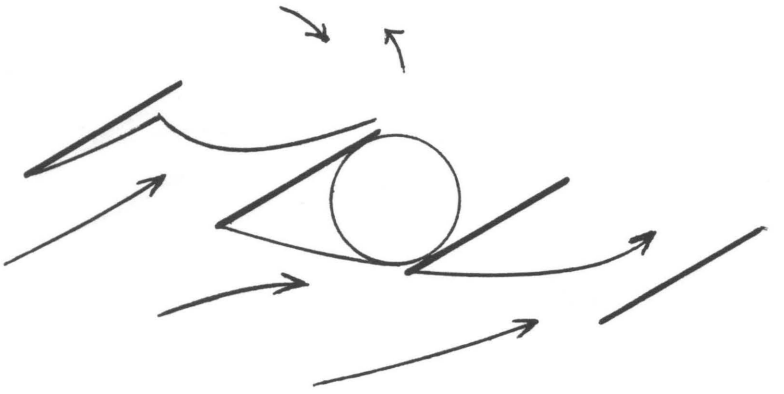

Fig. 78. Observed Flow; Stagger = 45, Angle of Attack = 30
(a) Picture 4, time = 26.50 ms.
(b) Diagram of Picture 4

(a)

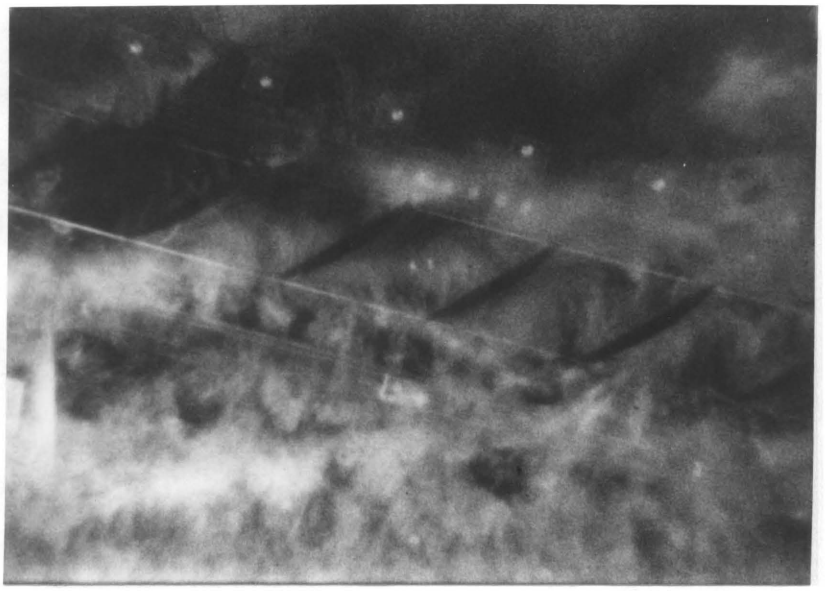

(b)

Fig. 79. Observed Flow; Stagger = 45, Angle of Attack = 30
(a) Picture 5, time = 39.00 ms.
(b) Diagram of Picture 5

(a)

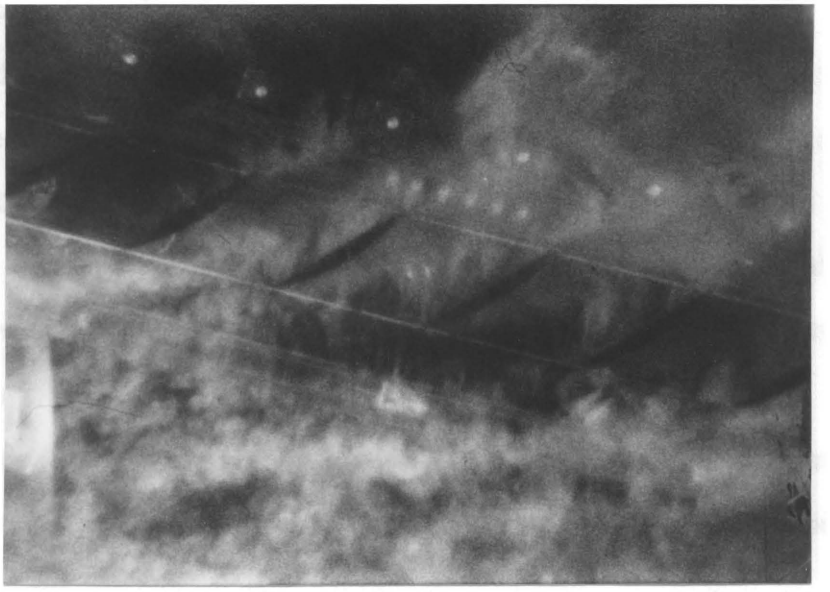

(b)

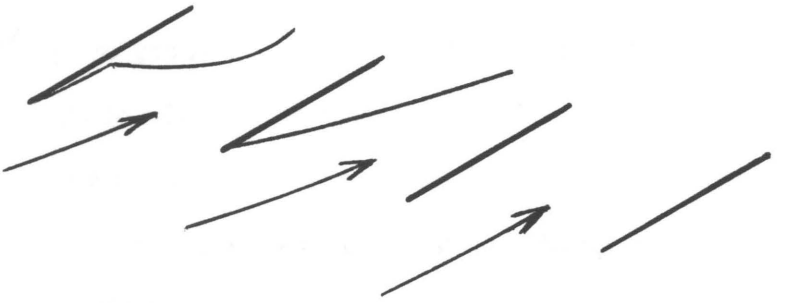

Fig. 80. Observed Flow; Stagger = 45, Angle of Attack = 30
(a) Picture 6, time = 56.75 ms.
(b) Diagram of Picture 6

Measured Results

The measured results of the propagating stall observations appear in Table I. The measured propagation speeds averaged 26.5 percent of the relative inlet velocity and ranged from 21.3 to 31.6 percent, a range of ± 20 percent of the average. Figures 81, 82, and 83 show the data and its relation to angle of attack, relative velocity, and stagger angle. Figure 84 shows the relation of the propagation velocity measurements to the component of the relative velocity which is tangent to the blade row.

In figures 81, 82, and 83, the solid lines represent a least squares linear approximation to the data. The slope of the lines are an indication of the dependence of the propagation velocity on each parameter. The slope of the least squares approximation is -0.0016/degree with respect to angle of attack, -0.0006/meter/second with respect to the relative velocity, and 0.0008/degree with respect to stagger angle. For the range of geometries tested, the maximum deviation of the ratio of propagation velocity to relative inlet velocity using the approximation is 0.021, less than 8 percent of the average. This shows that, for the range of tested geometries, the propagation velocity can be assumed constant with respect to angle of attack and stagger angle and linearly proportional to the relative inlet velocity.

Figure 84 is included for comparison of these results with previous results obtained from compressor tests because the tangential component of the relative velocity is analogous to the blade velocity in a compressor with purely axial entry flow. Since most propagating stall velocity data for compressors is recorded as a ratio to the blade velocity, these data are easily compared to other data. The line

Table I. Measured Propagation Speeds

ζ (degrees)	α (degrees)	W (m/sec)	V_p/W
36.5	20	16.9	0.163
36.5	22	16.9	0.277
36.5	25	16.5	0.238
36.5	30	16.9	0.279
36.5	35	16.9	0.292
45	20	16.5 16.6	0.168 0.207
45	25	16.6 16.4	0.262 0.286
45	30	16.5 16.7	0.271 0.260
36.5	30	48.0	0.247
36.5	35	48.3	0.231
45	25	47.4	0.316
45	30	46.9	0.213

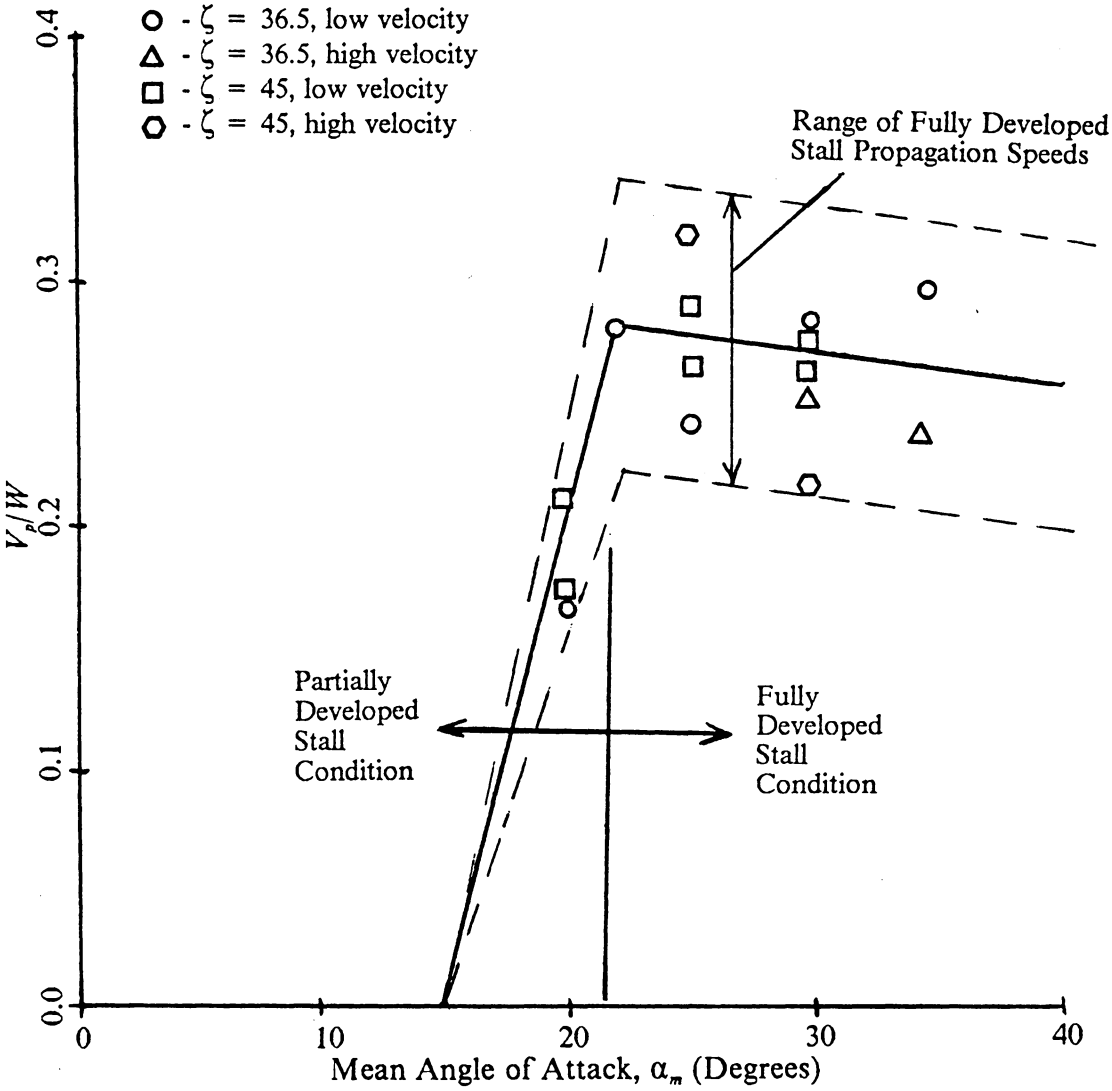

Fig. 81. Variation of Non-Dimensionalized Stall Propagation Speed with Mean Angle of Attack

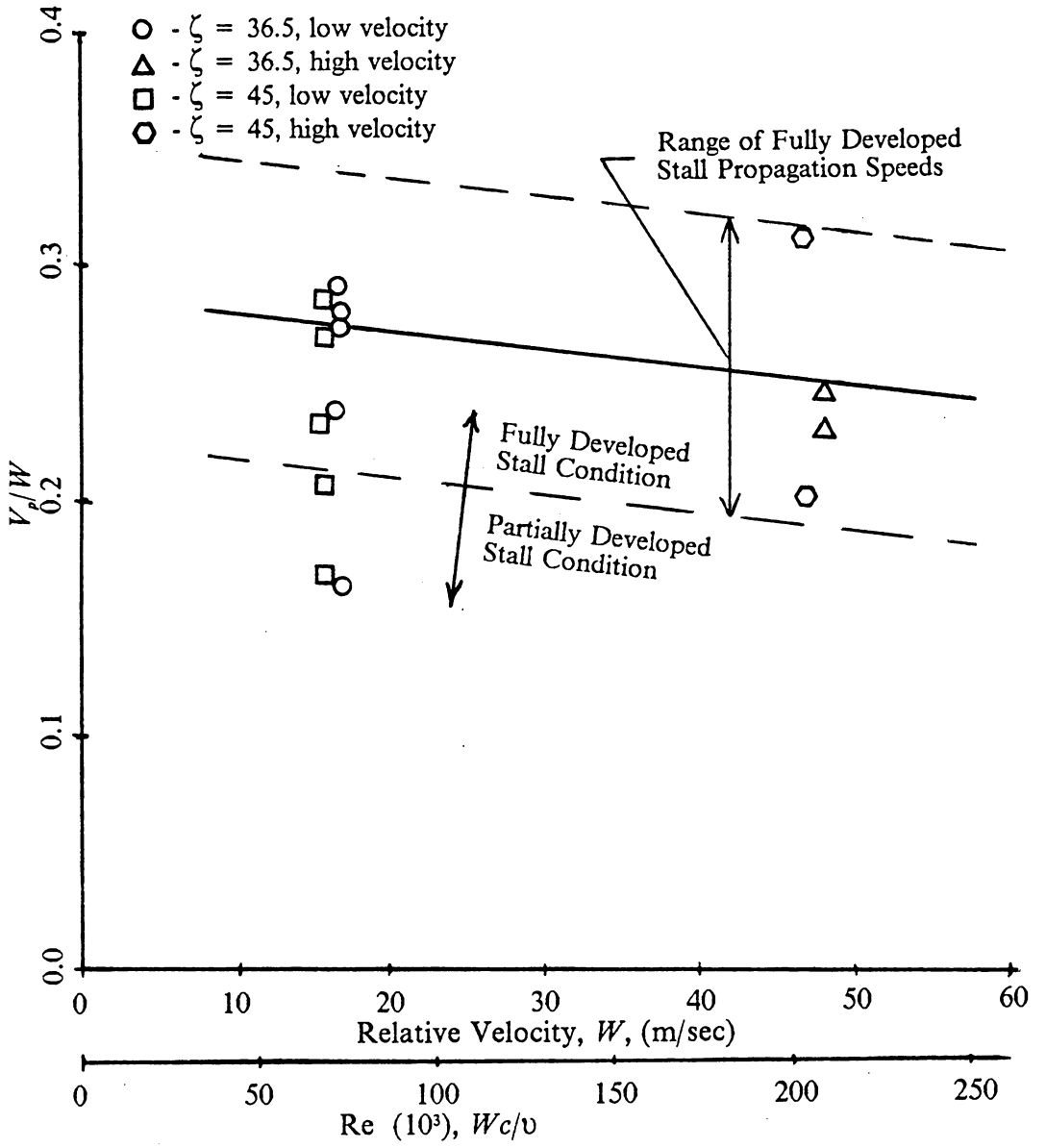

Fig. 82. Variation of Non-Dimensionalized Stall Propagation Speed with Relative Inlet Velocity

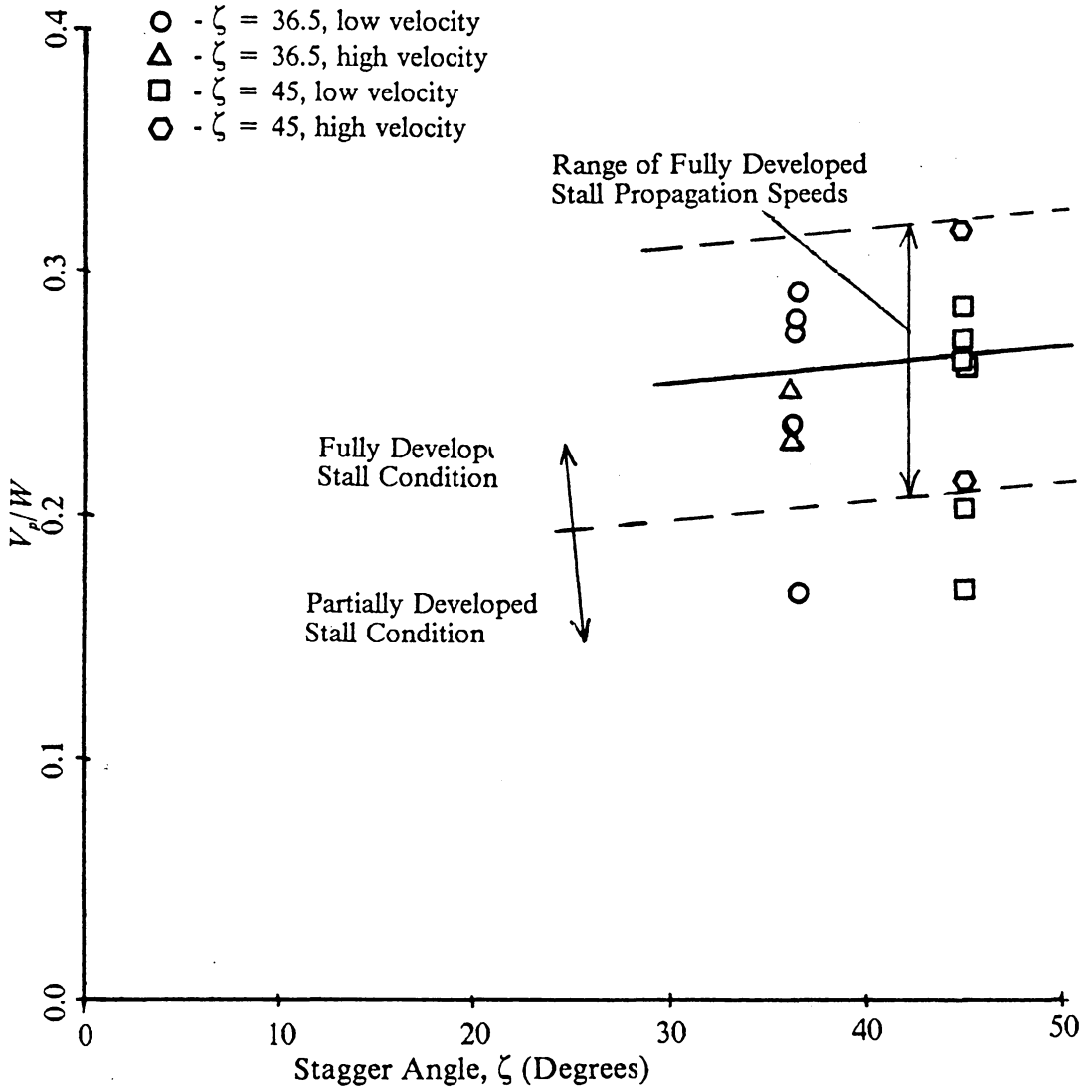

Fig. 83. Variation of Non-Dimensionalized Stall Propagation Speed with Stagger Angle

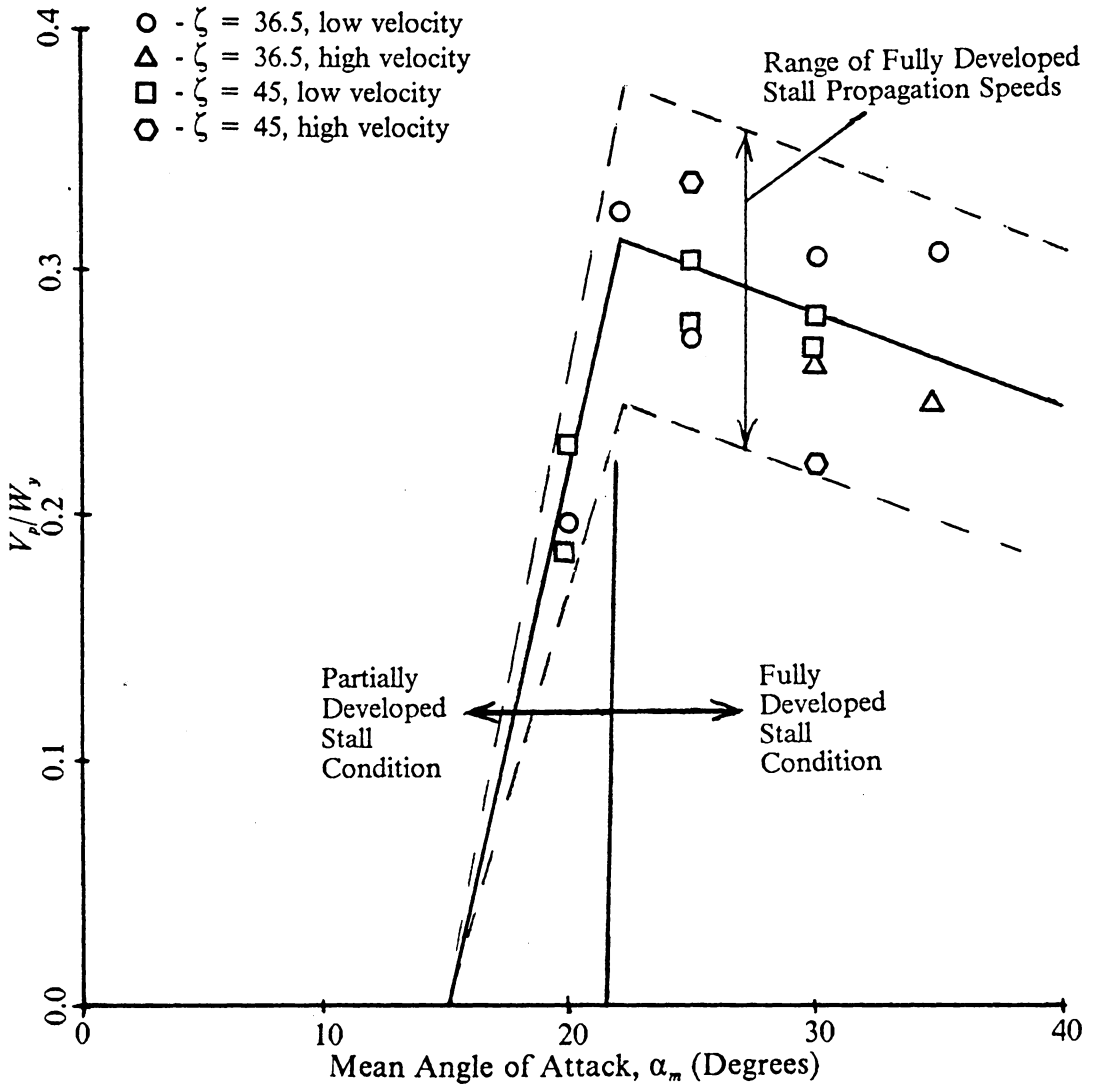

Fig. 84. Variation of Stall Propagation Speed, When Normalized Using the Tangential Component of the Relative Velocity, with Mean Angle of Attack

is again a least squares approximation to the data. When compared with Fig. 81, the propagation velocity is seen to be more dependent on the tangential component of the velocity relative to the blade row than on the total relative velocity. This is so because the tangential component of the velocity is a function of the relative velocity, angle of attack, and stagger angle. Thus, the sum effects of all these parameters is included in a representation of the propagation velocity as a function of the tangential relative velocity.

Another important observation is that the propagation speed at the stall inception point, noted by the measurements at an angle of attack of 20 degrees, is less than the propagation speed at higher angles of attack, which are relatively constant. At 20 degrees, the passage became only partially blocked before shedding occurred. This 20 degree case corresponds to blade 3 of Fig. 5. This is the developing stall region. Then, at angles of attack greater than 20 degrees, full blockage of the blade passages occurred. These latter measurements are associated with stalling behavior as diagrammed on blade 4 of Fig. 5, and are in the fully-developed stall region. The stalling behavior changes over this variation in angle of attack, which explains why there is a variation in the measured propagation speeds. It is believed that the measurements at an angle of attack of 20 degrees correspond to a part span stall condition which is known at occur at the stall inception point in compressors. The measurements at the higher angles of attack are believed to correspond to a full span stall condition in a compressor. It is known, as previously mentioned, that the larger stall cells in compressors propagate at higher speeds, relative to the rotor, than the smaller cells, so this appears reasonable. The con-

clusion reached from this observation is that the propagation speed is dependent on the amount of blockage in the stalled passages and the type of separation experienced by the blades, and that once full blockage and leading edge separation occur, the propagation speed will remain constant.

The results show that the ratio of the propagation speed to the relative velocity is fairly constant for high angles of attack where a fully-developed stall condition has been reached. This ratio is similar to a Strouhal number based on the chord length. A Strouhal number is defined as:

$$Str = \frac{fl_c}{W}$$

where f is the shedding frequency, l_c is a characteristic length, and W is a relative velocity. The Strouhal number is commonly used to predict vortex shedding from a cylinder in cross-flow.

The propagation velocity ratio:

$$Str_c = \frac{V_p}{W}$$

is similar to a Strouhal number since:

1. Dividing the propagation distance by the associated time period corresponds to multiplying the blade spacing by the shedding frequency. Therefore, the

inverse of the time period associated with the propagation of the vortex is the shedding frequency which is the f term in the Strouhal equation. That is:

$$V_p \propto \frac{prop.dist.}{period} \propto f l_c$$

2. The relative inlet velocity used in normalizing the propagation velocity is the value of W in the Strouhal equation.

3. With the solidity is 1.0, the blade spacing is the same as the chord length and is the value l_c in the Strouhal equation. If the solidity were different than 1.0, dividing the propagation velocity by the solidity would yield the desired value for l_c.

Results obtained in this study are very similar to results obtained for vortex shedding over a cylinder in cross flow where a constant value of Str of 0.21 occurs over a range of Reynolds numbers $1000 \leq Re \leq 5000$. The results obtained in this study can then be represented as having a constant Str_c of 0.27 for $70000 \leq Re_c \leq 200000$. This indicates that the problem of propagating stall may be very closely related to vortex shedding over a cylinder.

The Vortex Shedding Mechanism

Perhaps the most important result of this investigation is an understanding of the shedding mechanism. The movies showed that the vortex grew in the passage to an extent that nearly completely blocked the passage. It then dissipated and smooth flow through the passage was resumed. After further study, it appeared that the reverse flow from the previously-stalled passage interfered with the developing vortex flow and, thus, dissipated the vortex in the passage. It seemed that the two flows met directly and stagnated the flow in the middle of the passage. This 'clump' of stagnant flow then caused the rest of the vortex to dissipate and completely block the passage. The incoming flow then flushed the stagnated cell through the passage and restored smooth flow through it. This process is diagrammed in Fig. 85. Using the photos for the three stagger angles at an angle of attack of 30 degrees, the shedding mechanism can be observed. Figures 27 through 32 show the constant separated boundary layer that developed at a stagger angle of 25 degrees. Figures 53 through 56, pictures 3 through 6, show the flush-out process for a stagger of 36.5 degrees in the center passage. This sequence best shows the observed shedding mechanism. Picture 3 shows the developing vortex in the center passage. Picture 4 shows the presence of the fully-developed vortex in the passage. Flush-out of the vortex occurs in picture 5. In this picture, the reverse flow has interacted with the vortex flow near the trailing edge of the stalled blade. Also, in this picture the vortex is stagnating and a 'wall' is forming between the blades at the edge of the vortex. The incoming flow 'pushes' against this wall, thus flushing the vortex out of the passage. In picture 6, smooth flow is being re-

stored to the passage. Figures 77 through 80 show the same process for the same angle of attack at a stagger angle of 45 degrees. Similar comparisons can be made using the photos for angles of attack of 20 and 25 degrees.

The following explanation of the flush-out mechanism is offered. As the vortex grows, more flow is diverted out of the stalled passage. The flow that still goes through the passage is jetted along the pressure side, around the vortex. This jetting of the flow creates a pressure difference along the rear face of the blade row behind the vortex. The pressure difference pulls flow from the previously-stalled passage into the area behind the vortex. This flow then feeds the vortex along the suction side of the passage while the jetting flow pulls the vortex along at the pressure side. When the separating boundary layer develops in the next passage, it begins to pull some of the jetting flow into it, thus further increasing the amount of reverse flow from the trailing passage. This causes the vortex to grow even more until it is large enough so that the reverse flow actually interferes with the vortex flow instead of feeding it. The two flows collide and the vortex is dissipated. The incoming flow then flushes the stagnated vortex out of the passage and restores smooth flow.

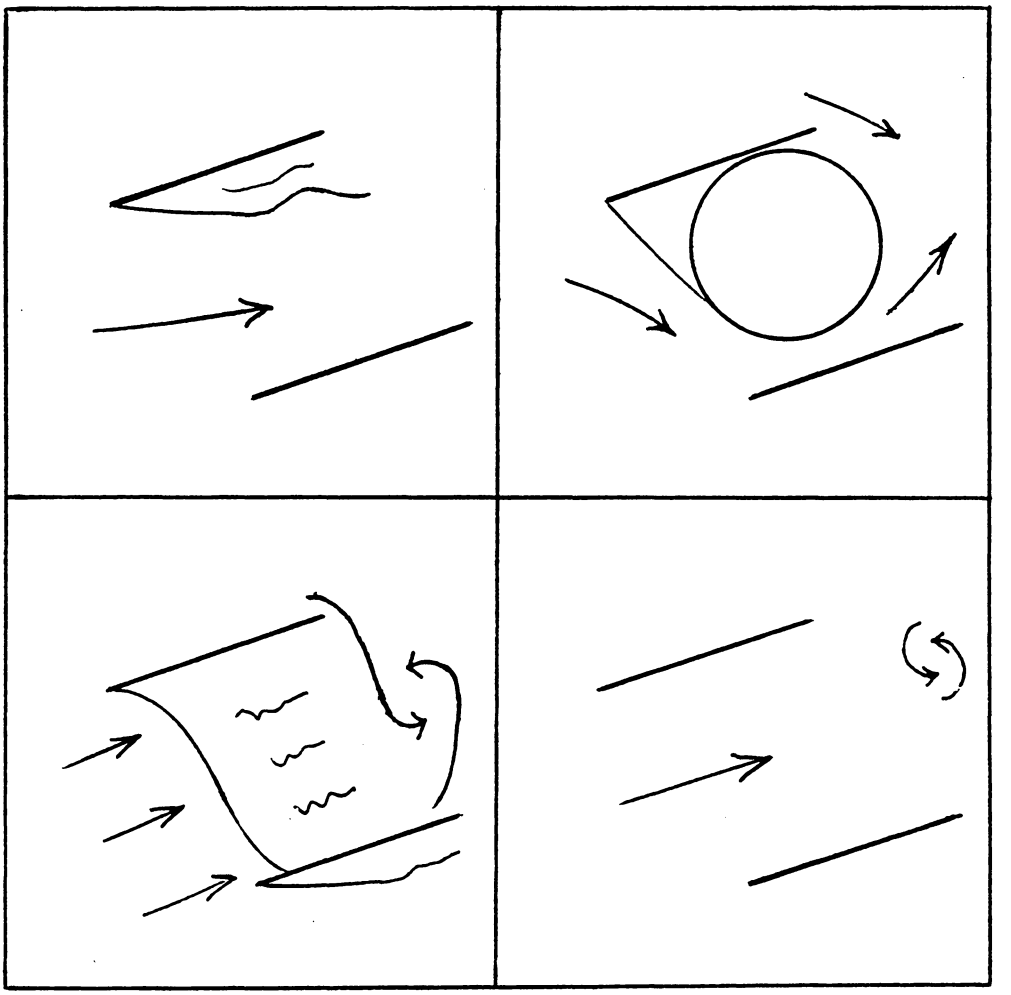

1) Developing vortex
2) Fully-developed vortex
3) Dissipation of vortex
4) Resumption of smooth flow

Fig. 85. Schematic of Flush-Out Process

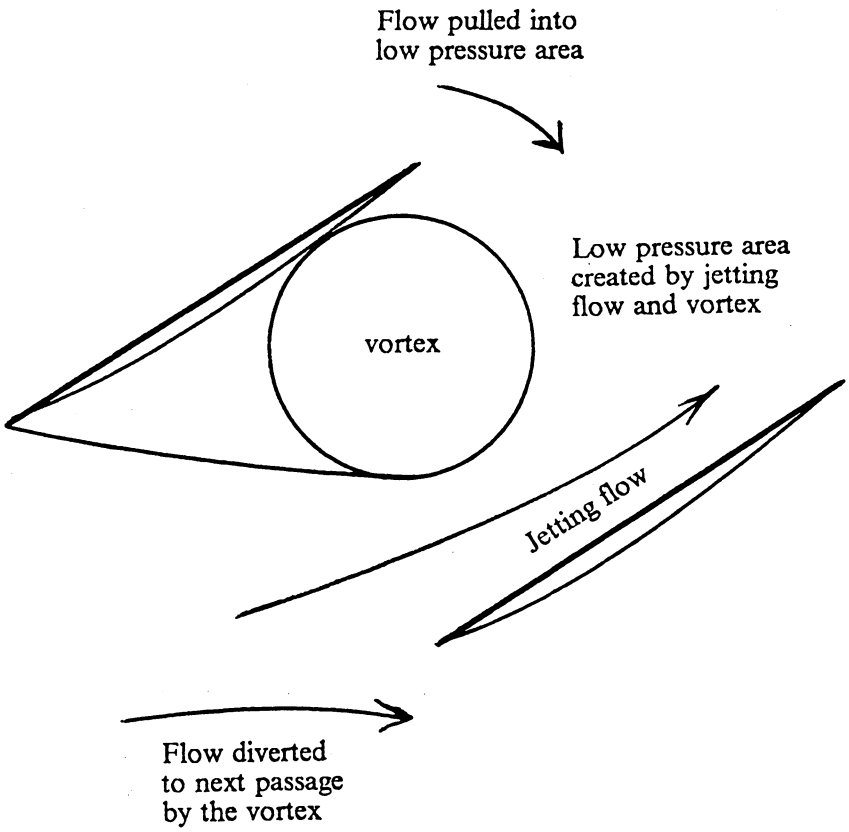

Fig. 86. Sketch of Interaction of Flow and Blading

Development of Geometric Model

The observations of the vortex shedding mechanism led to the development of a geometric model to predict vortex shedding and, thus, propagating stall inception. Steady flow behavior, as shown in the movies at a stagger angle of 25 degrees, or propagating stall behavior, as shown in the movies for staggers of 36.5 and 45 degrees, can be predicted. The model is based on the observations of the propagating stall flow, as shown in Figs. 39 through 56 and Figs. 63 through 80, and the cascade geometry. The fully-developed propagating stall process occurred with leading edge separation, a vortex was present in the center of the passage, and stall propagation occurred when the vortex was dissipated and flushed out by the incoming flow.

A schematic of the blade passage and the geometric notations appear in Fig. 87. Several assumptions were made, based on the observed shedding process, to develop the model. Assumptions were made concerning the importance of three-dimensional flow effects, the vortex model and its location in the passage, the point at which shedding occurred, and the boundary layer growth on the blades.

The analysis was made in two dimensions. This was necessary because the movies gave only a two-dimensional picture of the flow patterns. Based on Russ' work [22], the primary fully-developed stalling process resulted from the growth of a two-dimensional separated boundary layer. For this reason, a two-dimensional analysis is thought to be acceptable for determining the relation of the vortex

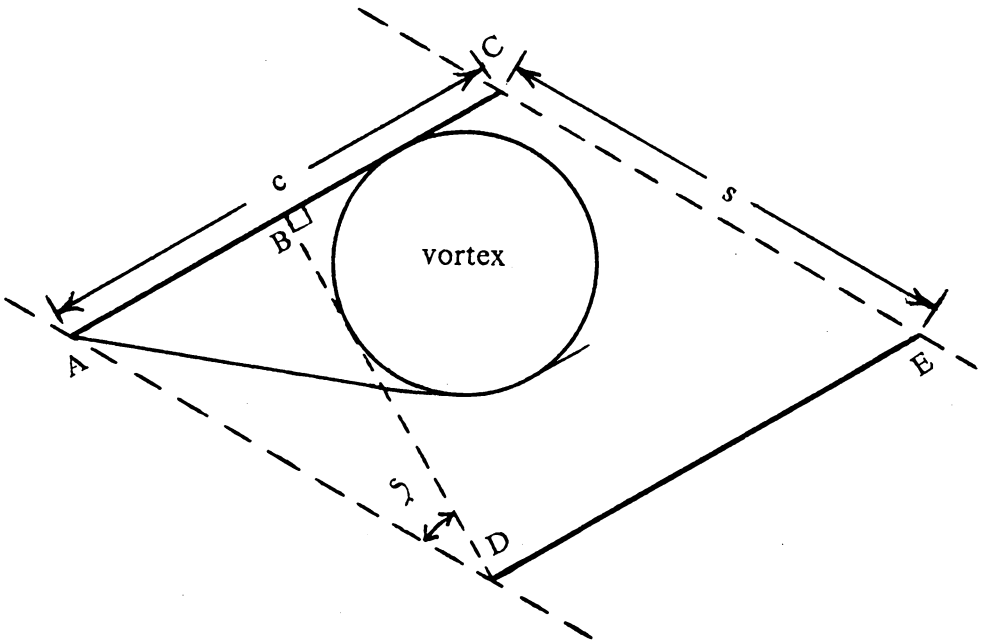

Fig. 87. Cascade Geometric Configuration and Notations

shedding process to the blade geometry. The cascade blades were flat-bottommed and were thus modeled as straight blades of negligible thickness.

The vortex was modeled in two dimensions as a circle. It lies completely within the boundary layer and its diameter is assumed to be equal to the maximum boundary layer thickness. Figure 87 shows the vortex position at the point of shedding. At this point, the vortex location in the passage was set so that the vortex was tangent to the perpendicular line from the leading edge of the leading blade to the stalled blade, line BD in Fig. 87. The vortex location was determined based on the observed position of the vortex development in the movies. The vortex size, at the point of shedding, was then defined as the largest diameter circle which is tangent to the stalled blade face, the perpendicular BD, and a third point which is related to the point where shedding occurred. Because the vortex dissipation resulted from the interference of the reverse flow with the flow of the vortex, the point where this occurred had to be defined. Observations showed that this occurred a short distance downstream of the trailing edge of the stalled blade. Therefore, the point at which vortex shedding begins, the 'flush-out' point, was defined to be the point at which the vortex circle intersected with the line connecting the trailing edges of the blades, line CE in Fig. 87. This became the limiting value for the vortex size, the flush-out diameter. This flush-out diameter, d_f, is dependent only on the blade geometry, so each different blade row has a distinct flush-out diameter.

Using basic geometry and the assumptions given, the vortex diameter at which flush-out occurs can be calculated. The derivation of this value appears in Appendix A. The final equation for calculating d_f is:

$$d_f = 2c\left[\frac{1 - (\sin\zeta)/\sigma}{1 + \tan(45 - \zeta/2)}\right]$$

This diameter is dependent on chord length, stagger angle, and solidity, but independent of angle of attack or flow velocity. This means that any compressor geometry will have only one flush-out diameter which is not changed by varying the operating conditions. The effects of the blade geometry on this flush-out diameter are:

1. Increasing the solidity, σ , (increasing the chord length or decreasing the blade spacing), increases the value of d_f.

2. Decreasing the stagger angle, ζ , increases the value of d_f.

The flush-out diameter equation gives a limiting value for the allowable vortex development in a blade passage. The size of the vortex which develops in the passage is very dependent on the flow conditions and is thus treated in an independent analysis.

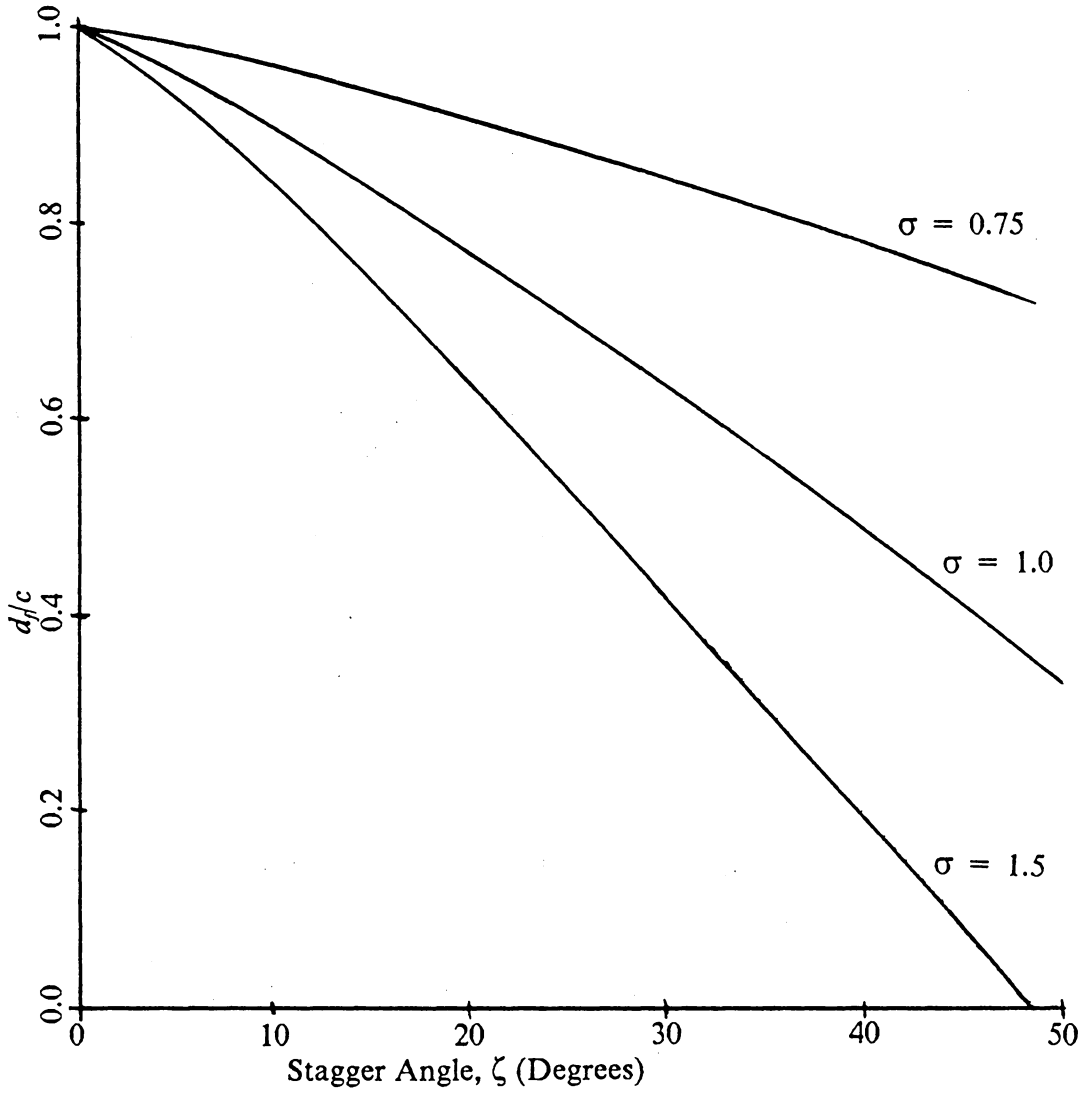

Fig. 88. Flush-Out Diameter vs. Stagger Angle, Solidity

Now, a model for predicting the growth of the separated boundary layer in the passage is needed. This will also be done geometrically. The development of the model assumes the edge of the boundary layer is impermeable. It is assumed that the boundary layer and vortex are fed entirely by the reverse flow along the blade at the suction side of the passage and that no flow from the incoming fluid enters the boundary layer. The incoming flow, in effect, sees a wedge whose outside edge is parallel to the flow at the leading edge of the stalled blade. Thus, the incoming flow undergoes no immediate changes in flow direction due to the blade or boundary layer. This defines the boundary layer growth at the leading edge of the blade to be directly related to the flow angle of the incoming flow. So, the slope of the boundary layer at the leading edge of the stalled blade is equal to the tangent of the angle of attack, as shown in Fig. 89. Also, it is assumed that the blade effects on the incoming flow are negligible up to the point where the flow is perpendicular to the leading edge of the leading blade. In Fig. 89, this gives linear boundary layer development between point A and point F, the point where the boundary layer intersects the perpendicular BD from the leading edge of the leading blade. Between points F and G, the boundary layer growth is assumed to be quadratic. Point G is the point on the boundary layer where it is thickest and, thus, the point where maximum blockage of the passsage occurs. Because the ultimate blockage occurs at the flush-out point and the edge of the vortex is fixed tangent to the perpendicular BD, point G is located a distance of half the flush-out diameter downstream of the beginning of quadratic boundary layer growth. This satisfies the assumed vortex position at the flush-out point. Since the boundary layer

thickness is a maximum, its growth rate is zero. This, along with the known boundary layer thickness and growth rate at point F which are calculated using the linear boundary layer development equation between points A and F, are the boundary conditions for the quadratic boundary layer development equation. The boundary layer growth behind the vortex, past point G, is less well defined and unnecessary for the analysis. It is therefore not modeled. The equations for the boundary layer thickness, δ , using the notation of Fig. 89, are derived in Appendix B and are:

$$\delta(x) = x \tan(\alpha)$$

if $x \leq x_0$, or

$$\delta(x) = d_f \tan(\alpha)\left[\frac{x}{d_f}(1 + 2\frac{x_0}{d_f}) - \frac{x^2 + x_0^2}{d_f^2}\right]$$

if $x_0 \leq x \leq x_0 + d_f/2$, where

$$x_0 = c\frac{\sin(\zeta)}{\sigma}$$

The values of x_0 and d_f are based on the blade geometry, but the major contributor to the growth of the boundary layer is the angle of attack.

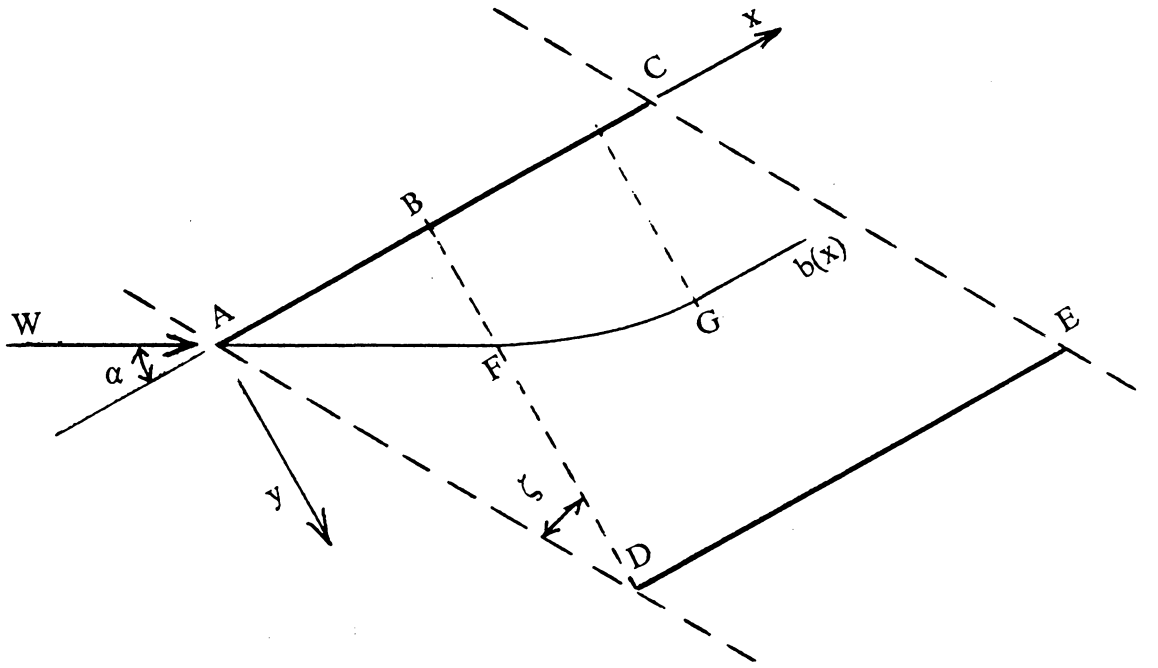

Fig. 89. Boundary Layer Geometric Model and Notations

Equations have been developed for determining the boundary layer growth in the blade passages and for determining a limiting value for the diameter of a developing vortex in the blade passage. The boundary layer thickness defines the diameter of the vortex. The vortex diameter will be calculated as being the diameter equal to the maximum boundary layer thickness. This is point G in Fig. 89 and it corresponds to the blockage of the blade passage. The equation for the vortex diameter, d_v, derived in Appendix B, is then:

$$d_v = \tan(\alpha)\left[x_0 + \frac{d_f}{4}\right]$$

The equations are used to predict flush-out by comparing the flush-out diameter and the developed vortex diameter. If the vortex diameter, d_v, is equal to or greater than the flush-out diameter, d_f, then shedding is predicted. Shedding, and thus, propagating stall inception, are predicted because the flow conditions encourage the growth of a vortex in the blade passage which will be large enough for the flush-out mechanism to affect the vortex. In very closely spaced blades, the flush-out diameter may be greater than the perpendicular spacing of the blades. In this case, the vortex would grow and block the passage before the flush-out diameter was reached. Therefore, an alternate shedding criteria is that shedding is also predicted if the vortex diameter is greater than the perpendicular blade spacing, l. The criteria for predicting the point of propagating stall inception are:

$$\frac{d_v}{d_f} \geq 1.0$$

or

$$\frac{d_v}{l} \geq 1.0$$

If these conditions are not met, stable, normal operation is predicted.

Since the flush-out diameter and perpendicular blade spacing are dependent only on the blade geometry, they are constant for all flow conditions. The vortex diameter, though, is primarily dependent on the angle of attack. Thus, the flow conditions necessary for inception of rotating stall for a given machine can be predicted. Similarly, for given flow conditions, blade geometries can be found for which rotating stall inception would not be predicted under normal operating conditions.

Discussion of Model

The theoretical models may be used in two ways. The first is to calculate the ratios d_v/d_f, the ratio of the vortex diameter to the flush out diameter, and d_v/l, the ratio of the vortex diameter to the perpendicular spacing of the blade, for varying angles of attack. Then, propagating stall inception would be predicted at the angle of attack at which either ratio reached unity. Another method is to calculate the angle of attack necessary for either ratio to reach unity. Since propagating stall initiates with an increase in angle of attack on one or more blades, the angle of attack necessary for propagating stall inception may be reached locally even if the mean angle of attack is lower. Thus, for known average flow conditions, particularly mean angle of attack, the flow distortion size necessary to cause propagating stall inception can be calculated. The stalled passage then creates the distortions which cause the stall cell to propagate. Since rotating stall results from flow distortions, this latter method is thought to be a better analysis method.

Figures 90 through 98 show the variations of d_v/d_f and d_v/l for various flow geometries. The figures show trends associated with changes in the blade geometry. Lowering the value of the vortex diameter or raising the value of the flush-out diameter or raising the perpendicular blade spacing, whichever is appropriate, reduces the ratios. Except for very high solidity machines, the flush-out diameter criterion is the determining relation, so increasing the blade spacing is of secondary concern. Reducing the diameter ratios reduces the chance of propagating stall inception.

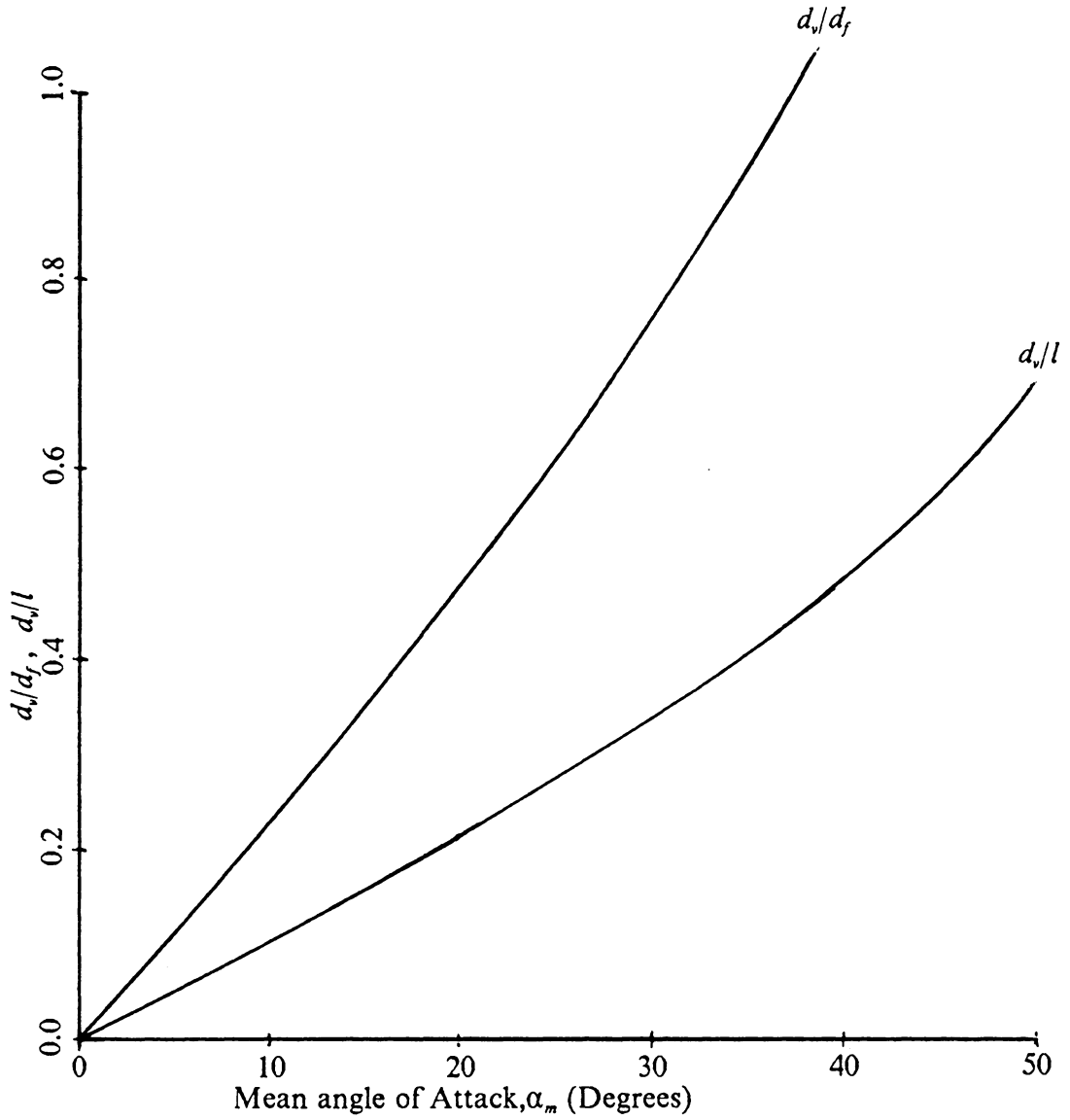

Fig. 90. Flush-Out Criteria; Solidity = 0.75, Stagger = 25

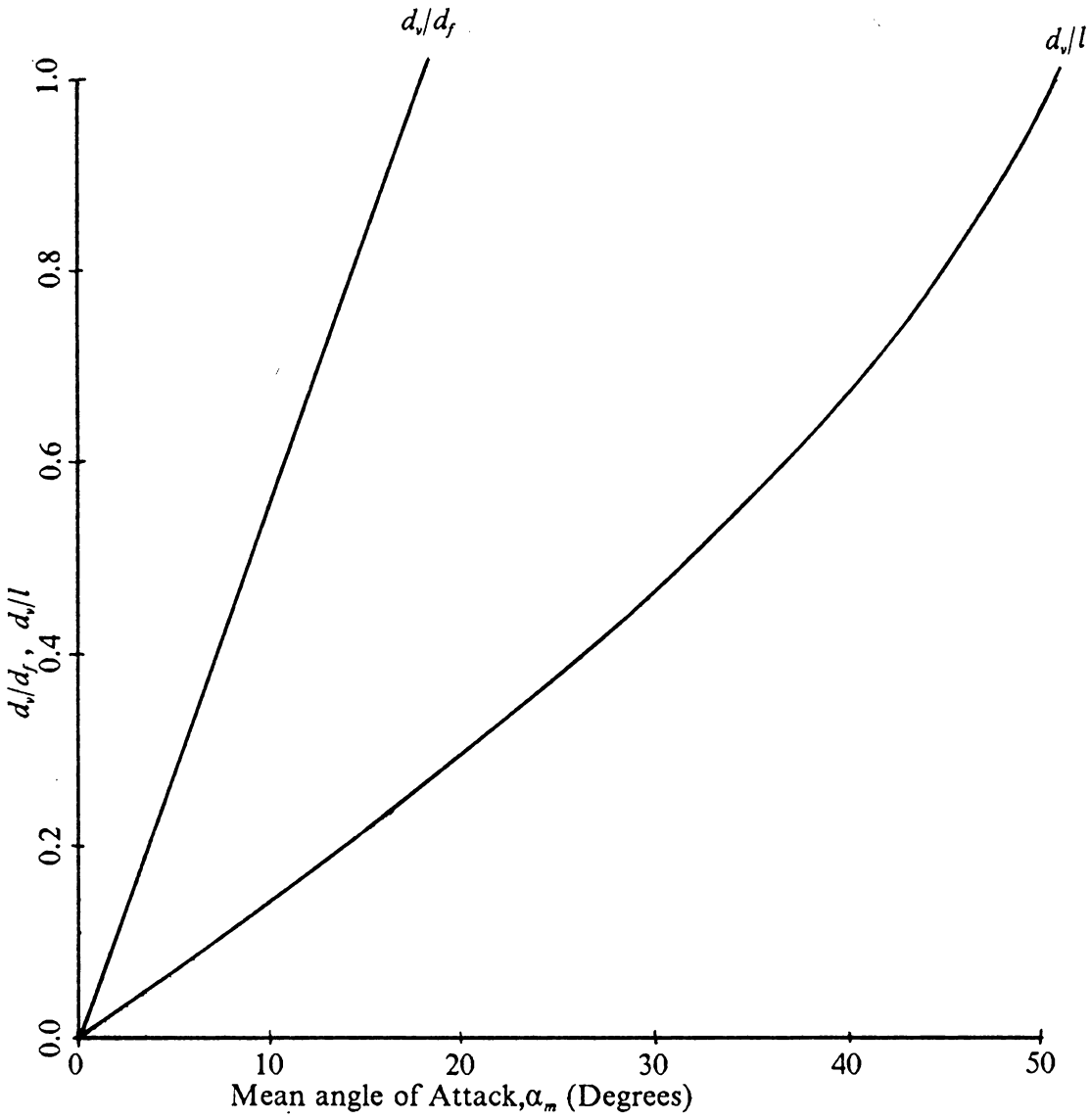

Fig. 91. Flush-Out Criteria; Solidity = 0.75, Stagger = 36.5

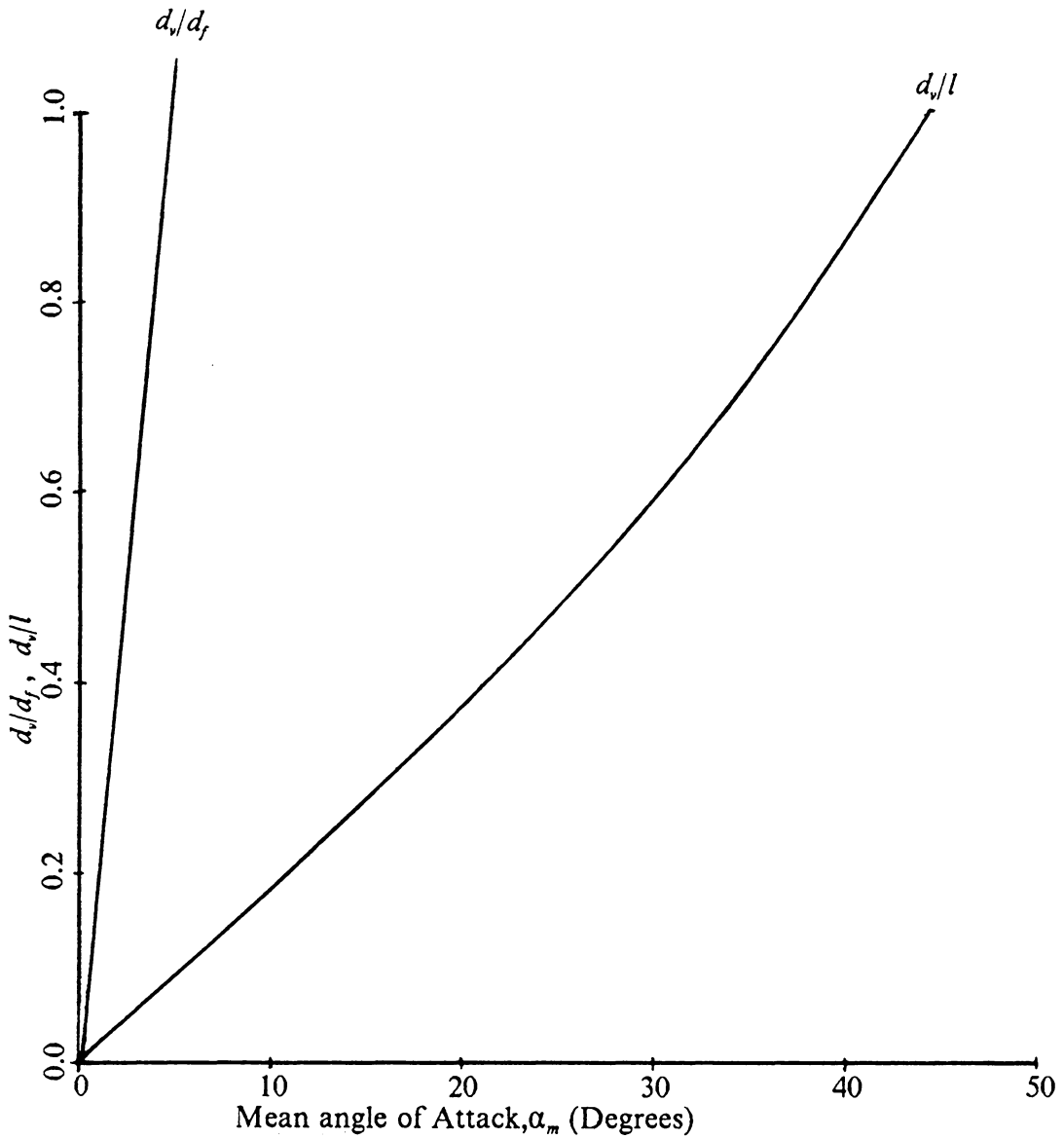

Fig. 92. Flush-Out Criteria; Solidity = 0.75, Stagger = 45

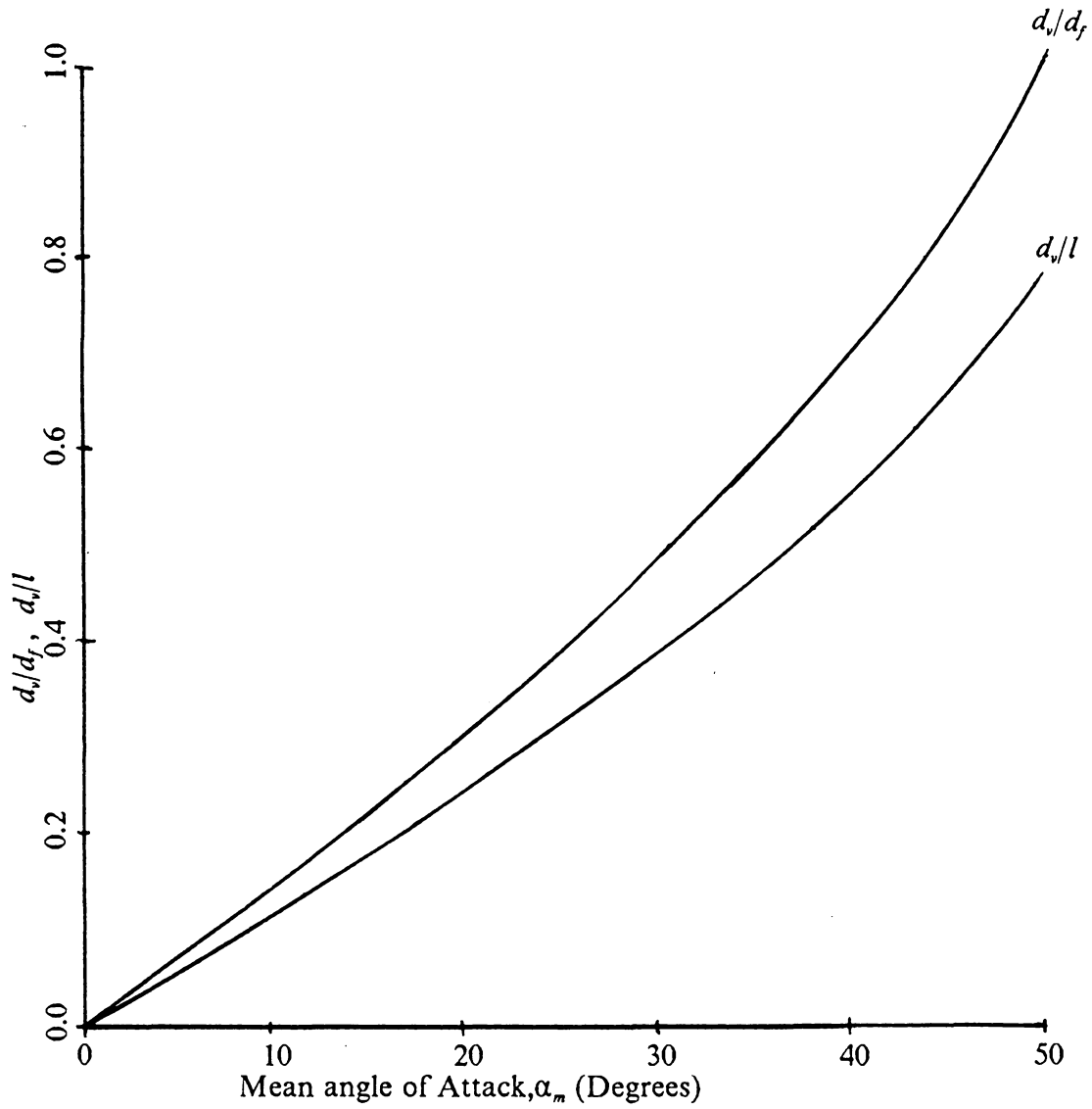

Fig. 93. Flush-Out Criteria; Solidity = 1.0, Stagger = 25

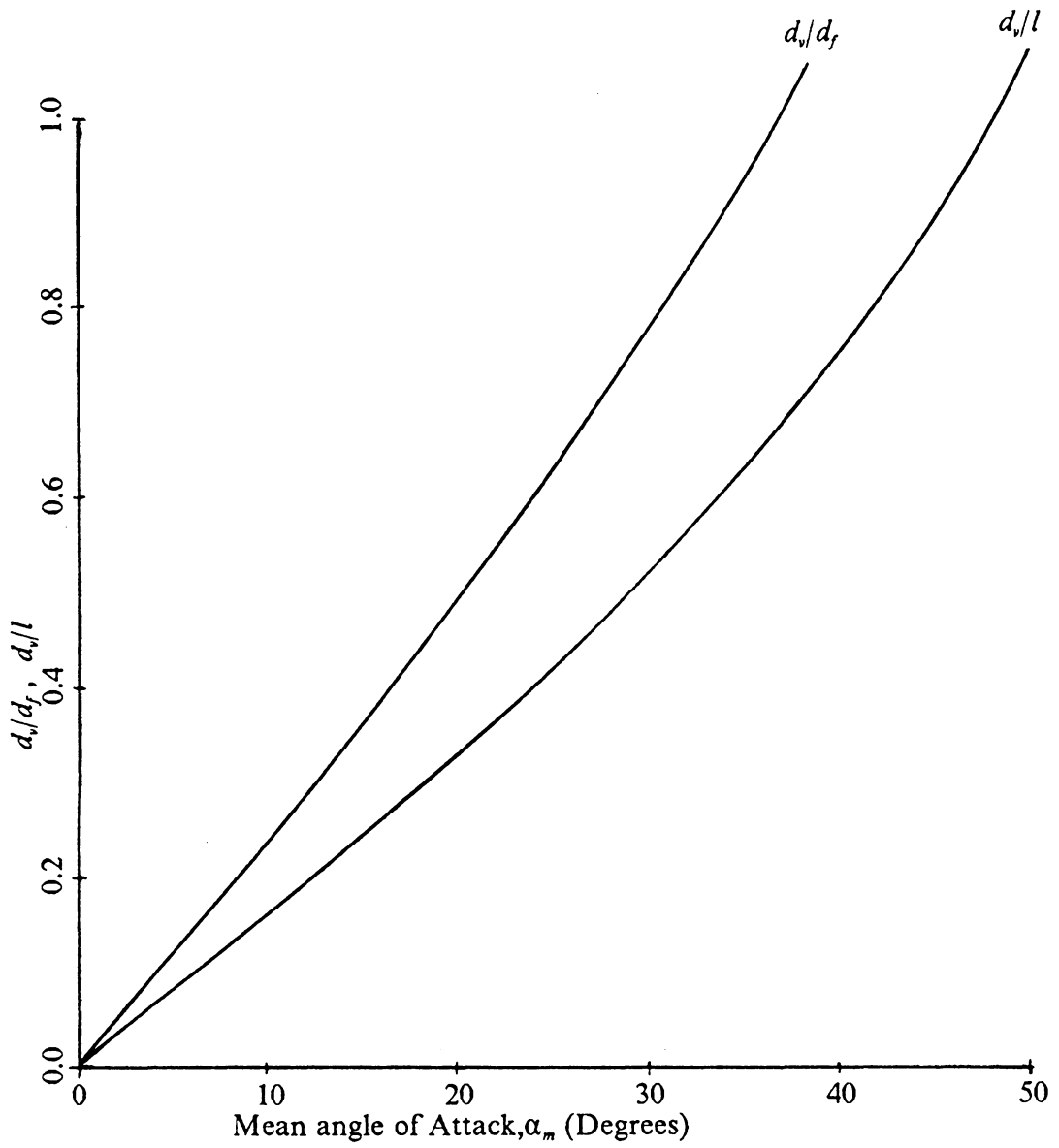

Fig. 94. . Flush-Out Criteria; Solidity = 1.0, Stagger = 36.5

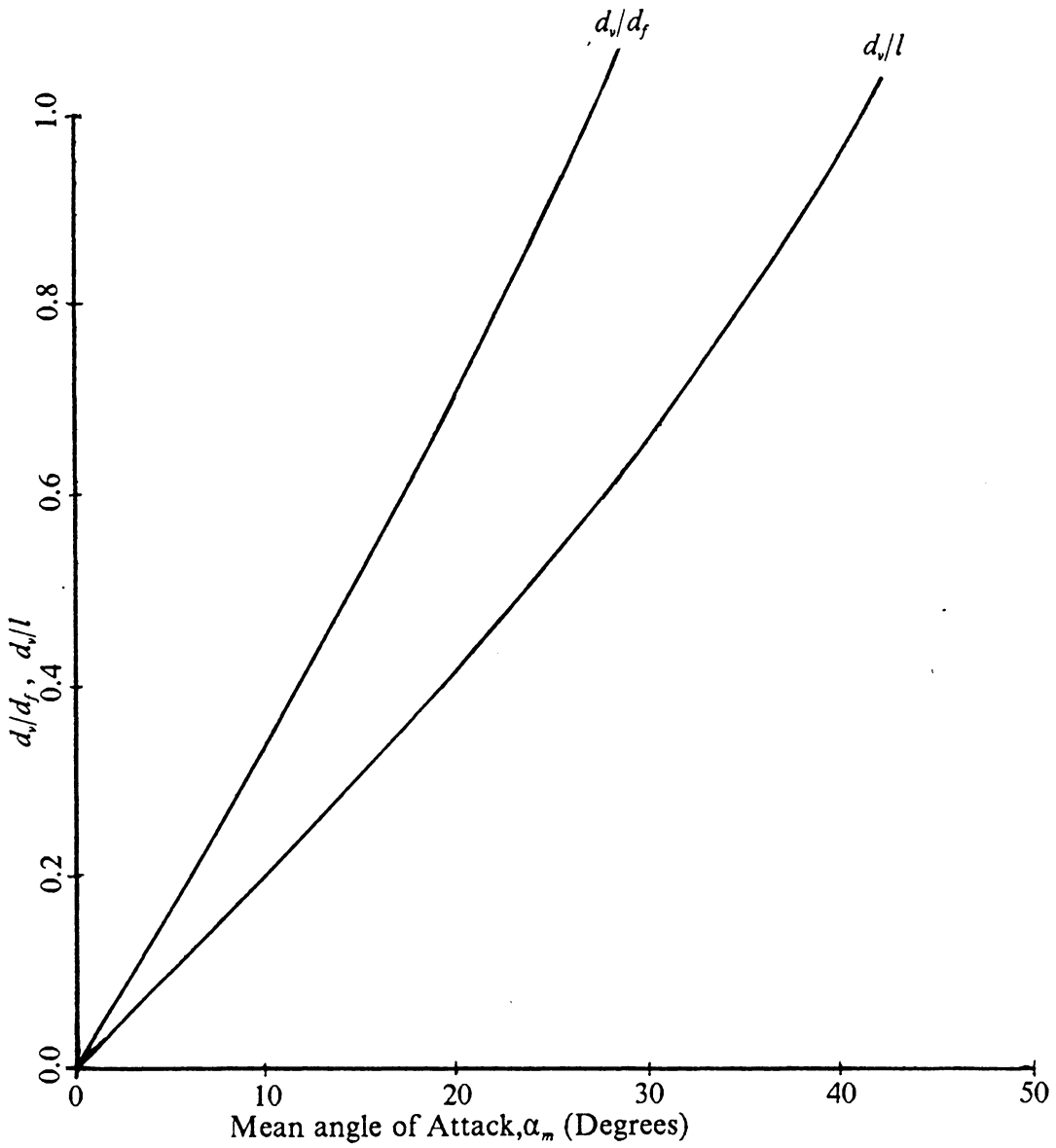

Fig. 95. Flush-Out Criteria; Solidity = 1.0, Stagger = 45

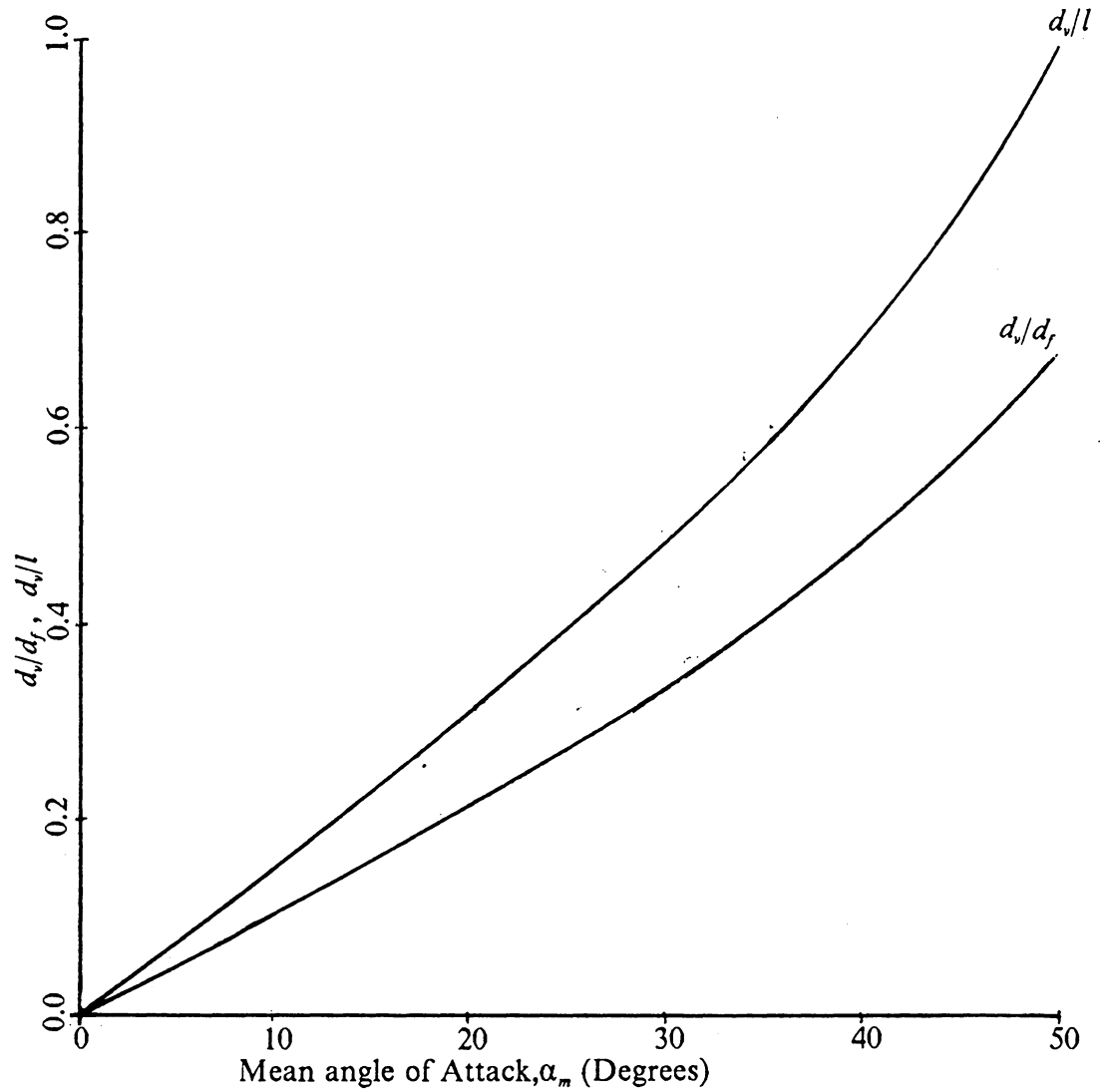

Fig. 96. Flush-Out Criteria; Solidity = 1.5, Stagger = 25

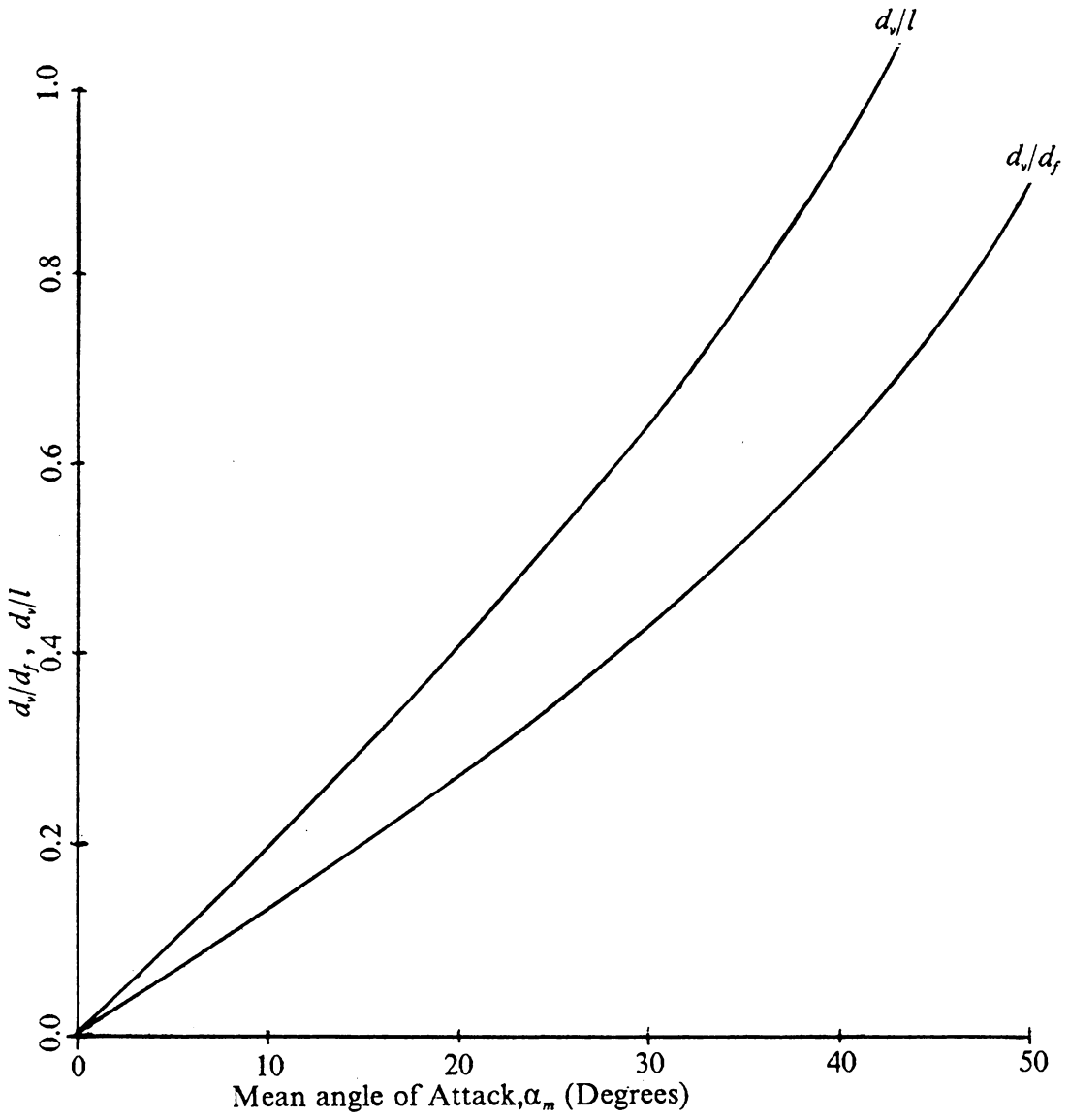

Fig. 97. Flush-Out Criteria; Solidity = 1.5, Stagger = 36.5

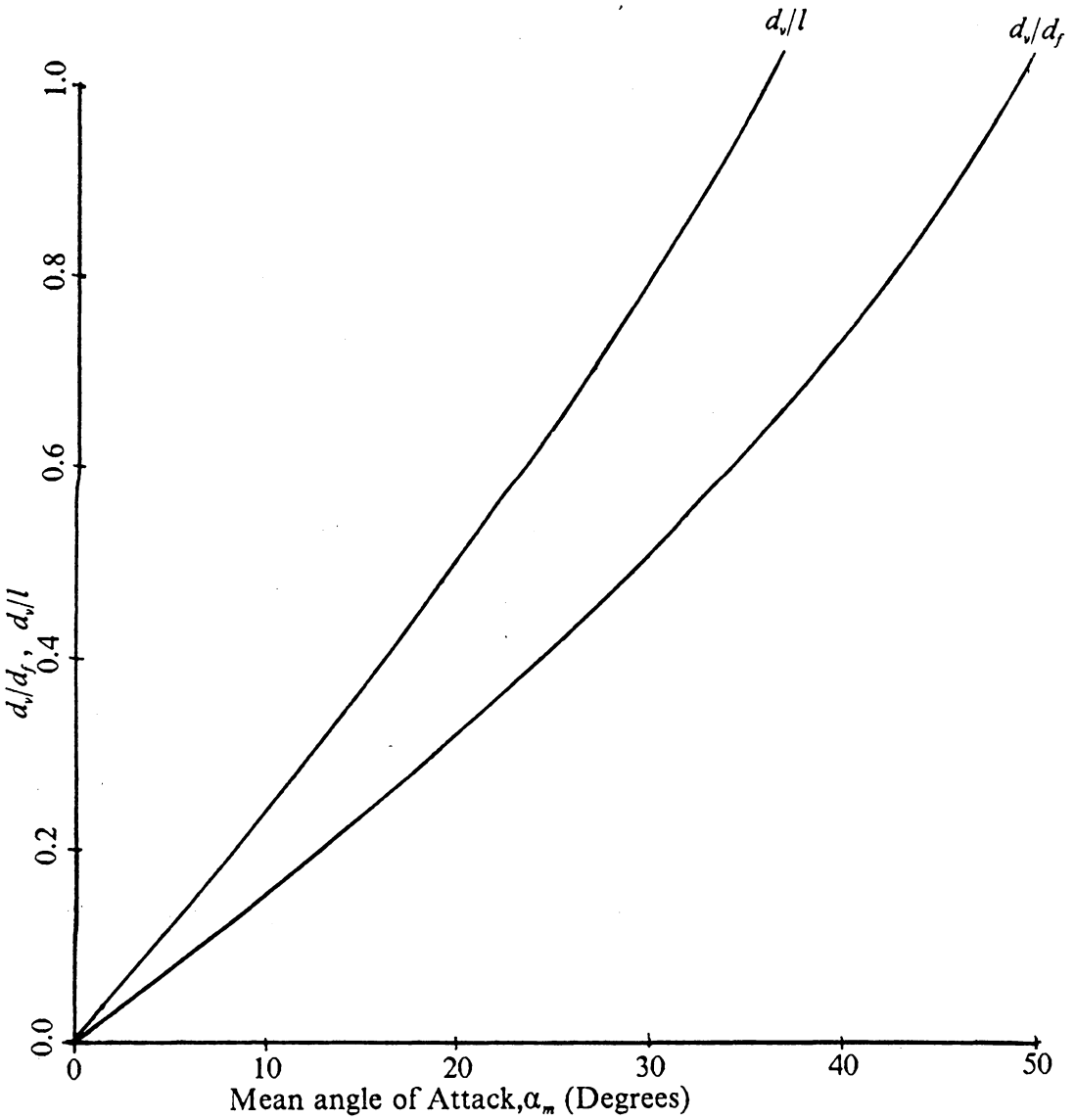

Fig. 98. Flush-Out Criteria; Solidity = 1.5, Stagger = 45

The vortex diameter can be reduced by reducing the boundary layer thickness. This is done by decreasing the angle of attack, which is equivalent to increasing the mass flow rate through a compressor. Increasing the flush-out diameter is done by increasing the solidity or by decreasing the stagger angle. The perpendicular distance between the blades is increased by increasing the stagger or decreasing the solidity. Thus, increasing the perpendicular blade spacing decreases the value of the flush-out diameter. Since the flush-out diameter relation is usually the critical factor, increasing the flush-out diameter is of primary concern to inhibit propagating stall inception.

One notable curiosity of the model is that the predicted angle of attack for propagating stall inception to occur is higher than the angle of attack where propagating stall inception actually occurred in the cascade. This may be due to fact that the flow through the cascade develops non-uniformities, perhaps the largest being the development of the boundary layer on the top wall of the cascade. This boundary layer contributes to the blockage of the flow in the top passage. This blockage increases the angle of attack on the next blade to an extent that a vortex, which satisfies the the flush-out criteria, develops in the next passage and propagating stall is initiated even though the necessary mean angle of attack has not been reached.

From the observation that propagating stall occurred at stagger angles of 36.5 and 45 degrees but not at a stagger angle of 25 degrees, it is suggested that the flow distortion caused by the development of the boundary layer on the top wall was sufficient to cause propagating stall inception at the higher stagger angles but, for

the range of geometries tested, not at the lower stagger angle. This can be explained by the fact that the 25 degree stagger angle case has more flow area in each passage. Then, for a relatively equal boundary layer development along the top wall, a lower percentage of flow area is blocked and less flow is diverted to the next passage. Since less flow is diverted from the top passage, a lower magnitude distortion is created in the next passage. At the 25 degree stagger angle, the flow distortion is sufficiently reduced so that stall propagation does not occur for the range of angles of attack tested. This and the model's prediction that the operation point for the 25 degree stagger angle is farther from the inception point than for the higher staggers explain why propagating stall occurred at stagger angles of 36.5 and 45 degrees but not at 25 degrees.

A second analysis method employing the geometric model to predict propagating stall inception is to calculate the flow disturbance size which causes propagating stall inception for known average flow conditions. Figures 99, 100, and 101 show the variation of the stall inception disturbance size with the mean angle of attack. These plots are generated by setting the value of the propagating stall inception criteria to 1.0 and calculating the angle of attack which satisfies this equation. Then, the flow disturbance magnitude, for known average flow conditions, is simply the difference of the calculated required local angle of attack and the mean angle of attack. This analysis method shows the flow disturbance size which initiates propagating stall as a function of the blade geometry and the average flow conditions. If an estimate for the actual flow disturbances experienced by the blading is known, it can be determined if propagating stall is likely be onset

in a cascade, and, by extension, if rotating stall will be onset in a compressor. From the graphs, Figs. 99, 100, and 101, it can be seen that reducing the stagger angle increases the flow distortion magnitude necessary for propagating stall inception, as does increasing the solidity. Also, reducing the angle of attack increases the necessary flow distortion size. These results agree with the results obtained using the first analysis method. Decreasing the stagger angle, decreasing the angle of attack, and increasing the solidity all make a cascade, or a compressor, more resistant to propagating, or rotating, stall inception, respectively.

With regard to recovery, the results help to explain the recovery process. It is known that when a compressor is operating in rotating stall, normal operation will resume if the flow coefficient is increased to a certain value. In the model, increasing the flow coefficient reduces the angle of attack on the blades. The stall cell propagates because the increased angle of attack on the next blade, caused by the stalled passage, is large enough to stall it. As the average angle of attack is decreased, the distortion size necessary to continue propagation and produce the required blockage is increased. At some point, the stall cessation point, the increase in angle of attack caused by the blockage in the stalled passage is not large enough to cause the next blade to flush-out its vortex. The stall cell dies out and the flow is redistributed along the blade row. This process corresponds to increasing the flow coefficient of a compressor which is operating in rotating stall and moving the operating point until the stall cessation line is encountered.

In summary, Two analysis methods have been developed employing the geometric model for propagating stall inception. Both show that increasing the

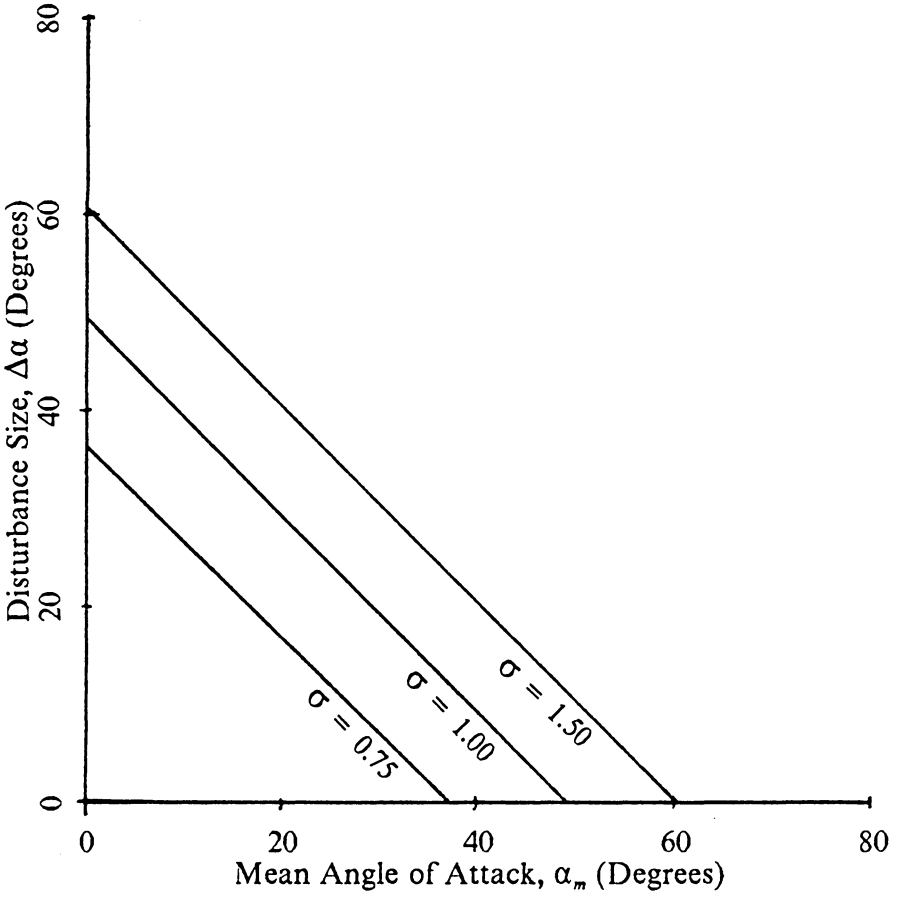

Fig. 99. Stall Inception Disturbance Size; Stagger = 25

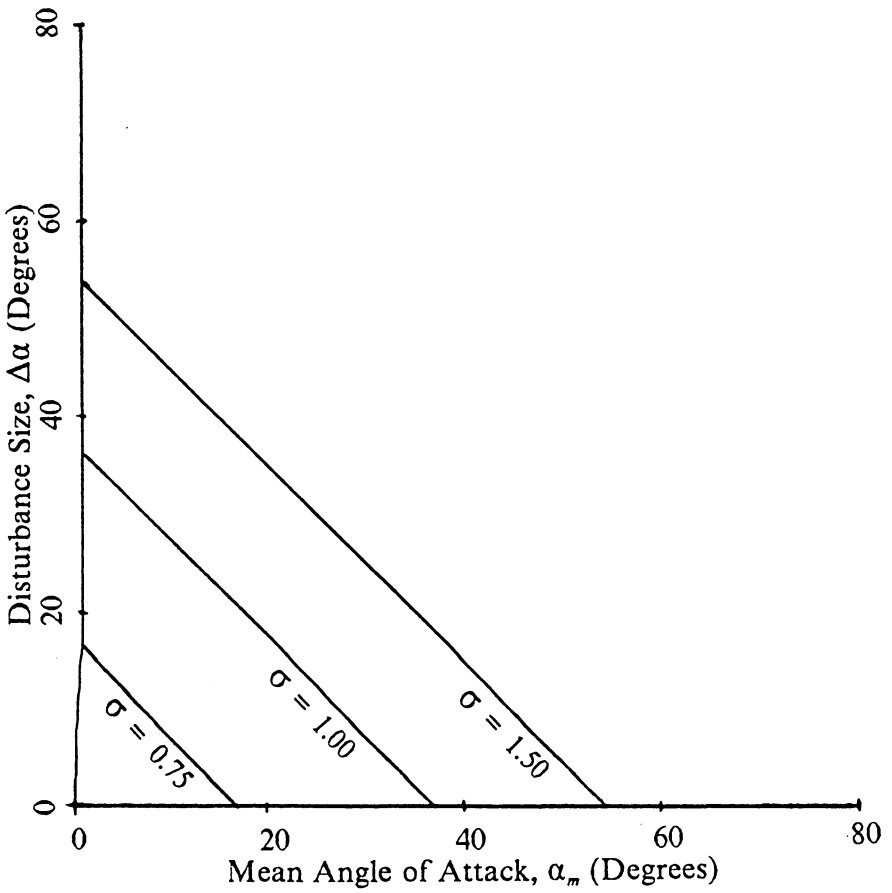

Fig. 100. Stall Inception Disturbance Size; Stagger = 36.5

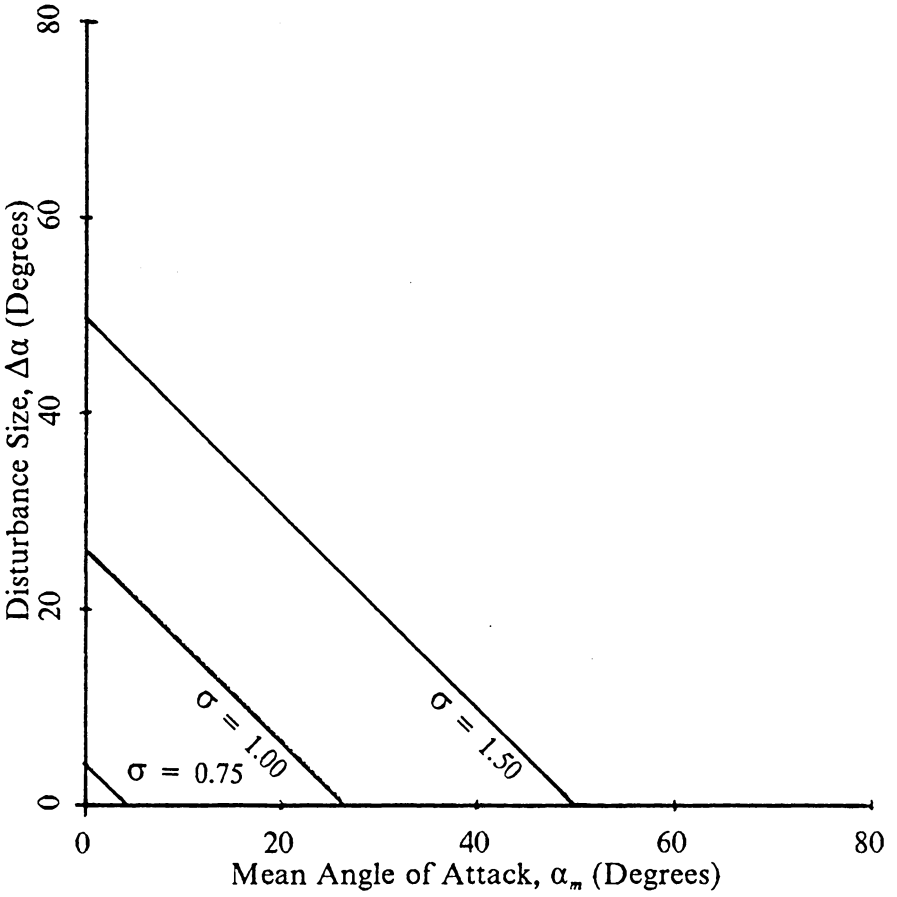

Fig. 101. Stall Inception Disturbance Size; Stagger = 45

solidity and decreasing the stagger angle of the blade row make a cascade more resistant to propagating stall inception, and, by extension, make a compressor more resistant to rotating stall inception. Also, reducing the angle of attack creates a more stable flow condition. The methods also show the relation of the models to the stall recovery process. Using the models, an estimate for the flow distortion size necessary to cause propagating stall inception for known mean flow conditions can be calculated. This gives an indication of the probability that propagating stall will occur. The models also show the effects of blade stagger angle and solidity on the propagating stall inception point.

Conclusions and Recommendations

Flow visualization movies showing flow through a cascade disclosed the presence of the periodic growth and shedding of a vortex between blade passages. This occurrence was observed at stagger angles of 36.5 and 45 degrees, but not at 25 degrees, for angles of attack of 20 degrees or more. The process observed was a propagating stall process which propagated along the blade row. Previous rotating stall models focused attention primarily on the losses incurred by a compressor during operation in rotating stall and did not concentrate on the effects of the blade geometry in predicting rotating stall inception. The movies, however, show the blade geometry and its effects on the local flow to be vital to propagating stall inception. From this work and previous research on blading effects, inferences on how the solidity, stagger angle, aspect ratio, and blade nose shape affect the inception point of propagating stall can be made.

The propagation speed of the vortex seen in the movies was measured using a viewing and counting process. Results have shown that, with respect to the angle of attack, the propagation speed is lower at the stall inception point where a developing stall condition exists. The observed lower propagation speeds for the partially-developed stall conditions are thought to be due to the reduced blockage of the blade passages and the different flow separation experienced by the blading. The ratios of the measured propagation speeds to the relative velocities, for fully-developed propagating stall, averaged 0.265 $\pm$ 20 percent. Least squares approxi-

mations to the data showed it to be only slightly dependent on the parameters of angle of attack, relative inlet velocity, and stagger angle. Thus, for the range of tested geometries in the fully-developed propagating stall region, the propagation speed can be represented as independent of the stagger angle and angle of attack and proportional to the relative velocity and blockage in the blade passages.

The findings that a propagating stall condition existed at stagger angles of 36.5 and 45 degrees but not at 25 degrees indicated that the stagger angle has an effect on propagating stall inception. The observed vortex growth and subsequent shedding was used as the basis for a two-dimensional geometric model for stall inception. The vortex shedding was the result of the reverse flow from the previously stalled passage interfering with the vortex flow, thus dissipating it and causing full blockage in the blade passage. Then, the incoming flow flushed the stagnated vortex out of the passage. The vortex was modeled in two dimensions as a circle which grew in the blade passages and was contained in the boundary layer along the suction side of the stalled passage. Based on the observed vortex shedding mechanism, a characteristic diameter was calculated to predict the point at which shedding would occur. The 'flush-out' diameter, d_f, was based solely on the geometry of the blading, specifically the stagger angle, the solidity, and the chord length. Using this model and a model for the boundary layer growth along the blade, the inception point of propagating stall can be predicted. The model showed that blade geometries with low stagger angles and high solidities are more resistant to propagating stall inception. Lower angles of attack, which correspond to higher flow rates in a compressor, are also more resistant to initiation of propagating stall.

In previous research efforts, the effects of aspect ratio, endwall boundary layer growth, and blade nose shape on rotating stall have been investigated by Koch and Smith [20, 21], Russ [22], and Cheers and Funnel [19]. Compressors with low aspect ratios have been shown to stall at lower flow rates than those with higher aspect ratios. They are thus more resistant to rotating stall inception. The endwall boundary layer growth, which is affected by the blade shape and tip clearance, contributes to flow area blockage. However, the endwall boundary layer growth is a separate phenomenon from propagating stall and it is felt that extended endwall boudary layer growth may retard the transition to leading edge stall and give better recovery ability to a compressor. Thus, endwall boundary layer growth may be a stabilizing factor in controlling propagating or rotating stall. The shape of the nose of the blade is also an important factor in determining the type of stalling behavior experienced by the blade. Rounder noses on blades have been shown to give a gradual, steady transition from trailing edge to leading edge separation. Sharper noses, however, give abrupt an abrupt transition to leading edge separation, from which it is more difficult to return to trailing edge separation. Since, as shown in this study, the primary propagating stalling behavior is associated with leading edge separation, it is suggested that blading with rounded noses and which develop thicker endwall boundary layers will be more resistant to propagating, or rotating, stall inception and will exhibit better recovery characteristics.

Recovery from rotating stall has been shown to be related to the shape of the compressor operating characteristic. Characteristics with closely-spaced stalled and unstalled operating lines have better recovery capability. In regard to the geomet-

ric model, recovery occurs because the angle of attack has been sufficiently reduced so that the disturbance caused by the stalling of a blade is not large enough to continue the propagation process. It should be noted, however, that blade designs which require large disturbances for propagating stall inception may experience severe recovery problems if propagating stall does occur. Blade geometry affects the shape of the compressor characteristic and the model helps to explain the recovery process.

What should be done to further the understanding of propagating and rotating stall? Research is needed to supply information on additional geometry effects on propagating stall inception and on propagation speed. Research along the following lines is suggested.

1. Test different solidity cases to determine the effect of solidity on propagation speed and to test the predicted effect on stall inception.

2. Test blades with different nose shapes to determine the effect on propagating stall inception, as suggested by the work of Cheers and Funnell.

3. Test blading with different aspect ratios to include in the model the effects of aspect ratio.

4. Test blading which encourages endwall boundary layer development to qualify the inferences made from the work of Koch and Smith [20,21], and Russ[22].

5. Test blades of varying turning angles to determine the turning angle effect on propagation speed and stall inception (the model is based on research done on flat-bottomed blades which have been modeled as flat plates).

6. Test different stagger angles to test the predictions of the model.

7. Measure the flow in a stalled passage to determine the exact location of the vortex and flush-out point to improve on the assumptions made about these parameters in the model.

8. Conduct flow measurements to determine importance of three-dimensional flow effects on propagating stall.

9. Test at different velocities to determine the linearity of propagation speed with relative velocity.

10. Test in compressors to determine correlation between the model based on cascade testing and actual compressor performance.

Further investigation along these lines will extend and improve upon the current model for predicting propagating stall inception and propagation speed.

In conclusion, the results have shown that propagating stall inception is very dependent on the blade geometry, while the propagation speed is not. The propagation speed is related to the blockage of the flow area in the blade passage and the relative velocity to the blades. After a fully-developed stall condition is reached,

the propagation velocity is independent of the the angle of attack but is correlated with a Strouhal number. The fully-developed propagating stall condition is characterized by the development of a two-dimensional leading edge separated boundary layer on a blade which develops a vortex, completely blocking the involved passage. A geometric model has been developed, based on the stagger angle and solidity, to predict stall inception. Further research should allow for inclusion of the effects of aspect ratio, turning angle, blade nose shape, and tip clearance in the geometric model.

From the research that has been done to date, blading with low stagger angles are more resistant to propagating stall inception. Further, it is predicted that high solidities, low aspect ratios, and round blade noses make a cascade more resistant to propagating stall inception, and, by inference, make a compressor more resistant to the inception of rotating stall. Designing so as to prevent propagating or rotating stall inception could lead to serious recovery problems, so compromise is indicated. The geometric model that has been developed is based on the local flow dynamics and knowledge of the effects of blade geometry on propagating stall, which appear essential to accurately modeling the propagating stall phenomenon.

Bibliography

1. Emmons, H. W., C. E. Pearson, and H. P. Grant, "Compressor Surge and Stall Propagation," Transactions of the American Society of Mechanical Engineers, May 1955, pg. 455-469.

2. Iura, T., and W. D. Rannie, "Experimental Investigations of Propagating Stall in Axial-Flow Compressors," Transactions of the American Society of Mechanical Engineers, April 1954, pg. 463-471.

3. Stenning A. H., and A. P. Friebel, "Stall Propagation in a Cascade of Airfoils," ASME Paper, No. 57-5A-29, 1957.

4. Sears, W. R.,"Rotating Stall in Axial Compressors," Journal of Applied Mathematics and Physics, Vol. 6, 1955, pg. 429-455.

5, Marble, F. E., "Propagation of Stall in a Compressor Blade Row," Journal of the Aeronautical Sciences, Vol. 22, 1955, pg. 541-554.

6. Emmons, H. W., R. E. Kronauer, and J. A. Rockett, "A Survey of Stall Propagation - Experiment and Theory," Journal of Basic Engineering, Sept. 1959, pg. 409-416.

7. Spalart, P. R., "Two Recent Extensions of the Vortex Method," Unsteady Flows in Turbomachines, Von Karman Institute for Fluid Dynamics; Lecture series 1984-02, Feb. 20-24, 1984.

8. Takata, H., and S. Nagano, "Nonlinear Analysis of Rotating Stall," Journal of Engineering for Power, Oct. 1972, pg. 279-293.

9. Adamczyk, J. J., and F. O. Carta, "Unsteady Fluid Dynamic Response of an Axial-Flow Compressor Stage with Distorted Inflow," Project Squid Technical Report UARL-2-PU, 1973.

10. Sexton, M. R., and W. F. O'Brien, "A Model for Dynamic Loss Response in Axial-Flow Compressors," ASME Paper, No. 81-gt-154, March 1981.

11. Greitzer, E. M., "Surge and Rotating Stall in Axial Flow Compressors. Part I: Theoretical Compression System Model," Journal of Engineering for Power, Vol. 98, April 1976, pg. 190-198.

12. Greitzer, E. M., "Surge and Rotating Stall in Axial Flow Compressors. Part II: Experimental Results and Comparison with Theory," Journal of Engineering for Power, Vol. 98, April 1976, pg. 199-217.

13. Greitzer, E. M., "Review - Axial Compressor Stall Phenomena," Journal of Fluids Engineering, Vol. 102, June 1980, pg. 134-151.

14. Moore, F. K., "A Theory of Rotating Stall of Multistage Axial Compressors: Part I - Small Disturbances," Journal of Engineering for Gas Turbines and Power, Vol. 106, April 1984, pg. 313-320.

15. Moore, F. K., "A Theory of Rotating Stall of Multistage Axial Compressors: Part II - Finite Disturbances," Journal of Engineering for Gas Turbines and Power, Vol. 106, April 1984, pg. 321-326.

16. Moore, F. K., "A Theory of Rotating Stall of Multistage Axial Compressors: Part III - Limit Cycles," Journal of Engineering for Gas Turbines and Power, Vol. 106, April 1984, pg. 327-336.

17. Day, I. J., E. M. Greitzer, and N. A. Cumpsty, "Prediction of Compressor Performance in Rotating Stall," Journal of Engineering for Power, Vol. 100, Jan. 1978, pg. 1-14.

18. Lieblein, S., "Loss and Stall Analysis of Compressor Cascades," Journal of Basic Engineering, Vol. 81, Sept. 1959, pg. 387-400.

19. Cheers, F., and G. C. Funnell, "Note on the Speed of Stall Propagation in a Cascade of Aerofoils," The Aeronautical Quarterly, May 1965, pg. 179-186.

20. Koch, C. C., and L. H. Smith, "Loss Sources and Magnitudes in Axial-Flow Compressors," Journal of Engineering for Power, Vol. 98, July 1976, pg. 411-424.

21. Koch, C. C., "Stalling Pressure Rise Capapability of Axial Flow Compressor Stages," Journal of Engineering for Power, Vol. 103, Oct. 1981, pg. 645-656.

22. Russ, W., Personal communication, 1986.

23. Mathioudakis, K., and F. A. E. Breugalmans, "Structure of Rotating Stall Cells: 1. - Absolute Motion," Unsteady Flows in Turbomachines, Von Karman Institute for Fluid Dynamics; Lecture series 1984-02, Feb. 20-24, 1984.

24. Mathioudakis, K., and F. A. E. Breugalmans, "Structure of Rotating Stall Cells: 2. - Relative Motion," Unsteady Flows in Turbomachines, Von Karman Institute for Fluid Dynamics; Lecture series 1984-02, Feb. 20-24, 1984.

25. Cumpsty, N. A., and E. M. Greitzer, "A Simple Model for Compressor Stall Cell Propagation," Journal of Engineering for Power, Vol. 104, Jan. 1982, pg. 170-176.

26. Zika, V. J., "Approximation of Rotating Stall by Finite-Discontinuity Modeling," ASME Paper, No. 81-WA/FE-15, 1981.

27. Cousins, W. T., and W. F. O'Brien, "Axial-Flow Compressor Stage Post-Stall Analysis," AIAA Paper, No. AIAA-85-1349, 1985.

28. Tkacik, P. T., M. S. Thesis, Virginia Polytechnic Institute and State University, 1982.

29. Yocum, A., Personnel communication, 1986.

30. Tamaki, T., and S. Nagano, "Experimental Evaluation of an Axial-Flow Transonic Compressor," ASME Paper, No. 76-GT-34, 1976.

31. Pandolfi, M., and G. Colasurdo, "Numerical Investigations on the Generation and Developement of Rotating Stall," ASME Paper, No. 78-WA/GT-5, 1978.

32. Cossar, B. F. J., W. C. Moffatt, and R. E. Peacock, "Compressor Rotating Stall in Uniform and Nonuniform Flow," Journal of Engineering for Power, Vol. 102, Oct. 1980, pg. 762-769.

33. Gostelow, J. P., Cascade Aerodynamics, 1st ed., Pergamon Press, Oxford, 1984.

34. Schlichting, H., Translated by J. Kestin, Boundary-Layer Theory, 6th ed., Mcgraw-Hill Book Company, New York, 1968.

APPENDICES

Appendix A: Derivation of Flush Out Diameter

A geometric parameter has been developed which is a limiting size for vortex growth in a blade passage during operation in rotating stall. This parameter is the flush out diameter, the diameter at which vortex shedding occurs. The derivation of this parameter follows.

The model on which the derivation is based is a two-dimensional model as shown in Fig. A-1. The vortex is modeled as a circle that is tangent to the blade, which is modeled as a thin flat blade, and the perpendicular from the leading edge of the leading blade. In the figure, The vortex is tangent to blade AC at point G and to perpendicular BD at point F. Shedding occurs when the vortex diameter is large enough that it intersects the trailing face of the blades, line CE. This intersection occurs at point H.

Using basic geometry, the vortex diameter necessary for shedding to occur can be calculated. It is easily shown that:

$$m = c - s\sin(\zeta)$$

Angle ACE is:

$$ACE = 90 + \zeta$$

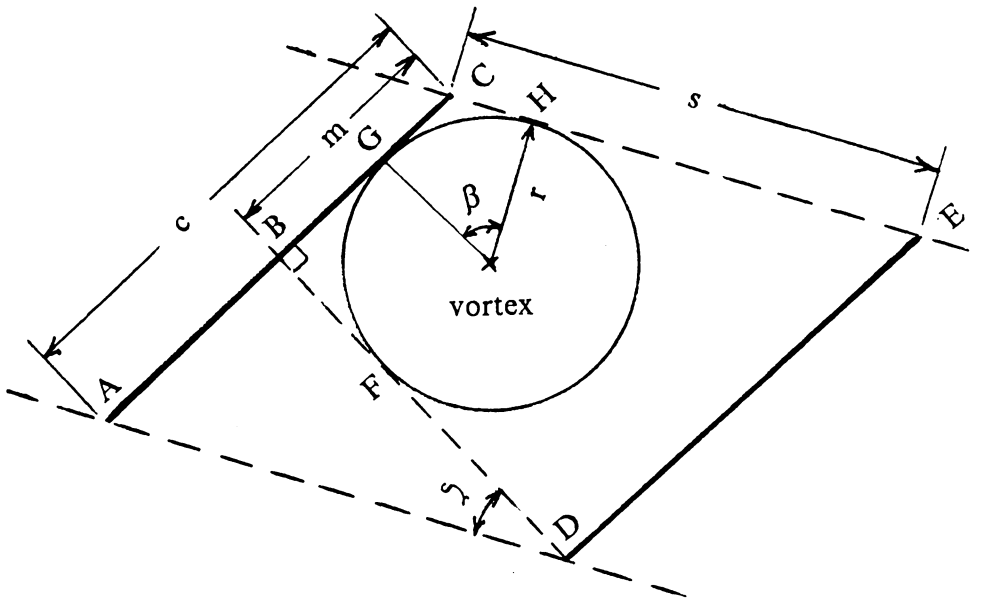

Fig. A-1. Model for Flush Out Diameter Derivation

Since the vortex is tangent at points F, G and H:

$$\beta = 90 - \zeta$$

which yields another equation for m:

$$m = r + r\tan(\beta/2)$$

or,

$$m = r[1 + \tan(45 - \zeta/2)]$$

Combining the two equations for m gives:

$$r = \frac{c - s\sin(\zeta)}{1 + \tan(45 - \zeta/2)}$$

Since $d_f = 2r$, rearranging gives:

$$d_f = 2c\left[\frac{1 - \sin(\zeta)/\sigma}{1 + \tan(45 - \zeta/2)}\right]$$

Appendix B: Derivation of Boundary Layer Growth and Vortex Diameter Model

A geometric model has been developed for the boundary layer and vortex growth along the suction side of a blade. The theoretical model is based on the geometry and coordinate system in Fig. B-1. The blade is modeled as a straight blade of negligible thickness.

The boundary layer growth is assumed to be linear between the stalled blade's leading edge and the perpendicular from the leading edge of the next blade. Quadratic boundary layer growth is assumed from this point to a point which lies a distance of half the flush out diameter downstream, st which point the boundary layer thickness is a maximum. The growth downstream of this point is unimportant to the model. Using the notation of Fig. B-1, the boundary layer growth is linear between points A and F and quadratic between points F and G.

The linear boundary layer growth is proportional to the tangent of the angle of attack. The general equation for the boundary layer thickness, $\delta(x)$, has the form,

$$\delta(x) = Ax + B$$

and has the following boundary conditions:

$$\delta(0) = 0$$

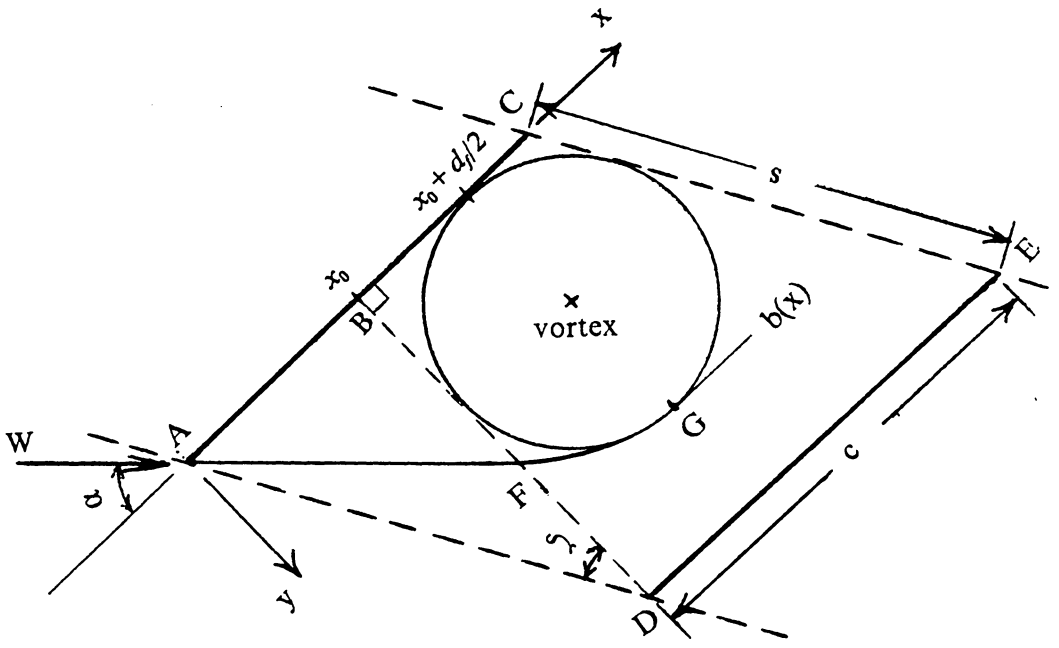

Fig. B-1. Model for Boundary Layer Growth

and

$$\frac{d\delta}{dx}(0) = \tan(\alpha)$$

This gives the following equation for the blockage in the linear growth section:

$$\delta(x) = x\tan(\alpha)$$

for $x \leq x_o$, where

$$x_0 = s\sin(\zeta) = c\left[\frac{\sin(\zeta)}{\sigma}\right]$$

In the quadratic growth region, between points F and G, the boundary layer growth equation has the following form:

$$\delta(x) = Ax^2 + Bx + C$$

The following boundary conditions are applied:

$$\delta(x_0) = x_0\tan(\alpha)$$

$$\frac{d\delta}{dx}(x_0) = \tan(\alpha)$$

$$\frac{d\delta}{dx}(x_0 + d_f/2) = 0$$

The equation for the bondary layer thickness when $x_0 \leq x \leq x_0 + d_f/2$ is:

$$\delta(x) = d_f \tan(\alpha)\left[\frac{x}{d_f}(1 + 2\frac{x_0}{d_f}) - \frac{x^2 + x_0^2}{d_f^2}\right]$$

The vortex diameter used in the analysis is taken to be the maximum boundary layer thickness. This occurs at $x = x_0 + d_f/2$. At this value of x the boundary layer thickness is:

$$d_v = \delta(x_0 + d_f/2) = \tan(\alpha)\left[x_0 + \frac{d_f}{4}\right]$$

Appendix C: Data

Definition of terms, Occurrence Frequency Data

OCCURRENCE	-	Observation of the development of a vortex
NO.	-	The number of the observation
FT	-	Foot number on the film where the occurrence was observed
FRAME	-	Frame number on the film where the occurrence was observed
DFRAME	-	Number of frames separating occurrences
PERIOD	-	Time period calculated from DFRAME and film speed < sec. > , (or PER.)
FREQUENCY	-	1.0 / PERIOD < hz > , (or FREQ.)
MEAN	-	Average value of DFRAME
STD.DEV.	-	Standard deviation of DFRAME

Definition of terms, Propagating Data

CELL	-	A vortex occurrence which blocks a passage
NO.	-	The number of the observation
FRAMES	-	The number of frames to follow the propagation of the stall cell
PASS.	-	The number of blade passages through which the stall cell propagates
PERIOD	-	The time period calculated from FRAMES and the film speed < sec. >
FREQ.	-	1.0 / PERIOD < hz >
VPROP	-	The calculated propagation velocity < ft/sec >
W	-	The relative inlet velocity < ft/sec >

Stagger angle= 36.5 , Angle of attack= 20 , Inlet velocity= 55.4 ft/sec.

OCCURRENCES IN CENTER PASSAGE

THERE ARE 5 OCCURRENCES

NO.	FT FRAME		DFRAME	PERIOD <SEC>	FREQUENCY <HZ>
0	7.0	0.0			
1	18.0	23.0	463.0	0.115750	8.64
2	20.0	7.0	64.0	0.016000	62.50
3	29.0	36.0	389.0	0.097250	10.28
4	43.0	10.0	534.0	0.133500	7.49
5	62.0	21.0	771.0	0.192750	5.19

THE 2 ENTRY IS NOT INCLUDED IN THE STATS

MEAN= 539.2500 STD.DEV.= 165.4537 PER.= 0.134812 FREQ.= 7.4177

CALCULATION OF PROPAGATION SPEED FROM PROPAGATING DATA

THERE ARE 4 PROPAGATING STALL CELLS NOTED

NO.	FRAMES	PASS.	PERIOD SEC.	FREQ. HZ.	VPROP FT/SEC	VPROP/W
1	173.000	2.000	0.02162500	46.243	9.8651	0.17807
2	263.000	3.000	0.02191666	45.627	9.7338	0.17570
3	88.000	1.000	0.02200000	45.455	9.6970	0.17504
4	115.000	1.000	0.02875000	34.783	7.4203	0.13394

MEAN= 94.2916 STD.DEV.= 0.138205E+02

AVERAGE VALUES

PER.= 0.023573 FREQ= 42.422 VPROP= 9.0499 VPROP/W= 0.16336

Stagger angle= 36.5 , Angle of attack= 22 , Inlet velocity= 55.3 ft/sec.

OCCURRENCES IN CENTER PASSAGE

THERE ARE 6 OCCURRENCES

NO.	FT FRAME		DFRAME	PERIOD <SEC>	FREQUENCY <HZ>
0	0.0	27.0			
1	4.0	27.0	160.0	0.040000	25.00
2	6.0	25.0	78.0	0.019500	51.28
3	10.0	27.0	162.0	0.040500	24.69
4	11.0	12.0	25.0	0.006250	160.00
5	23.0	22.0	490.0	0.122500	8.16
6	36.0	0.0	498.0	0.124500	8.03

MEAN= 235.5000 STD.DEV.= 206.8311 PER.= 0.058875 FREQ.= 16.9851

CALCULATION OF PROPAGATION SPEED FROM PROPAGATING DATA

THERE ARE 3 PROPAGATING STALL CELLS NOTED

NO.	FRAMES	PASS.	PERIOD SEC.	FREQ. HZ.	VPROP FT/SEC	VPROP/W
1	142.000	3.000	0.01183333	84.507	18.0282	0.32601
2	102.000	2.000	0.01275000	78.431	16.7320	0.30257
3	69.000	1.000	0.01725000	57.971	12.3672	0.22364

MEAN= 55.7778 STD.DEV.= 0.115966E+02

AVERAGE VALUES

PER.= 0.013944 FREQ= 71.713 VPROP= 15.2988 VPROP/W= 0.27665

Stagger angle= 36.5 , Angle of attack= 25 , Inlet velocity= 54.1 ft/sec.

OCCURRENCES IN CENTER PASSAGE

THERE ARE 10 OCCURRENCES

NO.	FT FRAME		DFRAME	PERIOD <SEC>	FREQUENCY <HZ>
0	1.0	21.0			
1	2.0	10.0	29.0	0.007250	137.93
2	3.0	0.0	30.0	0.007500	133.33
3	4.0	10.0	50.0	0.012500	80.00
4	10.0	18.0	248.0	0.062000	16.13
5	11.0	25.0	47.0	0.011750	85.11
6	16.0	22.0	197.0	0.049250	20.30
7	21.0	31.0	209.0	0.052250	19.14
8	27.0	32.0	241.0	0.060250	16.60
9	46.0	18.0	746.0	0.186500	5.36
10	56.0	16.0	398.0	0.099500	10.05

THE 9 ENTRY IS NOT INCLUDED IN THE STATS
MEAN= 161.0000 STD.DEV.= 129.2478 PER.= 0.040250 FREQ.= 24.8447

CALCULATION OF PROPAGATION SPEED FROM PROPAGATING DATA

THERE ARE 6 PROPAGATING STALL CELLS NOTED

NO.	FRAMES	PASS.	PERIOD SEC.	FREQ. HZ.	VPROP FT/SEC	VPROP/W
1	94.000	2.000	0.01175000	85.106	18.1560	0.33560
2	167.000	3.000	0.01391666	71.856	15.3293	0.28335
3	118.000	2.000	0.01475000	67.797	14.4633	0.26734
4	114.000	2.000	0.01425000	70.175	14.9708	0.27672
5	131.000	1.000	0.03275000	30.534	6.5140	0.12041
6	97.000	2.000	0.01212500	82.474	17.5945	0.32522

MEAN= 66.3611 STD.DEV.= 0.320257E+02

AVERAGE VALUES
PER.= 0.016590 FREQ= 60.276 VPROP= 12.8589 VPROP/W= 0.23769

Stagger angle= 36.5 , Angle of attack= 30 , Inlet velocity= 55.5 ft/sec.

OCCURRENCES IN CENTER PASSAGE

THERE ARE 17 OCCURRENCES

NO.	FT FRAME		DFRAME	PERIOD <SEC>	FREQUENCY <HZ>
0	25.0	0.0			
1	26.0	34.0	74.0	0.018500	54.05
2	29.0	24.0	110.0	0.027500	36.36
3	33.0	6.0	142.0	0.035500	28.17
4	37.0	5.0	159.0	0.039750	25.16
5	39.0	24.0	99.0	0.024750	40.40
6	41.0	6.0	62.0	0.015500	64.52
7	45.0	31.0	185.0	0.046250	21.62
8	48.0	10.0	99.0	0.024750	40.40
9	51.0	20.0	130.0	0.032500	30.77
10	53.0	23.0	83.0	0.020750	48.19
11	56.0	18.0	115.0	0.028750	34.78
12	60.0	32.0	174.0	0.043500	22.99
13	65.0	27.0	195.0	0.048750	20.51
14	68.0	19.0	112.0	0.028000	35.71
15	71.0	31.0	132.0	0.033000	30.30
16	77.0	15.0	224.0	0.056000	17.86
17	79.0	25.0	90.0	0.022500	44.44

MEAN= 128.5294 STD.DEV.= 45.6989 PER.= 0.032132 FREQ.= 31.1213

CALCULATION OF PROPAGATION SPEED FROM PROPAGATING DATA

THERE ARE 9 PROPAGATING STALL CELLS NOTED

NO.	FRAMES	PASS.	PERIOD SEC.	FREQ. HZ.	VPROP FT/SEC	VPROP/W
1	165.000	3.000	0.01375000	72.727	15.5152	0.27975
2	164.000	3.000	0.01366666	73.171	15.6098	0.28146
3	150.000	3.000	0.01250000	80.000	17.0667	0.30773
4	111.000	2.000	0.01387500	72.072	15.3754	0.27723
5	222.000	4.000	0.01387500	72.072	15.3754	0.27723
6	229.000	4.000	0.01431250	69.869	14.9054	0.26876
7	101.000	2.000	0.01262500	79.208	16.8977	0.30468
8	217.000	4.000	0.01356250	73.733	15.7297	0.28362
9	189.000	3.000	0.01575000	63.492	13.5450	0.24423

MEAN= 55.0741 STD.DEV.= 0.379863E+01

AVERAGE VALUES
PER.= 0.013769 FREQ= 72.630 VPROP= 15.4943 VPROP/W= 0.27938

Stagger angle= 36.5 , Angle of attack= 35 , Inlet velocity= 55.5 ft/sec.

OCCURRENCES IN CENTER PASSAGE

THERE ARE 20 OCCURRENCES

NO.	FT FRAME		DFRAME	PERIOD <SEC>	FREQUENCY <HZ>
0	0.0	0.0			
1	0.0	22.0	22.0	0.005500	181.82
2	1.0	10.0	28.0	0.007000	142.86
3	1.0	39.0	29.0	0.007250	137.93
4	3.0	19.0	60.0	0.015000	66.67
5	4.0	18.0	39.0	0.009750	102.56
6	5.0	32.0	54.0	0.013500	74.07
7	7.0	18.0	66.0	0.016500	60.61
8	8.0	11.0	33.0	0.008250	121.21
9	9.0	6.0	35.0	0.008750	114.29
10	10.0	17.0	51.0	0.012750	78.43
11	11.0	15.0	38.0	0.009500	105.26
12	12.0	18.0	43.0	0.010750	93.02
13	13.0	1.0	23.0	0.005750	173.91
14	16.0	29.0	148.0	0.037000	27.03
15	18.0	0.0	51.0	0.012750	78.43
16	19.0	34.0	74.0	0.018500	54.05
17	21.0	0.0	46.0	0.011500	86.96
18	24.0	5.0	125.0	0.031250	32.00
19	25.0	29.0	64.0	0.016000	62.50
20	28.0	38.0	129.0	0.032250	31.01

MEAN= 57.9000 STD.DEV.= 36.0188 PER.= 0.014475 FREQ.= 69.0846

CALCULATION OF PROPAGATION SPEED FROM PROPAGATING DATA

THERE ARE 5 PROPAGATING STALL CELLS NOTED

NO.	FRAMES	PASS.	PERIOD SEC.	FREQ. HZ.	VPROP FT/SEC	VPROP/W
1	138.000	3.000	0.01150000	86.957	18.5507	0.33425
2	105.000	2.000	0.01312500	76.190	16.2540	0.29286
3	110.000	2.000	0.01375000	72.727	15.5152	0.27955
4	54.000	1.000	0.01350000	74.074	15.8025	0.28473
5	111.000	2.000	0.01387500	72.072	15.3754	0.27703

MEAN= 52.6000 STD.DEV.= 0.386329E+01

AVERAGE VALUES
PER.= 0.013150 FREQ= 76.046 VPROP= 16.2231 VPROP/W= 0.29231

Stagger angle= 45 , Angle of attack= 20 , Inlet velocity= 54.2 ft/sec.

OCCURRENCES IN CENTER PASSAGE

THERE ARE 3 OCCURRENCES

NO.	FT FRAME		DFRAME	PERIOD <SEC>	FREQUENCY <HZ>
0	0.0	0.0			
1	15.0	22.0	622.0	0.155500	6.43
2	28.0	18.0	516.0	0.129000	7.75
3	62.0	26.0	1368.0	0.342000	2.92

THE 3 ENTRY IS NOT INCLUDED IN THE STATS
THE 1 ENTRY IS NOT INCLUDED IN THE STATS

MEAN= 516.0000 STD.DEV.= 0.0 PER.= 0.129000 FREQ.= 7.7519

CALCULATION OF PROPAGATION SPEED FROM PROPAGATING DATA

THERE ARE 3 PROPAGATING STALL CELLS NOTED

NO.	FRAMES	PASS.	PERIOD SEC.	FREQ. HZ.	VPROP FT/SEC	VPROP/W
1	163.000	2.000	0.02037500	49.080	10.4703	0.19318
2	299.000	3.000	0.02491666	40.134	8.5619	0.15797
3	302.000	3.000	0.02516666	39.735	8.4768	0.15640

MEAN= 93.9444 STD.DEV.= 0.107888E+02

AVERAGE VALUES
PER.= 0.023486 FREQ= 42.578 VPROP= 9.0834 VPROP/W= 0.16759

Stagger angle= 45 , Angle of attack= 20 , Inlet velocity= 54.5 ft/sec.

OCCURRENCES IN CENTER PASSAGE

THERE ARE 11 OCCURRENCES

NO.	FT FRAME		DFRAME	PERIOD <SEC>	FREQUENCY <HZ>
0	0.0	0.0			
1	3.0	25.0	145.0	0.036250	27.59
2	5.0	29.0	84.0	0.021000	47.62
3	19.0	14.0	545.0	0.136250	7.34
4	28.0	35.0	381.0	0.095250	10.50
5	33.0	21.0	186.0	0.046500	21.51
6	43.0	5.0	384.0	0.096000	10.42
7	44.0	3.0	38.0	0.009500	105.26
8	60.0	16.0	653.0	0.163250	6.13
9	61.0	31.0	55.0	0.013750	72.73
10	75.0	17.0	546.0	0.136500	7.33
11	87.0	20.0	483.0	0.120750	8.28

MEAN= 318.1816 STD.DEV.= 223.8226 PER.= 0.079545 FREQ.= 12.5714

CALCULATION OF PROPAGATION SPEED FROM PROPAGATING DATA

THERE ARE 8 PROPAGATING STALL CELLS NOTED

NO.	FRAMES	PASS.	PERIOD SEC.	FREQ. HZ.	VPROP FT/SEC	VPROP/W
1	119.000	2.000	0.01487500	67.227	14.3417	0.26315
2	75.000	1.000	0.01875000	53.333	11.3778	0.20877
3	77.000	1.000	0.01925000	51.948	11.0823	0.20334
4	142.000	2.000	0.01775000	56.338	12.0188	0.22053
5	157.000	2.000	0.01962500	50.955	10.8705	0.19946
6	169.000	2.000	0.02112500	47.337	10.0986	0.18530
7	162.000	2.000	0.02025000	49.383	10.5350	0.19330
8	156.000	2.000	0.01950000	51.282	10.9402	0.20074

MEAN= 75.5625 STD.DEV.= 0.760844E+01

AVERAGE VALUES

PER.= 0.018891 FREQ= 52.936 VPROP= 11.2931 VPROP/W= 0.20721

Stagger angle= 45 , Angle of attack= 25 , Inlet velocity= 54.3 ft/sec.

OCCURRENCES IN CENTER PASSAGE

THERE ARE 9 OCCURRENCES

NO.	FT	FRAME	DFRAME	PERIOD <SEC>	FREQUENCY <HZ>
0	0.0	0.0			
1	1.0	39.0	79.0	0.019750	50.63
2	24.0	15.0	896.0	0.224000	4.46
3	36.0	11.0	476.0	0.119000	8.40
4	43.0	16.0	285.0	0.071250	14.04
5	50.0	17.0	281.0	0.070250	14.23
6	53.0	18.0	121.0	0.030250	33.06
7	59.0	10.0	232.0	0.058000	17.24
8	60.0	30.0	60.0	0.015000	66.67
9	67.0	32.0	282.0	0.070500	14.18

MEAN= 301.3333 STD.DEV.= 257.4373 PER.= 0.075333 FREQ.= 13.2743

CALCULATION OF PROPAGATION SPEED FROM PROPAGATING DATA

THERE ARE 5 PROPAGATING STALL CELLS NOTED

NO.	FRAMES	PASS.	PERIOD SEC.	FREQ. HZ.	VPROP FT/SEC	VPROP/W
1	144.000	2.000	0.01800000	55.556	11.8519	0.21827
2	137.000	2.000	0.01712500	58.394	12.4574	0.22942
3	99.000	2.000	0.01237500	80.808	17.2391	0.31748
4	176.000	3.000	0.01466666	68.182	14.5455	0.26787
5	101.000	2.000	0.01262500	79.208	16.8977	0.31119

MEAN= 59.8333 STD.DEV.= 0.102273E+02

AVERAGE VALUES

PER.= 0.014958 FREQ= 66.852 VPROP= 14.2619 VPROP/W= 0.26265

Stagger angle= 45 , Angle of attack= 25 , Inlet velocity= 53.9 ft/sec.

OCCURRENCES IN CENTER PASSAGE

THERE ARE 15 OCCURRENCES

NO.	FT FRAME		DFRAME	PERIOD <SEC>	FREQUENCY <HZ>
0	0.0	0.0			
1	0.0	27.0	27.0	0.006750	148.15
2	1.0	29.0	42.0	0.010500	95.24
3	2.0	15.0	26.0	0.006500	153.85
4	3.0	32.0	57.0	0.014250	70.18
5	5.0	2.0	50.0	0.012500	80.00
6	5.0	33.0	31.0	0.007750	129.03
7	11.0	34.0	241.0	0.060250	16.60
8	13.0	9.0	55.0	0.013750	72.73
9	15.0	4.0	75.0	0.018750	53.33
10	16.0	10.0	46.0	0.011500	86.96
11	23.0	16.0	286.0	0.071500	13.99
12	25.0	13.0	77.0	0.019250	51.95
13	26.0	30.0	57.0	0.014250	70.18
14	30.0	0.0	130.0	0.032500	30.77
15	53.0	14.0	934.0	0.233500	4.28

THE 15 ENTRY IS NOT INCLUDED IN THE STATS

MEAN= 85.7143 STD.DEV.= 80.2605 PER.= 0.021429 FREQ.= 46.6667

CALCULATION OF PROPAGATION SPEED FROM PROPAGATING DATA

THERE ARE 6 PROPAGATING STALL CELLS NOTED

NO.	FRAMES	PASS.	PERIOD SEC.	FREQ. HZ.	VPROP FT/SEC	VPROP/W
1	101.000	2.000	0.01262500	79.208	16.8977	0.31350
2	131.000	3.000	0.01091666	91.603	19.5420	0.36256
3	214.000	4.000	0.01337500	74.766	15.9502	0.29592
4	250.000	4.000	0.01562500	64.000	13.6533	0.25331
5	144.000	2.000	0.01800000	55.556	11.8519	0.21989
6	199.000	4.000	0.01243750	80.402	17.1524	0.31823

MEAN= 55.3194 STD.DEV.= 0.102288E+02

AVERAGE VALUES

PER.= 0.013830 FREQ= 72.307 VPROP= 15.4256 VPROP/W= 0.28619

Stagger angle= 45 , Angle of attack= 30 , Inlet velocity= 54.2 ft/sec.

OCCURRENCES IN CENTER PASSAGE

THERE ARE 22 OCCURRENCES

NO.	FT FRAME	DFRAME	PERIOD <SEC>	FREQUENCY <HZ>
0	0.0 0.0			
1	0.0 37.0	37.0	0.009250	108.11
2	3.0 36.0	119.0	0.029750	33.61
3	7.0 7.0	131.0	0.032750	30.53
4	9.0 2.0	75.0	0.018750	53.33
5	11.0 13.0	91.0	0.022750	43.96
6	12.0 35.0	62.0	0.015500	64.52
7	15.0 7.0	92.0	0.023000	43.48
8	16.0 30.0	63.0	0.015750	63.49
9	18.0 32.0	82.0	0.020500	48.78
10	23.0 20.0	188.0	0.047000	21.28
11	25.0 26.0	86.0	0.021500	46.51
12	32.0 7.0	261.0	0.065250	15.33
13	34.0 18.0	91.0	0.022750	43.96
14	37.0 2.0	104.0	0.026000	38.46
15	48.0 7.0	445.0	0.111250	8.99
16	50.0 2.0	75.0	0.018750	53.33
17	52.0 31.0	109.0	0.027250	36.70
18	57.0 5.0	174.0	0.043500	22.99
19	59.0 0.0	75.0	0.018750	53.33
20	64.0 35.0	235.0	0.058750	17.02
21	69.0 25.0	190.0	0.047500	21.05
22	74.0 7.0	182.0	0.045500	21.98

THE 15 ENTRY IS NOT INCLUDED IN THE STATS

MEAN= 120.0952 STD.DEV.= 61.0458 PER.= 0.030024 FREQ.= 33.3069

CALCULATION OF PROPAGATION SPEED FROM PROPAGATING DATA

THERE ARE 9 PROPAGATING STALL CELLS NOTED

NO.	FRAMES	PASS.	PERIOD SEC.	FREQ. HZ.	VPROP FT/SEC	VPROP/W
1	173.000	3.000	0.01441666	69.364	14.7977	0.27302
2	171.000	3.000	0.01425000	70.175	14.9708	0.27621
3	184.000	3.000	0.01533333	65.217	13.9130	0.25670

4	90.000	2.000	0.01125000	88.889	18.9630	0.34987
5	127.000	2.000	0.01587500	62.992	13.4383	0.24794
6	115.000	2.000	0.01437500	69.565	14.8406	0.27381
7	121.000	2.000	0.01512500	66.116	14.1047	0.26023
8	116.000	2.000	0.01450000	68.966	14.7126	0.27145
9	122.000	2.000	0.01525000	65.574	13.9891	0.25810

MEAN= 57.9444 STD.DEV.= 0.532617E+01

AVERAGE VALUES
PER.= 0.014486 FREQ= 69.032 VPROP= 14.7268 VPROP/W= 0.27171

Stagger angle= 45 , Angle of attack= 30 , Inlet velocity= 54.9 ft/sec.

OCCURRENCES IN CENTER PASSAGE

THERE ARE 18 OCCURRENCES

NO.	FT FRAME		DFRAME	PERIOD <SEC>	FREQUENCY <HZ>
0	0.0	0.0			
1	0.0	32.0	32.0	0.008000	125.00
2	1.0	38.0	46.0	0.011500	86.96
3	2.0	31.0	33.0	0.008250	121.21
4	3.0	39.0	48.0	0.012000	83.33
5	6.0	3.0	84.0	0.021000	47.62
6	9.0	8.0	125.0	0.031250	32.00
7	11.0	12.0	84.0	0.021000	47.62
8	14.0	11.0	119.0	0.029750	33.61
9	15.0	26.0	55.0	0.013750	72.73
10	17.0	18.0	72.0	0.018000	55.56
11	19.0	16.0	78.0	0.019500	51.28
12	20.0	12.0	36.0	0.009000	111.11
13	22.0	18.0	86.0	0.021500	46.51
14	28.0	7.0	229.0	0.057250	17.47
15	32.0	33.0	186.0	0.046500	21.51
16	39.0	0.0	247.0	0.061750	16.19
17	40.0	6.0	46.0	0.011500	86.96
18	42.0	12.0	86.0	0.021500	46.51

MEAN= 94.0000 STD.DEV.= 65.0457 PER.= 0.023500 FREQ.= 42.5532

CALCULATION OF PROPAGATION SPEED FROM PROPAGATING DATA

THERE ARE 9 PROPAGATING STALL CELLS NOTED

NO.	FRAMES	PASS.	PERIOD SEC.	FREQ. HZ.	VPROP FT/SEC	VPROP/W
1	190.000	4.000	0.01187500	84.211	17.9649	0.32723
2	199.000	4.000	0.01243750	80.402	17.1524	0.31243
3	287.000	4.000	0.01793750	55.749	11.8931	0.21663
4	157.000	2.000	0.01962500	50.955	10.8705	0.19801
5	137.000	2.000	0.01712500	58.394	12.4574	0.22691
6	229.000	4.000	0.01431250	69.869	14.9054	0.27150
7	218.000	4.000	0.01362500	73.394	15.6575	0.28520
8	215.000	4.000	0.01343750	74.419	15.8760	0.28918
9	229.000	4.000	0.01431250	69.869	14.9054	0.27150

MEAN= 59.8611 STD.DEV.= 0.105956Ė+02

AVERAGE VALUES
PER.= 0.014965 FREQ= 66.821 VPROP= 14.2552 VPROP/W= 0.25966

Stagger angle= 36.5 , Angle of attack= 30 , Inlet velocity= 157.5 ft/sec.

OCCURRENCES IN CENTER PASSAGE

THERE ARE 37 OCCURRENCES

NO.	FT FRAME		DFRAME	PERIOD <SEC>	FREQUENCY <HZ>
0	0.0	14.0			
1	0.0	25.0	11.0	0.002750	363.64
2	2.0	19.0	74.0	0.018500	54.05
3	3.0	12.0	33.0	0.008250	121.21
4	3.0	31.0	19.0	0.004750	210.53
5	7.0	0.0	129.0	0.032250	31.01
6	9.0	30.0	110.0	0.027500	36.36
7	10.0	23.0	33.0	0.008250	121.21
8	11.0	31.0	48.0	0.012000	83.33
9	13.0	17.0	66.0	0.016500	60.61
10	14.0	26.0	49.0	0.012250	81.63
11	15.0	27.0	41.0	0.010250	97.56
12	17.0	12.0	65.0	0.016250	61.54
13	18.0	6.0	34.0	0.008500	117.65
14	19.0	9.0	43.0	0.010750	93.02
15	20.0	24.0	55.0	0.013750	72.73
16	21.0	7.0	23.0	0.005750	173.91
17	21.0	32.0	25.0	0.006250	160.00
18	23.0	11.0	59.0	0.014750	67.80
19	23.0	34.0	23.0	0.005750	173.91
20	26.0	27.0	113.0	0.028250	35.40
21	27.0	10.0	23.0	0.005750	173.91
22	28.0	33.0	63.0	0.015750	63.49
23	31.0	8.0	95.0	0.023750	42.11
24	32.0	15.0	47.0	0.011750	85.11
25	34.0	21.0	86.0	0.021500	46.51
26	35.0	22.0	41.0	0.010250	97.56
27	36.0	36.0	54.0	0.013500	74.07
28	39.0	12.0	96.0	0.024000	41.67
29	40.0	22.0	50.0	0.012500	80.00
30	41.0	26.0	44.0	0.011000	90.91
31	42.0	24.0	38.0	0.009500	105.26
32	44.0	3.0	59.0	0.014750	67.80
33	45.0	6.0	43.0	0.010750	93.02
34	46.0	34.0	68.0	0.017000	58.82
35	47.0	26.0	32.0	0.008000	125.00
36	48.0	22.0	36.0	0.009000	111.11
37	49.0	18.0	36.0	0.009000	111.11

MEAN= 53.0811 STD.DEV.= 27.8621 PER.= 0.013270 FREQ.= 75.3564

CALCULATION OF PROPAGATION SPEED FROM PROPAGATING DATA

THERE ARE 5 PROPAGATING STALL CELLS NOTED

NO.	FRAMES	PASS.	PERIOD SEC.	FREQ. HZ.	VPROP FT/SEC	VPROP/W
1	57.000	2.000	0.00712500	140.351	29.9415	0.19010
2	24.000	1.000	0.00600000	166.667	35.5556	0.22575
3	17.000	1.000	0.00425000	235.294	50.1961	0.31871
4	18.000	1.000	0.00450000	222.222	47.4074	0.30100
5	22.000	1.000	0.00550000	181.818	38.7879	0.24627

MEAN= 21.9000 STD.DEV.= 0.466905E+01

AVERAGE VALUES
PER.= 0.005475 FREQ= 182.649 VPROP= 38.9650 VPROP/W= 0.24740

Stagger angle= 36.5 , Angle of attack= 35 , Inlet velocity= 158.4 ft/sec.

OCCURRENCES IN CENTER PASSAGE

THERE ARE 27 OCCURRENCES

NO.	FT	FRAME	DFRAME	PERIOD <SEC>	FREQUENCY <HZ>
0	0.0	0.0			
1	0.0	21.0	21.0	0.005250	190.48
2	1.0	2.0	21.0	0.005250	190.48
3	1.0	33.0	31.0	0.007750	129.03
4	4.0	12.0	99.0	0.024750	40.40
5	4.0	29.0	17.0	0.004250	235.29
6	5.0	15.0	26.0	0.006500	153.85
7	5.0	34.0	19.0	0.004750	210.53
8	6.0	14.0	20.0	0.005000	200.00
9	7.0	7.0	33.0	0.008250	121.21
10	7.0	17.0	10.0	0.002500	400.00
11	7.0	38.0	21.0	0.005250	190.48
12	8.0	11.0	13.0	0.003250	307.69
13	9.0	2.0	31.0	0.007750	129.03
14	9.0	21.0	19.0	0.004750	210.53
15	10.0	15.0	34.0	0.008500	117.65
16	11.0	32.0	57.0	0.014250	70.18
17	12.0	21.0	29.0	0.007250	137.93
18	13.0	33.0	52.0	0.013000	76.92
19	14.0	19.0	24.0	0.006000	166.67
20	14.0	27.0	18.0	0.004500	222.22
21	15.0	19.0	32.0	0.008000	125.00
22	15.0	38.0	19.0	0.004750	210.53
23	16.0	28.0	30.0	0.007500	133.33
24	17.0	30.0	42.0	0.010500	95.24
25	18.0	13.0	23.0	0.005750	173.91
26	18.0	30.0	17.0	0.004250	235.29
27	19.0	16.0	26.0	0.006500	153.85

THE 18 ENTRY IS NOT INCLUDED IN THE STATS
THE 19 ENTRY IS NOT INCLUDED IN THE STATS

MEAN= 26.2222 STD.DEV.= 17.1682 PER.= 0.006555 FREQ.= 152.5425

CALCULATION OF PROPAGATION SPEED FROM PROPAGATING DATA

THERE ARE 6 PROPAGATING STALL CELLS NOTED

NO.	FRAMES	PASS.	PERIOD SEC.	FREQ. HZ.	VPROP FT/SEC	VPROP/W
1	22.000	1.000	0.00550000	181.818	38.7879	0.24487
2	36.000	2.000	0.00450000	222.222	47.4074	0.29929
3	68.000	3.000	0.00566666	176.471	37.6471	0.23767
4	82.000	3.000	0.00683333	146.342	31.2195	0.19709
5	49.000	2.000	0.00612500	163.265	34.8299	0.21989
6	76.000	3.000	0.00633333	157.895	33.6842	0.21265

MEAN= 23.3055 STD.DEV.= 0.322562E+01

AVERAGE VALUES
PER.= 0.005826 FREQ= 171.633 VPROP= 36.6151 VPROP/W= 0.23116

Stagger angle= 45 , Angle of attack= 25 , Inlet velocity= 154.2 ft/sec.

OCCURRENCES IN CENTER PASSAGE

THERE ARE 8 OCCURRENCES

NO.	FT FRAME		DFRAME	PERIOD <SEC>	FREQUENCY <HZ>
0	0.0	0.0			
1	1.0	10.0	50.0	0.012500	80.00
2	3.0	31.0	101.0	0.025250	39.60
3	12.0	18.0	347.0	0.086750	11.53
4	15.0	30.0	132.0	0.033000	30.30
5	19.0	31.0	161.0	0.040250	24.84
6	27.0	9.0	298.0	0.074500	13.42
7	34.0	11.0	282.0	0.070500	14.18
8	40.0	11.0	240.0	0.060000	16.67

MEAN= 201.3750 STD.DEV.= 105.5379 PER.= 0.050344 FREQ.= 19.8634

CALCULATION OF PROPAGATION SPEED FROM PROPAGATING DATA

THERE ARE 2 PROPAGATING STALL CELLS NOTED

NO.	FRAMES	PASS.	PERIOD SEC.	FREQ. HZ.	VPROP FT/SEC	VPROP/W
1	17.000	1.000	0.00425000	235.294	50.1961	0.32553
2	18.000	1.000	0.00450000	222.222	47.4074	0.30744

MEAN= 17.5000 STD.DEV.= 0.707107E+00

AVERAGE VALUES

PER.= 0.004375 FREQ= 228.571 VPROP= 48.7619 VPROP/W= 0.31622

Stagger angle= 45 , Angle of attack= 30 , Inlet velocity= 154.0 ft/sec.

OCCURRENCES IN CENTER PASSAGE

THERE ARE 9 OCCURRENCES

NO.	FT FRAME		DFRAME	PERIOD <SEC>	FREQUENCY <HZ>
0	0.0	0.0			
1	1.0	3.0	43.0	0.010750	93.02
2	2.0	5.0	42.0	0.010500	95.24
3	3.0	27.0	62.0	0.015500	64.52
4	4.0	7.0	20.0	0.005000	200.00
5	5.0	13.0	46.0	0.011500	86.96
6	7.0	34.0	101.0	0.025250	39.60
7	21.0	7.0	533.0	0.133250	7.50
8	22.0	29.0	62.0	0.015500	64.52
9	30.0	0.0	291.0	0.072750	13.75

THE 7 ENTRY IS NOT INCLUDED IN THE STATS
THE 9 ENTRY IS NOT INCLUDED IN THE STATS

MEAN= 53.7143 STD.DEV.= 25.2370 PER.= 0.013429 FREQ.= 74.4681

CALCULATION OF PROPAGATION SPEED FROM PROPAGATING DATA

THERE ARE 3 PROPAGATING STALL CELLS NOTED

NO.	FRAMES	PASS.	PERIOD SEC.	FREQ. HZ.	VPROP FT/SEC	VPROP/W
1	23.000	1.000	0.00575000	173.913	37.1015	0.24098
2	58.000	2.000	0.00725000	137.931	29.4253	0.19112
3	26.000	1.000	0.00650000	153.846	32.8205	0.21318

MEAN= 26.0000 STD.DEV.= 0.300000E+01

AVERAGE VALUES
PER.= 0.006500 FREQ= 153.846 VPROP= 32.8205 VPROP/W= 0.21318

The vita has been removed from the scanned document